CRANFIELD UNIVERSITY

**Syed Kumail Haider**

# Oxygen Carrier and Reactor Development for Chemical Looping Processes and Enhanced $CO_2$ Recovery

School of Energy, Environment & Agrifood

Doctorate of Philosophy

Academic Year: 2015 - 2016

Supervisors: Dr K. Patchigolla, Professor J.E. Oakey

Subject Advisor: Professor E.J. Anthony

April 2016

CRANFIELD UNIVERSITY

School of Environment, Energy & Agrifood
Centre for Combustion, Carbon Capture & Storage

Doctorate of Philosophy

Academic Year 2015 - 2016

**SYED KUMAIL HAIDER**

# *Oxygen Carrier and Reactor development for Chemical Looping Processes and Enhanced $CO_2$ Recovery*

Supervisors: Dr K. Patchigolla & Professor. J.E. Oakey

Subject Advisor: Professor E.J. Anthony

April 2016

This thesis is submitted in partial fulfilment of the requirements for the degree of PhD

# ABSTRACT

This thesis's main focus is a $CO_2$ capture technology known as chemical looping combustion (CLC). The technology is a novel form of combustion and fuel processing that can be applied to gas, solid and liquid fuels. By using two interconnected fluidised-bed reactors, with a bed material capable of transferring oxygen from air to the fuel, a stream of almost pure $CO_2$ can be produced. This stream is undiluted with nitrogen and is produced without any direct process efficiency loss from the overall combustion process. The heart of the process is the oxygen carrier bed material, which transfers oxygen from an air to fuel reactor for the conversion of the fuel. Oxygen carrier materials and their production should be of low relative cost for use in large-scale systems.

The first part of this research centres on development and investigative studies conducted to assess the use of low-cost materials as oxygen carriers and as supports. Mixed-oxide oxygen carriers of modified manganese ore and iron ore were produced by impregnation. While copper (II) oxide supported on alumina cement and CaO have been produced by pelletisation. These oxygen carriers were investigated for their ability to convert gaseous fuels in a lab-scale fluidised bed, and characterised for their mechanical and chemical suitability in the CLC process. The modified ores and pelletised copper-based oxygen carriers' mechanical properties were enhanced by their production methods and in the case of the modified iron ore, significant oxygen uncoupling was observed. The copper-based oxygen carriers particularly those containing alumina cement showed high conversion rates of gaseous fuels and improved mechanical stability.

The second part of this research thesis focuses on the design philosophy, commissioning and operation of a dual-fast bed chemical looping pilot reactor. Based on the operational experience, recommendations for modifications to the CLC system are discussed. In support, a parallel hydrodynamic investigation has been conducted to validate control and operational strategies for the newly-designed reactor system. It was determined that the two fast bed risers share similar density and pressure profiles. Stable global circulation rate is flexible and could be maintained despite being pneumatically controlled. Reactor-reactor leakage via the loop-seals is sensitive to loop seal bed-height, and inlet fluid velocity but can be maintained as such to ensure no leakage is encountered.

Keywords: Climate change, Carbon capture, Circulating fluidised bed, Metal oxide, Ore, Oxygen uncoupling (CLOU)

# ACKNOWLEDGEMENTS

I would like to first thank my supervisors, Professor John Oakey and Dr Kumar Patchigolla for their advice, support and for granting me the opportunity to conduct this interesting research.

I am indebted to Professor Edward (Ben) Anthony for his continuous commitment and tutelage in order to see me through this degree. I whole-heartedly believe that without his kind support, honest advice and academic vigour, this embodiment of my work would not have been possible.

Thanks to Professor Vasilije Manovic for his contributions to my successful publications. I would like to thank Dr Stuart Scott for his advice and arranging my research visit to conduct investigations his laboratory. Thanks to Felix Donat for his support during this research visit. To my Swedish co-authors, notably Professor Henrik Leion and Dr Golnar Azimi, for their fruitful discussions and support during my research secondment, tack så mycket.

I would like to thank Dr Lunbo Duan for the scientific coaching he provided during my time as a research student. It was a pleasure to work with you.

A big thank you must go to the technical team in building 43a; Howard, Peter, Kevin and Euan. I would especially like to express my thanks to Martin Roskilly for all of his exceptional efforts and support. His encouragement never wavered, nor did his sarcasm. I will surely miss working alongside you.

I would like to thank María and Danilo, for their contributions in the laboratory, but more importantly for their support and friendship.

Lastly, I want to thank my family for their unconditional love and prayers. To my Aunty Saeeda and beloved parents, who never doubted I would reach my goals, even in times when I doubted myself. I dedicate this work to you.

Syed. K. Haider

Cranfield, 31st March 2016

# TABLE OF CONTENTS

ABSTRACT ..... i
ACKNOWLEDGEMENTS ..... iii
LIST OF FIGURES ..... viii
LIST OF TABLES ..... xiii
LIST OF EQUATIONS ..... xiv
GLOSSARY ..... xv
1 Introduction ..... 1
1.1 Greenhouse Gas & Climate Change ..... 1
1.2 Carbon capture and storage ..... 4
1.2.1 $CO_2$ Capture processes ..... 5
1.2.2 High-temperature solid-looping cycles ..... 8
1.2.3 Calcium looping ..... 10
1.3 Chemical looping Combustion and Oxygen Uncoupling ..... 11
1.4 PhD scope ..... 15
1.5 Key issues ..... 15
1.6 Key gaps in knowledge ..... 17
1.7 PhD aims and objectives ..... 17
1.8 Outline of PhD thesis ..... 19
2 Literature Survey ..... 21
2.1 Introduction ..... 21
2.2 Oxygen carriers fundamentals for CLC/CLOU ..... 21
2.2.1 Research and development of oxygen carriers ..... 22
2.2.1 Mass balance and oxygen carrier transport capacity ..... 22
2.2.2 Thermodynamic Considerations ..... 24
2.2.3 Heat Balance ..... 26
2.2.4 Attrition and agglomeration ..... 27
2.2.5 Economic comparison ..... 29
2.2.6 Environmental Considerations ..... 32
2.2.7 Copper–based oxygen carriers ..... 32
2.2.8 Manganese-based oxygen carriers ..... 34
2.2.9 Iron-based oxygen carriers ..... 35
2.2.10 Combined-oxide based oxygen carriers ..... 37
2.2.11 Low-cost for oxygen carrier materials ..... 39
2.3 Chemical looping scale up ..... 41
2.3.1 Scaling rules with dimensionless parameters ..... 43
2.3.2 Fuel types used in CLC ..... 45
2.3.3 Status of current CLC reactors ..... 47
2.3.4 Large scale development ..... 52
3 Development of iron and manganese ore-based oxygen carriers ..... 53
3.1 Scope ..... 53

3.1.1 Impregnation background ..... 54
3.2 Methodology ..... 55
3.2.1 Particle preparation ..... 55
3.2.2 Experimental Setup ..... 58
3.2.3 Experimental Conditions ..... 59
3.2.4 Oxygen Carrier Characterisation ..... 60
3.2.5 Data Evaluation ..... 61
3.3 Results and Discussion ..... 62
3.3.1 Particle Characterisation ..... 62
3.3.2 Oxygen Release ..... 66
3.3.3 Syngas conversion ..... 68
3.3.4 Methane Conversion ..... 72
3.4 Conclusions ..... 75
4 Development of copper-based oxygen carriers ..... 77
4.1 Scope ..... 77
4.2 Methodology ..... 78
4.2.1 Particle Preparation ..... 78
4.2.2 Ball mill production method ..... 79
4.2.3 Pelletisation Method ..... 82
4.2.4 Oxygen carrier characterisation ..... 84
4.2.5 Lab-scale experimental setup ..... 84
4.2.6 Experimental conditions ..... 85
4.2.7 Data evaluation ..... 87
4.3 Results and discussion ..... 88
4.3.1 Particle characterisation ..... 88
4.3.2 Carbon monoxide conversion ..... 94
4.3.3 Methane conversion ..... 100
4.4 Conclusions ..... 101
5 Development of Cranfield PACT CLC ..... 103
5.1 Pilot-plant reactor design ..... 103
5.2 Operation strategy analysis ..... 106
5.2.1 Operational Constraints ..... 107
5.2.2 Feasible operation strategies ..... 109
5.3 PACT facility commissioning ..... 110
5.4 Operation of PACT CLC in CLOU with Cu-based oxygen carrier ..... 115
6 Hydrodynamic investigation in a cold-flow model for CLC ..... 117
6.1 Cold-flow model design ..... 117
6.2 Methodology ..... 119
6.2.1 Experimental procedures ..... 120
6.3 Results and Discussion ..... 122
6.3.1 Minimum fluidisation and transport velocities ..... 122
6.3.2 Density profiles at varying velocities ..... 125

6.3.3 Solid circulation rate ..... 127
6.3.4 Gas bypass leakage ..... 129
6.4 Conclusions ..... 131
7 Conclusions and Future Work ..... 133
7.1 Conclusions ..... 133
7.1.1 Oxygen carrier development ..... 133
7.1.2 Pilot plant operational strategy ..... 137
7.2 Research findings comparison with research objectives ..... 139
7.3 Future work and recommendations ..... 141
7.3.1 Future oxygen carrier development ..... 141
7.3.2 Future pilot plant modifications ..... 142
REFERENCES ..... 143
APPENDICES ..... 159
Appendix A ..... 159
Appendix B ..... 167
Appendix C ..... 169

# LIST OF FIGURES

Figure 1-1 Observed globally averaged combined land and ocean surface temperature anomaly 1850-2012 (IPCC, 2014) ..... 1

Figure 1-2 Global anthropogenic energy-related greenhouse-gas emissions by type (IEA, 2015) ..... 2

Figure 1-3 (Left) Market share of primary energy sources up to 2014 and their predicted trend till 2035 (Right) Energy demand by fuel source between 1994-2014 and predicted demand by fuel source 2014-2035 (BP, 2013) ... 3

Figure 1-4 Overview of the complete CCS process (UKCCSRC, 2016)..... 5

Figure 1-5 Block diagram illustrating post-combustion, pre-combustion and oxy-combustion systems from (Figueroa et al., 2008) ..... 7

Figure 1-6 General Ca-looping scheme for post-combustion capture ..... 10

Figure 1-7 Simplified chemical looping combustion scheme ..... 12

Figure 2-1 Equilibrium constant $K_{eq}$ for the reduction of $H_2$ and CO with varying redox systems (Adánez et al., 2012)..... 25

Figure 2-2 SEM Images for 75%wt Fe2O3 particles a) as prepared b) after 50 cycles, from (Kidambi et al., 2012) ..... 29

Figure 2-3 Equilibrium oxygen concentration over the manganese and copper redox systems releasing oxygen as a function of temperature..... 34

Figure 2-4 Binary phase diagram of (MnyFe1-y)Ox in an O2 partial pressure of 0.05 atm from (Azimi et al., 2013) ..... 38

Figure 2-5 (Left) 10kW for gaseous fuels (Right) 100kW for solid fuels at Chalmers..... 48

Figure 2-6 (Left) schematic view (Right) image of 50kW CLC pilot plant ICB-CSIC from (Adánez et al., 2014) ..... 49

Figure 2-7 TUV 120kW CLC pilot plant for gaseous fuels from (Penthor et al., 2015)..... 50

Figure 3-1 Overview of laboratory-scale fluidised-bed system ..... 58

Figure 3-2 Manganese elemental mapping by EDX of FeMn33 particle (particle size 125-180 μm) ..... 64

Figure 3-3 Iron elemental mapping by EDX of MnFe33 particle (particle size 125-180 μm)..... 64

Figure 3-4 X-ray diffraction spectra for FeMn33 ..... 65

Figure 3-5 X-ray diffraction spectra for MnFe33 ..... 65

Figure 3-6 Oxygen carrier conversion vs. oxygen concentration for inert period at 950°C ..... 67

Figure 3-7 Oxygen release during inert period (360s) at 950°C ..... 67

Figure 3-8 Oxygen carrier conversion vs. gas yield for reduction with syngas at 950°C ..... 69

Figure 3-9 Oxygen carrier conversion vs. gas yield for reduction with syngas at 850°C ..... 70

Figure 3-10 Average Syngas Conversion at 800 – 1000°C showing the effect of increasing cycle numbers ..... 71

Figure 3-11 Oxygen carrier conversion vs. gas yield for reduction with $CH_4$ at 950°C ..... 72

Figure 3-12 Oxygen carrier conversion vs. gas yield for reduction with $CH_4$ at 850°C ..... 73

Figure 3-13 Average Methane Conversion at 800 – 1000°C showing the effect increasing redox cycle numbers ..... 74

Figure 4-1 Ortho-Alesa ball mill; (left) milling ball bearings, (right) ball mill ..... 80

Figure 4-2 Particle size distribution of CuO after 24h of ball mill operation ..... 80

Figure 4-3 (left) Glatt TGM Granulator (right) 4 litre vessel with blades i) agitator, ii) chopper ..... 82

Figure 4-4 Oxygen Carriers produced by pelletisation method: (left) SEM image of multiple oxygen carriers, (right) range of produced samples ..... 83

Figure 4-5 Simplified scheme of fluid bed reactor for redox investigation ..... 85

Figure 4-6 XRD spectra of alumina supported oxygen carriers (Top)-Cu25Al75 (Centre)-Cu50Al50 (Bottom)-Cu75Al25 ▲-CuO (Tenorite) ♦-$Al_2O_3$(Corundum) ◊-$AlHO_2$ (Bohmite) ..... 89

Figure 4-7 XRD spectra for Ca-supported oxygen carriers (Top)-Cu25Ca75 (Centre)-Cu50Ca50 (Bottom)-Cu75Ca25 ▲-CuO (Tenorite) ♦-$CaH_2O_2$ (Portlandite) ■-$Ca_2CuO_3$ ..... 90

Figure 4-8 Cu25Al75 i) High resolution SFEG image (scale 500µm), ii) Global particle view EDX, iii) Cu elemental mapping EDX, iv) Al elemental mapping EDX ..... 92

Figure 4-9 Cu50Al50 i) High resolution SFEG image (scale 500µm), ii) Global particle view EDX, iii) Cu elemental mapping EDX, iv) Al elemental mapping EDX ..... 92

Figure 4-10 Cu75Al25 i) High resolution SFEG image (scale 500µm), ii) Global particle view EDX, iii) Cu elemental mapping EDX, iv) Al elemental mapping EDX ..... 92

Figure 4-11 Cu25Ca75 i) High resolution SFEG image (scale 500µm), ii) Global particle view EDX, iii) Cu elemental mapping EDX, iv) Ca elemental mapping EDX ..... 93

Figure 4-12 Cu5OCa50 i) High resolution SFEG image (scale 500µm), ii) Global particle view EDX, iii) Cu elemental mapping EDX, iv) Ca elemental mapping EDX ..... 93

Figure 4-13 Cu75Ca25 i) High resolution SFEG image (scale 500µm), ii) Global particle view EDX, iii) Cu elemental mapping EDX, iv) Ca elemental mapping EDX ..... 93

Figure 4-14 Redox cyclic behaviour over 25 cycles assessed by oxygen carrier conversion against the conversion of CO to $CO_2$ (Left) Cu25Al75, (Centre) Cu50Al50, (Right) Cu75Al25 ..... 95

Figure 4-15 High resolution SEM images showing morphology of Cu25Al75 (left) Fresh produced 5µm, (centre) After 25 redox cycles with CO 5µm (right), Multiple particles after 24 redox cycles with CO 500µm ..... 96

Figure 4-16 High resolution SEM images showing morphology of Cu50Al50 (left) Fresh produced 5µm, (centre) After 25 redox cycles with CO 5µm (right), Multiple particles after 24 redox cycles with CO 500µm ..... 96

Figure 4-17 High resolution SEM images showing morphology of Cu75Al25 (left) Fresh produced 5µm, (centre) After 25 redox cycles with CO 5µm (right), Multiple particles after 24 redox cycles with CO 500µm ..... 96

Figure 4-18 Redox cyclic behaviour over 25 cycles assessed by oxygen carrier conversion against the conversion of CO to $CO_2$ (Left) Cu25Ca75, (Centre) Cu50Ca50, (Right) Cu75Ca25 ..... 98

Figure 4-19 High resolution SEM images showing morphology of Cu25Ca75 (left) Fresh produced 5µm, (centre) After 25 redox cycles with CO 5µm (right), Multiple particles after 24 redox cycles with CO 500µm ..... 99

Figure 4-20 High resolution SEM images showing morphology of Cu50Ca50 (left) Fresh produced 5µm, (centre) After 25 redox cycles with CO 5µm (right), Multiple particles after 24 redox cycles with CO 500µm ..... 99

Figure 4-21 High resolution SEM images showing morphology of Cu75Ca25 (left) Fresh produced 5µm, (centre) After 25 redox cycles with CO 5µm (right), Multiple particles after 24 redox cycles with CO 500µm ..... 99

Figure 4-22 Redox cyclic behaviour of Cu25Al75 and Cu25Ca75 over 25 cycles assessed by oxygen carrier conversion against the conversion of $CH_4$ to $CO_2$ ..... 101

Figure 5-1 Cranfield dual interconnected CFB design (not to scale) – 1a Distributer nozzles, 1b Wind box and Magnified distributer nozzles, 2 Main riser, 3a Loop-seal, 3b Loop-seal distributer nozzles, 4 Return leg, 5 Primary cyclone, 6 Secondary cyclone ..... 104

Figure 5-2 Simplified flowchart of PACT CLC reactor ..... 107

Figure 5-3 Wind box pressure at ignition during commissioning test..... 111

Figure 5-4 Air reactor temperature profile at ignition during commissioning test ..... 112

Figure 5-5 (Left) Gas analysis during one reactor operation (Bed temperature: 850-880 °C) / (Right) Mass-based conversion of oxygen carrier and conversion of $CH_4$ ..... 113

Figure 5-6 Installed PACT CLC facility (Left) Top of risers of dual CFB (Top Right) Multi-gas supply manifold (Bottom Right) Particulate filter system and flare ..... 114

Figure 5-7 Oxygen releasing with the temperature (total duration: 30mins) ... 116

Figure 5-8 Agglomerated copper-based oxygen carriers fused to the gas distributor ..... 116

Figure 6-1 Components of CFM (bottom left) gas distributor (top left) loop-seal (centre) Top of CFB risers and cyclones (right) Lower section of CFB and return legs and loop-seals ..... 118

Figure 6-2 Minimum fluidisation velocity of molochite..... 123

Figure 6-3 Minimum fluidisation velocity of FE100 ..... 123

Figure 6-4 Geldart particle classification of molochite and FE100 (Adapted from(Geldart, 1973))..... 124

Figure 6-5 Density profiles at varying fluidisation velocities (molochite static bed height 550mm) ..... 126

Figure 6-6 Density profiles at varying fluidisation velocities (Fe100 static bed height 230mm) ..... 126

Figure 6-7 Pressure profile of both risers at steady state (static bed height 550mm)..... 127

Figure 6-8 Solid transfer rate at varying velocity and static bed height (molochite) ..... 128

Figure 6-9 Solid transfer rate at varying velocity and static bed height (FE100) ..... 129

Figure 6-10 Leakage ratio at varying fluidising gas velocities and loop seal bed heights..... 131

Figure A-1 Installation of the risers, cyclones and trace heating elements..... 157

Figure A-2 Installation of return legs, and reactor insulation ..... 158

Figure A-3 (left) Gas preheaters (right) Trace heating control units ..... 158

Figure A-4 Installed loop seals and flexible joints for reactor expansion relief 159

Figure A-5 Engineering scheme of CLC reactor..... 160

Figure A-6 Design of candle particulate filter. Two per riser, designed to allow continuous operation if one becomes full or blocked..... 161

Figure A-7 Design of feed lock hopper for the oxygen carrier feeding..... 162

Figure A-8 Design of primary and secondary cyclones ..... 163

Figure A-9 Primary cyclone modification to enhance entry velocity and cyclonic effect. Plate installed (indicated in red) to reduce cyclone inlet aperture. 164

Figure C-1 XRD spectra of CuO 60% Al2O3 40% after commissioning test, showing no interaction between active oxide and support material..... 167

# LIST OF TABLES

Table 1-1 Current status of efficiencies and efficiency losses of coal and gas plants coupled with various carbon capture technologies and their development targets for 2020 adapted from (APGTF, 2011) ..... 8

Table 2-1 Oxygen ratio $R_O$ for various redox systems adapted from (Jerndal, Mattisson and Lyngfelt, 2006) ..... 24

Table 2-2 Standard heat of reaction of different redox systems (Adánez et al., 2012) ..... 26

Table 2-3 Comparison of various oxygen carrier production techniques ..... 31

Table 2-4 Reactor patterns and characteristics ..... 43

Table 2-5 Pilot plant operation >10kWth with solid fuels adapted from (Fennell and Anthony, 2015) ..... 46

Table 2-6 Summary of chemical looping units larger than $10kW_{th}$ ..... 51

Table 2-7 Dimensions of $1MW_{th}$ CLC facility at the Technical University of Damstadt from (Ströhle, Orth and Epple, 2014) ..... 52

Table 3-1 Oxygen Carriers Samples ..... 56

Table 3-2 Composition analyses of ores ..... 57

Table 3-3 Experimental gaseous conditions ..... 60

Table 3-4 Physical Properties of Oxygen Carriers ..... 63

Table 4-1 Properties of reagents used in oxygen carrier preparation ..... 79

Table 4-2 Typical product yield from 1kg of CuO + Al300 ..... 81

Table 4-3 Experimental conditions, gases and flowrates ..... 86

Table 4-4 Oxygen carrier characterisation properties ..... 88

Table 5-1 Gas conditions for bubbling-bed commissioning test ..... 113

Table 6-1 Operational conditions of CLC vs CFM ..... 119

Table 6-2 CFM similarity with Glicksman scaling laws ..... 120

# LIST OF EQUATIONS

Equation 1-1 ..... 12
Equation 1-2 ..... 12
Equation 1-3 ..... 13
Equation 1-4 ..... 13
Equation 1-5 ..... 14
Equation 1-6 ..... 14
Equation 2-1 ..... 23
Equation 2-2 ..... 23
Equation 2-3 ..... 23
Equation 2-4 ..... 23
Equation 2-5 ..... 38
Equation 2-6 ..... 44
Equation 3-1 ..... 61
Equation 3-2 ..... 61
Equation 3-3 ..... 61
Equation 3-4 ..... 62
Equation 3-5 ..... 62
Equation 4-1 ..... 87
Equation 4-2 ..... 87
Equation 4-3 ..... 87
Equation 6-1 ..... 121

# GLOSSARY

## ABBREVIATIONS

| | |
|---|---|
| APGTF | Advanced power generation technology forum |
| ASU | Air separation unit |
| AR | Air reactor |
| BET | Brunauer Emmett Teller |
| BP | British Petroleum |
| CCS | Carbon capture and storage |
| CFB | Circulating fluidised bed |
| CFM | Cold flow model |
| CLC | Chemical looping combustion |
| CLOU | Chemical looping with oxygen uncoupling |
| CSIC/ICB | Instituto de Carboquimica (Spanish research council) |
| EDX | Energy dispersive x-ray spectroscopy |
| FR | Fuel reactor |
| HTLC | High temperature looping cycles |
| IPCC | Intergovernmental panel on climate change |
| LCV | Lower calorific value |
| LS | Loop seal |
| OC | Oxygen carrier |
| PACT | Pilot scale advanced $CO_2$ capture technology |
| PEL | Point efficiency loss |
| SEM | Scanning electron microscope |
| SFEG | Schottky Field Emission Gun |
| TS | Total Solids |
| UNFCCC | United nations framework convention on climate change |
| XRD | X-ray diffraction spectroscopy |

## NOMENTCLATURE

| | | |
|---|---|---|
| Ar | | Archimedes Number |
| $a_{oc}$ | | Mass fraction of active oxygen carrier |
| D | [m] | Internal Diameter |
| d | | Stoichiometric coefficient of $O_2$ |
| dp | [*$10^{-6}$ m] | Particle Diameter |

| | | |
|---|---|---|
| Fr | | Froude Number |
| g | [m $s^{-2}$] | Gravitational acceleration |
| $G_S$ | [kg $m^{-2}$ $s^{-1}$] | Solid circulation rate |
| L | [m] | Length of riser |
| $LR_{CO2}$ | | $CO_2$ Leakage ratio |
| $M_o$ | [0.016 kg $mol^{-1}$] | Atomic weight of oxygen |
| $m_{oc}$ | [kg] | Mass of oxygen carrier sample |
| $m_{ox}$ | [kg] | Mass of fully oxidised oxygen carrier |
| $m_{red}$ | [kg] | Mass of fully oxidised oxygen carrier |
| $n_{tot,in}$ | [mol $s^{-1}$] | Total molar flow in |
| $n_{tot,out}$ | [mol $s^{-1}$] | Total molar flow out |
| $P_i$ | [mol %] | Partial pressure of component *i* |
| $P_{CO2}$ | [vol %] | $CO_2$ % at analysis point |
| $Q_{riser}$ | [L*$m^{-1}$] | Flow rate in riser |
| $Q_{LS}$ | [L*$m^{-1}$] | Flow rate in loop seal |
| Re | | Reynolds number |
| $R_o$ | | Oxygen carrier transport capacity |
| $U_0$ | [m $s^{-1}$] | Superficial fluidisation |
| $U_{mf}$ | [m $s^{-1}$] | Minimum fluidisation velocity |
| $U_{tr}$ | [m $s^{-1}$] | Transport velocity |
| $X_i$ | | Mass based oxygen carrier conversion |

## GREEK LETTERS

| | | |
|---|---|---|
| $\gamma_i$ | | Conversion of component *i* |
| $\Delta H_c^0$ | [kJ $mol^{-1}$] | Standard enthalpy of heat of combustion |
| $\Delta H_r^0$ | [kJ $mol^{-1}$] | Standard enthalpy of heat of reaction |
| $\Delta p$ | [Pa] | Pressure drop |
| $\xi_S$ | | Solid concentration |
| $\varphi$ | | Particle sphericity |
| $\mu$ | [Pa $s^{-1}$] | Gas viscosity |
| $\rho_g$ | [kg $m^{-3}$] | Gas density |
| $\rho_s$ | [kg $m^{-3}$] | Solid density |
| $\omega$ | | Degree of oxygen carrier conversion |

# 1 Introduction

## 1.1 **Greenhouse Gas & Climate Change**

Global warming and its effect on climate change pose alarming consequences for many inhabitants around the world. Global warming has been linked to the reduction of polar ice sheets, warming of the oceans and disruptions in weather cycles, causing severe droughts in some areas and increased flooding in others (Hughes, 2000). The increase in frequency of these climate related disasters could see the large-scale displacement of populations and cause a major vulnerability for food security and supply. The effect of global warming and climate change has gained attention within recent years. Global temperature recordings over the past one and a half centuries, for which several independent datasets exist (Stocker et al., 2013), shows the average surface temperature increasing in two distinct phases as seen in Figure 1-1; between the decades of 1910 and 1940, where the temperature rose 0.35ºC and between 1970 and the recent period of 2010, where a rise of 0.55ºC is observed (IPCC, 2014).

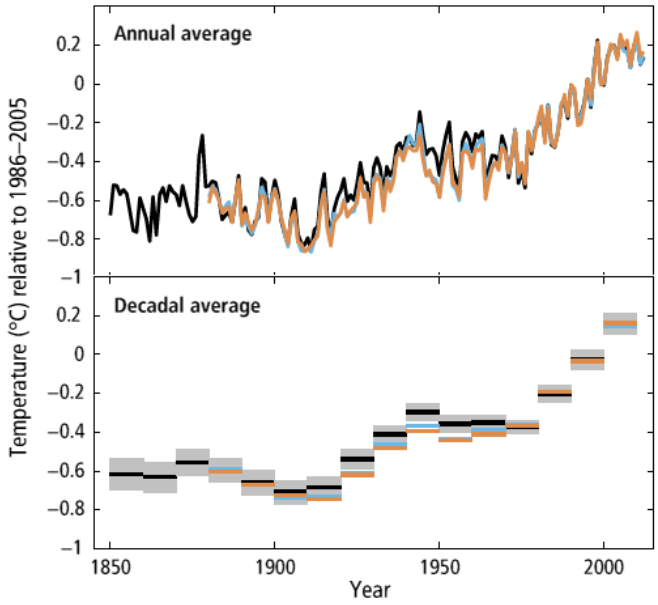


**Figure 1-1 Observed globally averaged combined land and ocean surface temperature anomaly 1850-2012 (IPCC, 2014)**

The significance of these thirty and forty-year spans respectively, is their association with heightened industrial activity during these decades. This, in turn leads to the conclusion, that the observed rise in global temperatures is a direct result of human activity. The majority of the scientific community accepts that the acceleration of climate change is directly linked to anthropogenic greenhouse gases (Hansen, 2004). Anthropogenic carbon dioxide ($CO_2$) has been identified as the main contributor to the greenhouse gas effect through its emissions in power generation and industrial processes (Shakun et al., 2012). Other greenhouse gases such as nitrous oxide ($N_2O$) and methane ($CH_4$) pose a greater greenhouse potential, 265 and 28 times higher than $CO_2$ respectively, but are present in the atmosphere in ppb as compared to $CO_2$, which is in the order of 1000 times greater in concentration as shown in Figure 1-2 (IPCC, 2007).

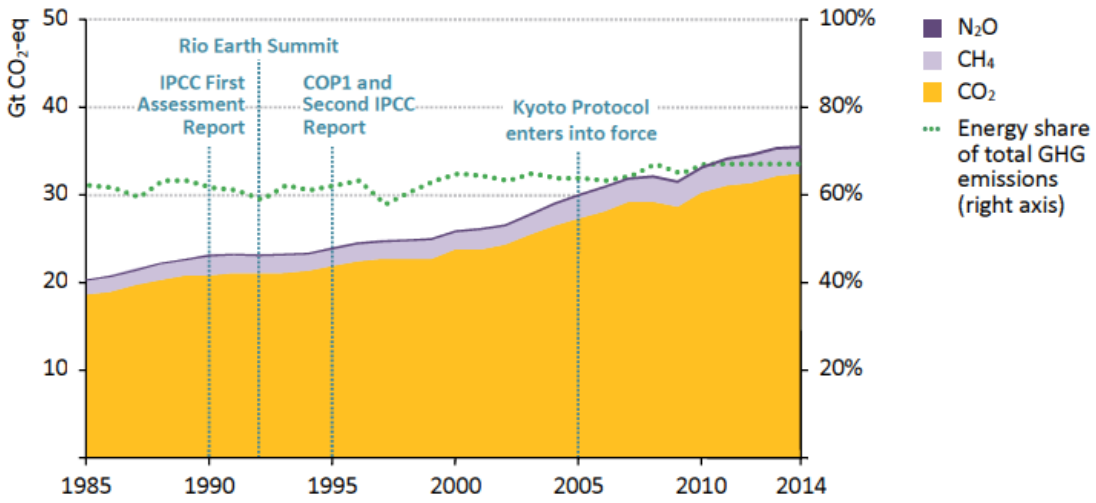


**Figure 1-2 Global anthropogenic energy-related greenhouse-gas emissions by type (IEA, 2015)**

The bulk of this $CO_2$ currently comes from the combustion of fossil fuels, and approximately 40% of global emissions are a result of power generation and another 45% is produced by industrial processes and transportation (IEA, 2010).

The 2015 climate change summit (Paris COP21) led to global policies where it was agreed to keep the average global temperature below 2ºC above pre-

industrial levels, in accordance with the best available science (UNFCCC, 2015). For this to be achievable, countries are required to significantly cut their emissions of greenhouse gases by the year 2030.

With the current and predicted trends for growth in the world economy, energy use is projected to increase by 34% between 2014 and 2035 (BP, 2013). It is expected that renewable and low carbon sources of energy are likely to play a key role in future energy supply while the dependence on fossil fuels, namely coal must be reduced. Figure 1-3 in the 2016 BP energy outlook estimates, renewables and low carbon sources of energy (renewables including biofuels, hydro and nuclear) will contribute approximately 40% supply to the growth in energy demand by the year 2035. Therefore, fossil fuels will still account for the supply of the remaining 60% of the 34% predicted growth in energy demand, and approximately 80% of the entire energy mix.

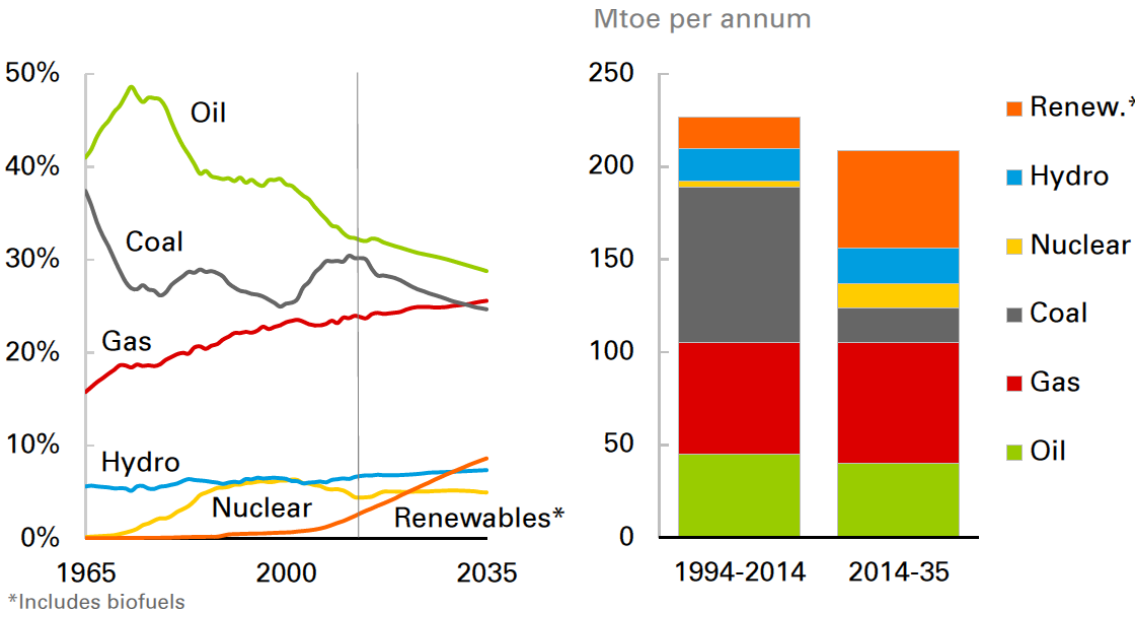


**Figure 1-3 (Left) Market share of primary energy sources up to 2014 and their predicted trend till 2035 (Right) Energy demand by fuel source between 1994-2014 and predicted demand by fuel source 2014-2035 (BP, 2013)**

Transitioning to low $CO_2$ emitting sources of power generation is likely to be slow and the transition requires an overhaul of the energy network. Such adoption will require the industrial materiality of alternative low carbon and

renewable technologies and it is argued that it may take up to 30 years (Kramer and Haigh, 2009).

Nuclear energy is likely only ever serve base load supply, with minimal plant flexibility and slow response to grid demands. While an increase share in renewables to the energy mix will give rise to greater intermittency of energy supply. Fast response fossil fuelled power generation will thus still be required to compensate for peak demands in the grid and will still be the major source of energy supply for the foreseeable future. The way in which fossil fuels are utilised in the transition period is particularly important, as responsible usage is the key pathway to emission reductions. A switch to cleaner fossil fuels such as natural gas instead of coal and the co-firing of coal with biomass are possible strategies (BP, 2013) for near term $CO_2$ mitigation, but to ensure the targets set at the Paris climate summit are achieved, the $CO_2$ from these combustion intensive processes will still have to be captured.

A possible strategy to mitigate the $CO_2$ produced from carbon intensive power generation and industrial processes is carbon capture and storage (CCS). The CCS strategy can offer a near term solution for $CO_2$ emission reductions while the necessary policy, markets, networks and distribution are optimised for low carbon sources of energy (Kramer and Haigh, 2009). Most carbon capture processes require energy and therefore the capture sector of the CCS strategy incurs efficiency penalties for power generation processes.

## 1.2 **Carbon capture and storage**

CCS encompasses a class of technologies, the accumulative processes of which remove $CO_2$ emissions from point sources of combustion e.g. large-scale power generation units. The entire process consists of three main steps; firstly the resultant $CO_2$ emissions are captured from the flue gas source; it is then compressed to a pressure suitable for transportation conditions in a pipeline (approximately 80 bar); lastly it is pumped into a designated sub-surface site for long-term storage (D'Alessandro, Smit and Long, 2010). A diagram illustrating the CCS process is shown in Figure 1-4. For the capture of the $CO_2$ from sources such as power plants and $CO_2$ intensive industries, pre-combustion,

post-combustion, oxy-fuel processes and high-temperature looping cycles are some of the most well investigated technologies. A recent review of the developments of each of these capture processes is available elsewhere (Boot-Handford et al., 2014).

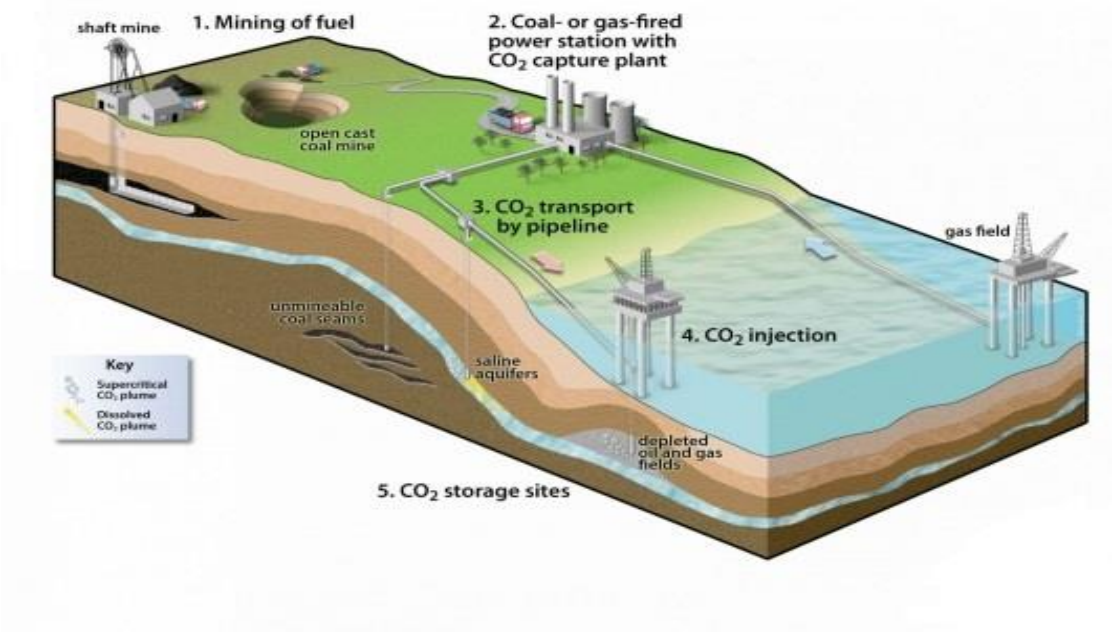


**Figure 1-4 Overview of the complete CCS process (UKCCSRC, 2016)**

### 1.2.1 $CO_2$ Capture processes

In post-combustion processes, as the name suggests, the capture of $CO_2$ occurs after the combustion process and the $CO_2$ is separated from the resultant flue gas. The advantage of this approach is that the combustion process is largely unaffected, thus allowing one to potentially retrofit such a capture system (Wilcox, 2012). Post-combustion capture currently consists of the following techniques and processes; absorption, adsorption, membrane absorption and cryogenic separation. Absorption processes' are currently the closest to commercial deployment, with operational demonstration plants such as; Boundary Dam (Canada) and Petra Nova (USA). The fundamental absorption process achieves the uptake of $CO_2$ into a bulk phase of another material. This is typically a solvent in a liquid phase, by which absorption takes place through chemical interaction with the $CO_2$ or utilising the solvents solubility gradient (Global CCS Institute, 2011). In a typical pulverised coal fired

power plant, the incorporation of full post-combustion capture processes can reduce the thermal efficiency by up to 10% from 38% for a base-case power plant to 28% for full post-combustion capture. The reduction in thermal efficiency comes from the capture element ensuing parasitic energy consumption and thus acting as a heat sink for low temperature waste heat which is uneconomical to recover (Global CCS Institute, 2011). For air-fired pulverised coal power plants, the $CO_2$ concentration present in the flue gas ranges between 4-14%, (Pires et al., 2011) therefore, to maintain high capture rates, the solvent must remain at a high concentration. The solvent reduces in efficacy over time and requires make-up, which incurs additional process cost. The solvent regeneration process impacts the thermal efficiency of the plant (Hester and Harrison, 2010). The extracted steam required for solvent regeneration causes a reduction of flow to the low-pressure steam turbine impacting the net energy production (Global CCS Institute, 2011).

In pre-combustion processes, the carbonaceous fossil fuel is decarbonised prior to the combustion process takes place. This decarbonisation step is achieved by means of gasification and then a subsequent steam reformation step (Wilcox, 2012). $CO_2$ is removed from the fuel gas stream, through absorption, adsorption and membrane separation. The highly calorific syngas is then ready for combustion (Pires et al., 2011). Whilst achieving a high concentration stream of $CO_2$ the pre-combustion capture process has associated energy penalties (7-9%) arising from the cryogenic separation of oxygen from air for the gasification step (Hester and Harrison, 2010).

Oxy-fuel combustion is the process in which the fossil fuel is combusted in an oxygen rich environment. The bulk nitrogen from air is removed prior to combustion via a cryogenic air separation unit (ASU) (Simmonds, Miracca and Gerdes, 2004). This separation technology is a commercially mature process, although still expensive. Due to the use of oxygen to combust the fuel, the extracted $CO_2$ is of high purity (90% dry basis) (Rackley, 2010). The combustion process takes place in boiler systems similar to air fired plants. Oxy-fuel combustion with $CO_2$ capture also requires a $CO_2$ purification unit,

which include a flue gas drying and conditioning sub-system and gas compressors (Global CCS Institute, 2011). During the combustion in such oxygen rich environments, the temperature of reaction can reach the limits of what the combustion plant can tolerate. In typical air firing processes, the temperature is limited by the presence of nitrogen in the air. In oxy-firing processes, $CO_2$ is recycled back into the combustion chamber to control the reaction temperature and allows for complete combustion of the fuel.

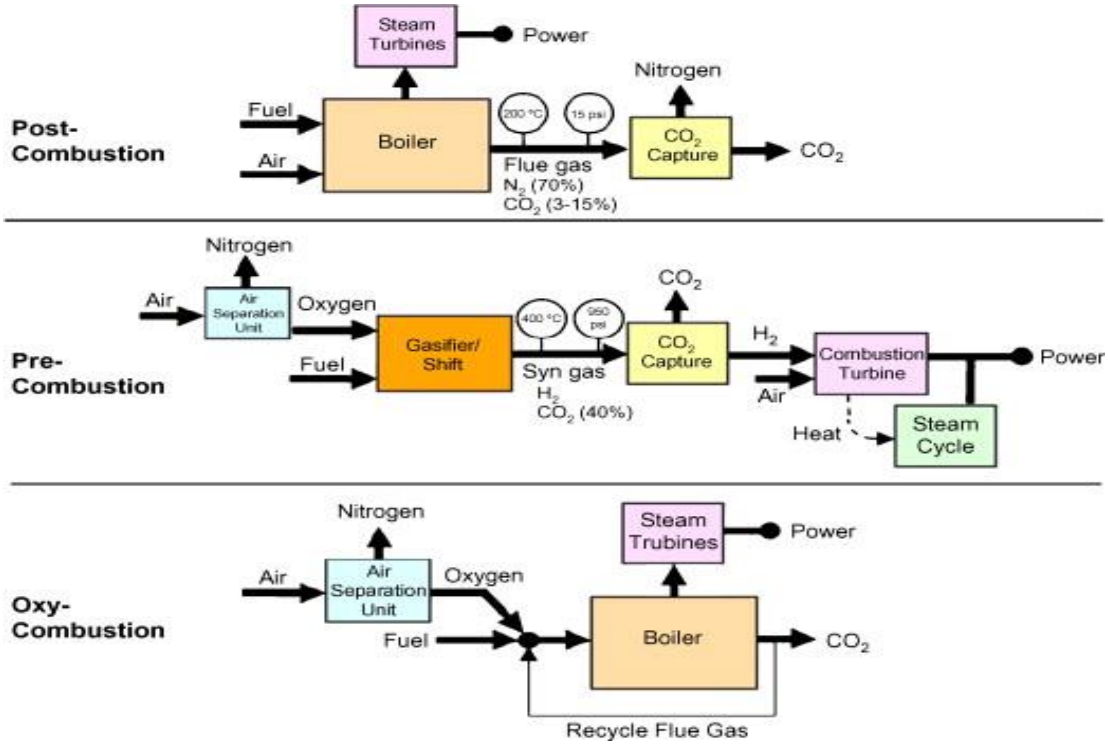


**Figure 1-5 Block diagram illustrating post-combustion, pre-combustion and oxy-combustion systems from (Figueroa et al., 2008)**

A block diagram of pre, post and oxy-fuel combustion systems and their means of implementation in power generation processes are illustrated in Figure 1-5.

Each of the capture technologies described above, have common disadvantages in that they require some form of additional energy input, which impacts the efficiency of the coupled power generation process. In case of post-combustion capture, there is the requirement for regenerating the $CO_2$ containing solvent. In pre-combustion there is an associated energy necessity for increased steam production and the separation of gases required after the

gasification process. Oxy-fuel capture requires a coupled ASU to produce oxygen, which is a particularly energy intensive process. Neither technology offers distinct advantages over its competitors (Fennell and Anthony, 2015). The advanced power generation technology forum published figures in their cleaner fossil fuel 2011 report discussing the current and 2020 target efficiency impacts on coupled $CO_2$ capture technologies (APGTF, 2011) as shown in Table 1-1. These figures take into account the energy penalty posed by the compression of $CO_2$ for transport. Currently, if post-combustion systems or oxy-fuel process are implemented in a pulverised coal plant, the thermal efficiency is reduced to 33-35% from 45%. Best-case scenarios aim to increase these efficiencies to 42-47% by 2020. Novel forms of carbon capture technologies are also being explored, namely high-temperature solid-looping cycles are attractive as alternatives to the processes previously discussed, due to lower efficiency losses ranging between 3-8% (Fennell and Anthony, 2015).

**Table 1-1 Current status of efficiencies and efficiency losses of coal and gas plants coupled with various carbon capture technologies and their development targets for 2020 adapted from (APGTF, 2011)**

| Technology | Current Efficiency Status | 2020 Target |
|---|---|---|
| Unabated coal plant (steam cycle) | Efficiency (LCV) -45% | Efficiency (LCV) - 50-55% |
| CCS coal – post-combustion | ~ 12% (PEL) | ~ 8% (PEL) |
| CCS coal – oxy-fuel combustion | ~ 10% (PEL) | ~ 8% (PEL) |
| CCS coal – pre-combustion | ~ 7-9% (PEL) | ~ 5-6% (PEL) |
| CCS gas – post-combustion | ~ 8% (PEL) | ~ 7% (PEL) |
| CCS gas – oxy-fuel combustion | ~ 11% (PEL) | ~ 8% (PEL) |

(LCV) – Lower calorific value (PEL) – Point Efficiency Loss

### 1.2.2 **High-temperature solid-looping cycles**

This class of technologies involves the utilisation of solids to transfer either $O_2$ (for chemical looping) or $CO_2$ (for Calcium looping) between two fluid-bed reactors. As discussed previously, the point efficiency loss is higher when pre

and post-combustion systems and oxy-fuel processes are implemented for as carbon capture strategies when compared to high-temperature looping cycles (HTLC). In the case of chemical looping, this is achieved by separating the combustion of fuel from air, which minimises flue-gas treatment (Lyngfelt, Leckner and Mattisson, 2001). Similarities can be drawn between chemical looping and oxy-fuel combustion in this regard, but the separation is inherent to the chemical looping process and does not require an ASU unlike oxy-fuel. Therefore, chemical looping boasts no additional efficiency penalty over what would be required for the compression of $CO_2$. Calcium looping (Ca-looping) achieves its reduced energy penalty by utilising the heat produced from the carbonation of sorbent and its integration into a steam cycle (Blamey et al., 2010).

HTLC have been proposed to use circulating fluidised bed (CFB) technology. The majority of research suggests both reactors could operate as CFBs, or one could possibly consist of a bubbling bed. The use of fluidised-bed technology is a particular advantage for HTLC as a carbon-capture process as the scale-up is easily achievable, given that large-scale CFB units already exist such as the Łagisza power plant (Poland) operating at 460MWe (CFB designed by Foster Wheeler).

Chemical looping and Ca-looping cycles require the transfer of hot solid material. The solids are known as sorbents (in Ca-looping) and oxygen carriers (in chemical looping). Although the processes and chemistry differ between the two technologies (detailed below) the requirements and their characteristics remain quite similar. In general these solids are expected to; pose low risk with respect to health and safety whilst possessing the required reaction chemistry needed for the reversible reactions they will undergo. They should also possess sufficient carrying/ sorption capacity for $O_2$ (Chemical looping) $CO_2$ (Ca-looping); be of relative low cost and demonstrate high mechanical stability with low tendencies towards attrition and agglomeration.

### 1.2.3 **Calcium looping**

Ca-looping is a cyclic method of capturing $CO_2$. Classically research has employed the technique towards post-combustion capture allowing a capture plant to be retrofitted to an existing power plant. Ca-looping utilises the CaO as the sorbent for the capture of $CO_2$.The CaO is derived from limestone and reacts with the $CO_2$ from process flue gases, producing $CaCO_3$ in a circulating fluidised-bed reactor named the carbonator. This reaction occurs at an approximate temperature of 650°C (dependent on the partial pressure of $CO_2$) and is exothermic. The solid material is then transferred to the second reactor known as the calciner, which is operated at a temperature range of 900-950°C in the presence of almost 100 vol% $CO_2$. The $CaCO_3$ decomposes at this temperature, thus releasing the captured $CO_2$ from the process flue gas (Abanades, 2002; Boot-Handford et al., 2014). This stream of $CO_2$ can then be compressed for transportation and subsequent utilisation or storage. The CaO is then transferred back to the carbonator so that the cyclic process can continue. A schematic of Ca-looping for post-combustion capture is shown in Figure 1-6.

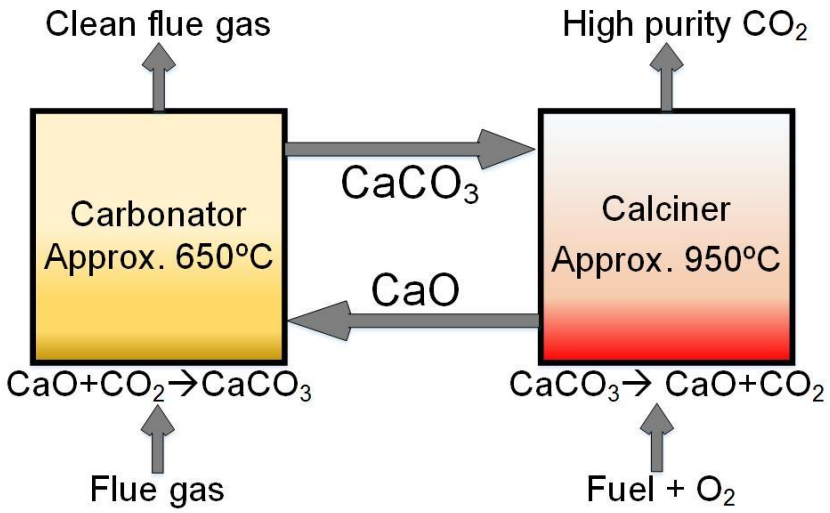


**Figure 1-6 General Ca-looping scheme for post-combustion capture**

## 1.3 **Chemical looping Combustion and Oxygen Uncoupling**

Chemical looping combustion (CLC), is a high temperature process, which can produce a resultant pure stream of $CO_2$ from the conversion of hydrocarbons without any energy penalty for flue gas separation. The process typically uses two interconnected fluidised-bed reactors, designated the air reactor and fuel reactor with a circulating oxygen carrier which travels between the two reactors (Ishida and Jin, 1996). In the process, the oxygen carrier (typically a transition-metal oxide) is oxidised in the air reactor according to Equation 1-1. The oxidised oxygen carrier is then transferred to the fuel reactor, in which it provides the necessary oxygen for the conversion of the fuel into combustion products, steam and $CO_2$ according to Equation 1-2. The water can be condensed out leaving a high purity stream of $CO_2$ suitable for compression, transport and storage (Lyngfelt, Leckner and Mattisson, 2001). The oxidation of the oxygen carrier is always an exothermic reaction, while the reduction reaction can be endothermic or exothermic, dependant on the specific oxygen carrier system utilised (Jerndal, Mattisson and Lyngfelt, 2006). The combination of reaction schemes in Equation 1-1 and Equation 1-2 produces an overall heating value, which is equal to the heating value of the conventional combustion process. A simplified reaction scheme is shown in Figure 1-7. The reduced form of the oxygen carrier is then transferred back to the air reactor, where it can be re-oxidised and the cyclic process can continue. The oxygen carrier effectively allows the fuel to be combusted in an oxygen-rich environment, in the absence of nitrogen containing air and therefore, does not pose any associated penalty for the separation of $CO_2$ from process flue gas (Lyngfelt, Leckner and Mattisson, 2001).

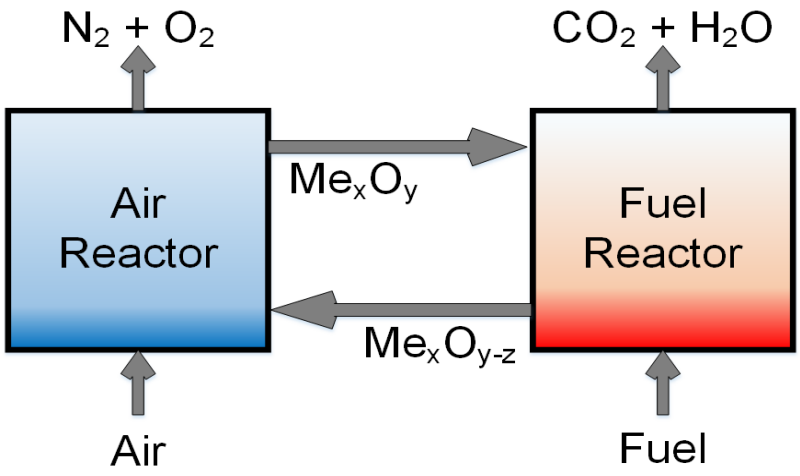


**Figure 1-7 Simplified chemical looping combustion scheme**

The concept of chemical looping was first introduced by Lewis and Gilliland who developed a cyclic process and a copper-based oxygen carrier as a means of producing a pure stream of $CO_2$ intended to be utilised in the carbonated beverage industry (Lewis and Gilliland, 1954). Ishida and Jin, first termed the process 'chemical looping' and recognised its potential for carbon capture and to decrease exergy losses associated with inefficiencies in heat-exchange and combustion processes (Ishida and Jin, 1994). Chemical looping combustion, in the configuration of two interconnected fluidised beds was then proposed by Lyngfelt et al, and the process was soon demonstrated for methane conversion in a 10kW reactor (Lyngfelt and Thunman, 2003; Lyngfelt, Leckner and Mattisson, 2001). To date, chemical looping has been demonstrated in several research laboratories around the world with pilot scale systems of up to 120kW (Adánez et al., 2012; Hossain and de Lasa, 2008; Lyngfelt, 2011).

$$M_yO_{x-1} + Air \rightarrow M_yO_x \qquad \textbf{Equation 1-1}$$

$$(2n+m)M_yO_x + C_nH_{2m} = (2n+m)M_yO_{x-1} + mH_2O + nCO_2 \qquad \textbf{Equation 1-2}$$

A major benefit of the chemical looping combustion process is its applicability to a range of varying fuels types, be they gaseous, liquid or solid. The bulk of research has concentrated on gaseous fuels so far, but current trends in research are directed to the utilisation of solid fuels such as biomass and coal (Adánez et al., 2012). Classically, chemical looping combustion requires solid fuel to first be gasified in the presence of either $CO_2$ or steam according to Equation 1-3 and Equation 1-4 (Leion, Mattisson and Lyngfelt, 2008). The solid oxygen carrier can then convert the resultant synthesis gas ($CO/H_2$) to $H_2O$ and $CO_2$.

$$C + H_2O \rightarrow CO + H_2 \qquad \textbf{Equation 1-3}$$

$$C + CO_2 \rightarrow 2CO \qquad \textbf{Equation 1-4}$$

In the classic chemical looping conversion of solid fuels, the gasification of the de-volatised char is a slow, rate limiting process, as the char is not directly converted by the oxygen carrier and must proceed through the intermediate gasification step (Wang and Anthony, 2008a). In CLC processes with solid fuels, an additional reactor is utilised to allow of conversion of unconverted fuel to char. This reactor is known as a carbon stripper and is typically of a bubbling bed-design. The carbon stripper separates unreacted char from bed material and returns it to the fuel reactor allowing for further conversion (Markström, Linderholm and Lyngfelt, 2012). A chemical looping process variant, known as chemical looping with oxygen uncoupling (CLOU) can allow for direct, rapid and complete conversion of a solid fuel (Imtiaz, Hosseini and Müller, 2013). The main difference for a CLOU system as compared to CLC for solids fuels is the use of a particular class of oxygen carriers. These can decompose at high temperatures and under low oxygen partial pressures, releasing gaseous oxygen (Equation 1-5), which can directly convert solid fuel (Equation 1-6), without the need of the otherwise slow gasification step. The overall heat of reaction is the same for CLC and CLOU, with only the release of oxygen facilitating fuel conversion being the major difference (Gayán et al., 2012a).

$$Me_xO_y \rightarrow Me_xO_{y-2} + O_2$$ **Equation 1-5**

$$C_2H_{2m} + \left(n + \frac{m}{2}\right) O_2 \rightarrow nCO_2 + mH_2O$$ **Equation 1-6**

It is typical for CFB boilers to operate at an air to fuel ratio of 1.2, however, when this technology is employed for CLC, this corresponds to an approximate oxygen concentration of 5% at the outlet of an air reactor. In CLC and CLOU, oxygen carriers should be able to be oxidised at or below this 5% oxygen partial pressure and at typical operational temperatures (800-1100°C). This would ensure full oxidation occurs in the air reactor (Imtiaz, Hosseini and Müller, 2013). Oxygen carriers operating outside of these parameters would require a greater air-fuel ratio and would be associated with greater thermal losses due to an increased flue gas stream exiting the air reactor.

A CLC based system will require a greater solids inventory than CLOU based systems due to faster fuel conversion of CLOU oxygen carriers. The CLOU process also offers advantages over CLC in the conversion of solid fuels by reducing the requirement for a carbon stripper, thus potentially reducing its system cost. CLOU can also have benefits for the conversion of gaseous fuels, where the inherent oxygen release associated with CLOU oxygen carries under the correct conditions will also react with fuels in the gas phase and can potentially reduce the requirement for maximised gas-solid contact.

## 1.4 **PhD scope**

The main focus of this thesis centres on two areas specific to chemical looping combustion. Firstly, the engineering challenges associated with operating a newly installed and fast-bed design, chemical looping combustion pilot plant for gaseous fuels are examined; Secondly, the development, production and experimental evaluation of low-cost oxygen carriers for chemical looping with gaseous fuels is investigated.

The research presented concentrates on investigating the key parameters required for successful commissioning and operation of the UKs largest chemical looping pilot scale reactor to date. It also contributes to the knowledge base with up-to-date research for possible oxygen carriers that can maintain the required performance for chemical looping processes, having been produced with methods that potentially offer relative ease of scale-up and use low-cost materials.

The majority of this work has been conducted at Cranfield University. Complementary experimental investigations detailed in this thesis, were carried out by the author as a part of research secondments at Chalmers University of Technology and Cambridge University. The investigations conducted were supported in part by the Engineering and Physical Sciences Research Council (EPSRC grant /I070912/1)

## 1.5 **Key issues**

Chemical looping is a fuel conversion technique that can produce pure streams of $CO_2$ from hydrocarbons without the requirement for ‘back-end’ energy intensive flue gas separation. In chemical looping, the separation of $CO_2$ is inherent due to the flue gas consisting of only $CO_2$ and $H_2O$. Therefore, following condensation of the flue gas, pure $CO_2$ can be obtained. The chemical looping process can facilitate the conversion of fossil fuels, intended for the supply of energy whilst mitigating their detrimental contributions to greenhouse gas emissions.

Cranfield University has recently installed its PACT (pilot-scale advanced capture technology) chemical looping reactor, rated at 50$kW_{th}$ input and this is the largest of its kind in the UK. The facility is of a dual fast-bed design. Its design benefits are the ease of scale up to small to medium scale for power generation systems. However this design has several engineering challenges that must be assessed and addressed for successful operation.

Operational constraints include difficulties in solid control and solid handling. Due to the system comprising of two identical riser dimensions, there is an inherent difficulty in managing the solids allowing for full combustion in the fuel reactor. The system is intended to use a dual fast-bed mode of operation. For full methane conversion corresponding to approximately 50$kW_{th}$ output, the solids handling requirement is extremely large, around 60g/s of oxygen carrier are required to be transferred from one reactor to another with a 60% CuO weight ratio oxygen carrier. The reactor system requires a control philosophy that accounts for the high solids recirculating in the system and their transfer rate. The use of a cold-flow model based on the existing facility, can provide the necessary and required hydrodynamic data that can translate directly into functional considerations that can be employed in an operational campaign for the reactor.

Another major requirement for the operation of the installed chemical looping reactor is the use of oxygen carriers suitable for the combustion of gaseous fuels. Oxygen carriers must possess certain physical and chemical properties that allow them to be suitable for the process. They must have the correct redox chemistry permitting the successful transfer of oxygen from air to the intended fuel for conversion, whilst maintaining structural integrity allowing for the cyclic process to be repeated as many times as possible. There is apparent trade-off between cost and performance in oxygen carriers. It is argued that highly engineered particles can maintain a higher level of performance, chemically and mechanically, when compared to cheaper, ‘simpler’ particles. But when considering a scaled up system, especially in the energy generation sector, these highly engineered particles will form the bulk of the operators cost, and it

is reasonable to believe these operators will prefer to utilise the cheaper alternatives as oxygen carriers. Therefore, there is a need to further research the use of low-cost materials for use as oxygen carriers and explore the possibilities for improving their chemical and mechanical properties, which would allow them to be used at scale in chemical looping processes.

The main focus will centre on producing oxygen carriers for chemical looping processes derived from low-cost materials, with methods of production for intended ease of scale-up. The oxygen carriers are assessed for their performance for fuel conversion and stability and therefore suitability in chemical looping processes.

## 1.6 **Key gaps in knowledge**

In chapter 2, a survey of existing literature has been carried out in order to define and clarify key points that require further research with regards to chemical looping cycles for fossil fuel conversion and carbon capture. The identified key gaps in knowledge are therefore the basis of the research presented in this doctoral thesis. They serve to provide the research's main aims and objectives detailed below.

## 1.7 **PhD aims and objectives**

Several key aims have been formulated with their corresponding objectives defined to facilitate the accomplishment of the research aims.

**Aim 1** To evaluate the fast-bed design chemical looping reactor at pilot scale and identifying its potential engineering issues that may arise from design configuration.

**Objective 1a** *Assess the newly designed chemical looping reactor's operability through a study of hydrodynamics through the operation of a hydrodynamically scaled cold flow model.*

**Objective 1b** *Evaluate the operability of a dual fast bed chemical looping pilot plant reactor. Detail engineering challenges addressed for an operation campaign.*

**Aim 2** Assess the requirement and feasibility for low cost materials in oxygen carrier performance for use in chemical looping processes. Detail characterisation and performance indicators to assess the produced oxygen carrier's efficacy towards oxygen transfer, oxidation and reduction cycles and gaseous fuel conversion.

**Objective 2a** *Conduct an experimental campaign exploring the use of ores as oxygen carriers for chemical looping combustion cycles with gaseous fuel. Assess these ores for potential oxygen release under inert conditions, for indications of their suitability for chemical looping with oxygen uncoupling processes. Assess employable methods for the possible improvement of the ores, in order to enhance their properties for increase efficacy and performance in chemical looping cycles.*

**Objective 2b** *Assess methods for producing oxygen carriers at a feasible scale for pilot plant operation. Evaluate oxygen carriers produced by feasible methods, in bench scale reactors to determine their performance in oxidation and reducing environments with gaseous fuels.*

**Objective 2c** *Conduct an experimental campaign exploring the use of feasible supports for Copper (II) oxide as oxygen carriers, whilst assessing their morphology, characterising their physical properties and fuel conversion performance. Characterisation techniques include scanning electron microscope (SEM), energy dispersive X-ray spectrometry (EDS) and x-ray diffraction spectroscopy (XRD)*

Based on the research aims and objectives outlined above, this doctoral thesis comprises of two distinct sections. The initial section's main focus comprises of several experimental campaigns, for the design, production and assessment of performance of low-cost oxygen carriers, for chemical looping combustion and chemical looping with oxygen uncoupling. The second section centres on the description and design philosophy of the pilot plant chemical looping reactor at Cranfield. The assessment of operation of the pilot-scale chemical looping reactor and engineering challenges that require addressing. This incorporates

the experimental investigation of detailed hydrodynamics of the chemical looping reactor system utilising a fully scaled cold flow model.

## 1.8 **Outline of PhD thesis**

The outline of this doctoral thesis's chapters with a brief description of the content covered is detailed below:

- **Chapter 2** presents a detailed literature review of chemical looping combustion, with particular emphasis on; the development of mixed oxides and low cost support materials for use in oxygen carrier development and current status of dual-CFB pilot plant design and operation.
- **Chapter 3** presents an experimental campaign for the use of ores in chemical looping processes. The investigation entails the doping of ores by active metal oxides through impregnation, to enhance their chemical and mechanical properties, in order to improve their performance in bench scale fluidised-bed testing.
- **Chapter 4** describes an experimental campaign utilising low-cost supports for copper (II) oxide based oxygen carriers, produced by the scalable method of pelletisation. The oxygen carrier's morphology is assessed, as is their efficacy for gaseous fuel conversion and potential stability in a fluidised-bed environment.
- **Chapter 5** presents a detailed description of Cranfield University's PACT chemical looping reactor and its design philosophy and commissioning.
- **Chapter 6** describes the requirement for hydrodynamic modelling of the chemical looping reactor. Here a description of a fully scaled cold-flow model and the experimental campaign for the determination of an operation and control philosophy is detailed. The results of the hydrodynamic study and concluding recommendations for operation and control are also discussed.
- **Chapter 7** details concluding remarks, contributions to the existing knowledge base and recommendations for future work and investigations, based on the findings detailed in the thesis.

# 2 Literature Survey

## 2.1 **Introduction**

This chapter presents a literature review of chemical looping combustion for $CO_2$ capture. The reviews' aim is to evaluate the existing knowledge, specifically the research and development concerning suitable oxygen carriers for the process for gaseous and solid fuel conversion. It will also provide an overview of chemical looping pilot plant studies conducted to date.

## 2.2 **Oxygen carriers fundamentals for CLC/CLOU**

CLC technology utilises a circulating solid material as an oxygen transfer medium for conversion of a carbonaceous fuel to combustion products. The process allows for the conversion of fuel to take place with oxygen in the direct absence of air. The circulating solid materials utilised in the CLC process are known as oxygen carriers. Oxygen carriers are an integral part of chemical looping, where proposed processes and reactor systems are required to be designed with the specific considerations of a particular oxygen carrier to be employed. Investigations into suitable oxygen carriers is one of the most prolific areas of research in the CLC field, with over 1000 oxygen carriers tested (Adánez et al., 2012; Hossain and de Lasa, 2008; Imtiaz, Hosseini and Müller, 2013; Lyngfelt, Johansson and Mattisson, 2008).

A suitable oxygen carrier to be utilised in the CLC process within a fluidised-bed system must satisfy the following criteria:

- Demonstrate sufficient reactivity for oxidation in air and the ability to convert the fuel to combustion products ($CO_2$ and $H_2O$)
- Sufficient oxygen carrier and transfer capacity
- Pose low risk to handlers health and environment
- Show a low tendency for attrition, fragmentation and agglomeration
- Have a low relative cost including costs for preparation/production

The majority of investigations utilise a fixed bed and thermo-gravimetric analysis (TGA) for characterisation studies to determine if a particular oxygen carrier is a

suitable candidate and shows promise for use in larger systems. The advantage of such effective screening process, is that oxygen carriers can be produced in small quantities (<50g) with precise formulation, composition being assured. Investigations can be completed within several hours, in systems that are not optimised for a specific oxygen carrier system, but rather a general reactor, which can be used many types of materials. TGA investigations allow insight into reactivity within oxidation and reduction cycles. However, they cannot provide an accurate prediction of a particular materials' ability to exist without significant deterioration in a fluidised bed for the relevant velocities. Far fewer materials have been tested at larger scales for long term operation as these investigations require suitable equipment sizes and increased research effort, thus incurring increased time and costs of such examinations.

### 2.2.1 **Research and development of oxygen carriers**

In the early stages of oxygen carrier development, research was focused on the redox systems of four main metals: nickel, iron, manganese and copper, with the majority of investigations utilising fixed bed or small lab-scale fluidised beds in order establish their reactivity towards gaseous fuels (Lyngfelt et al., 2004). The metal oxides were typically combined with an inert support material to limit their degradation, increase porosity, ionic conductivity and thus increase reactivity. In supported materials, the ratio of theoretical oxygen available for fuel conversion will decrease, but the reactivity can actually rise in comparison with unsupported materials (Ishida and Jin, 1994). While some investigations were performed on unsupported materials and metal ores, because of the attraction of their low relative cost, typically these materials degrade more rapidly or have low reactivity towards methane conversion (De Diego et al., 2004; Lee et al., 2005; Mattisson, Lyngfelt and Cho, 2001).

### 2.2.1 **Mass balance and oxygen carrier transport capacity**

The mass balance of the system allows one to determine the circulation rate required between the air and fuel reactors in a chemical looping system. The circulation rate to be calculated is dependent on the oxygen carrier system used and the type of fuel to be converted. As detailed by Abad et al., using the

assumptions of full fuel conversion the solid circulation rate $m_{oc}$ (kg $s^{-1}$) by means of the empirical Equation 2-1.

$$m_{OC} = \frac{1}{R_{OC}\Delta X_s}\frac{2dM_O}{\Delta H_C^O} \qquad \textbf{Equation 2-1}$$

The oxygen transport capacity ($R_{OC}$) is the most important attribute that quantifies the amount of oxygen that can be transferred between the air and fuel reactors. It provides a guide to the solid recirculation rate required to meet the mass balance of the system. Ultimately it is dependent on the species involved, though it should be noted that solid recirculation rate ($m_{oc}$) must increase as the transport capacity decreases. Here, $d$ is the stoichiometric coefficient for $O_2$, $M_O$ the atomic weight of oxygen (0.016kg $mol^{-1}$), $\Delta H_c^0$(kJ $mol^{-1}$) the standard enthalpy of heat from combustion of the fuel and $\Delta X$ is the change in conversions of solids exiting the air reactor and fuel reactor (Abad et al., 2007a). The solid conversion is defined in Equation 2-2 where $m$ is the actual mass of the oxygen carrier used in the investigation and $m_r$ and $m_o$ (kg) are the masses of the fully reduced and fully oxidised oxygen carriers. The transport capacity of a given oxygen carrier is dependent on the fraction of active oxygen transporting material present in a given oxygen carried according to Equation 2-3, where $R_O$ Equation 2-4 is dependent on the specific redox system being employed

$$X_S = \frac{m - m_r}{m_o - m_r} = \frac{m - m_r}{R_{OC} - m_o} \qquad \textbf{Equation 2-2}$$

$$R_{OC} = x_{OC}R_O \qquad \textbf{Equation 2-3}$$

$$R_O = \frac{m_O - m_r}{m_O} \qquad \textbf{Equation 2-4}$$

Table 2-1 shows the oxygen ratio for several redox systems that can be used as oxygen carriers. When an oxygen carrier is combined with a support material the oxygen ratio will decrease as per Equation 2-3.

**Table 2-1 Oxygen ratio $R_O$ for various redox systems adapted from (Jerndal, Mattisson and Lyngfelt, 2006)**

| Oxygen carrier systems | $R_O$ |
|---|---|
| NiO/Ni | 0.214 |
| CuO/Cu | 0.201 |
| $Cu_2O$/Cu | 0.112 |
| $Fe_2O_3$/$Fe_3O_4$ | 0.033 |
| $Mn_2O_3$/MnO | 0.101 |
| $Mn_3O_4$/MnO | 0.070 |

### 2.2.2 **Thermodynamic Considerations**

Suitable oxygen carriers must possess favourable redox characteristics towards gaseous fuel for conversion into combustion products. Following the thermodynamic investigations, Jerndal et al., identified the metal oxide systems; $Cu_2O$/Cu, $Mn_3O_4$/MnO, $Fe_2O_3$/$Fe_3O_4$, NiO/Ni and CoO/Co as the most attractive potential oxygen carriers. The iron, copper and manganese systems were found to completely convert CO to $CO_2$ at equilibrium in CLC conditions exhibiting equilibrium constants ($K_{eq}$) above $10^3$. In the case on the NiO/Ni and CoO/Co systems the equilibrium constant is approximately $10^2$ shown in Figure 2-1 indicating the conversion to combustion products is not complete and hindered with unfavourable thermodynamics (Adánez et al., 2012).

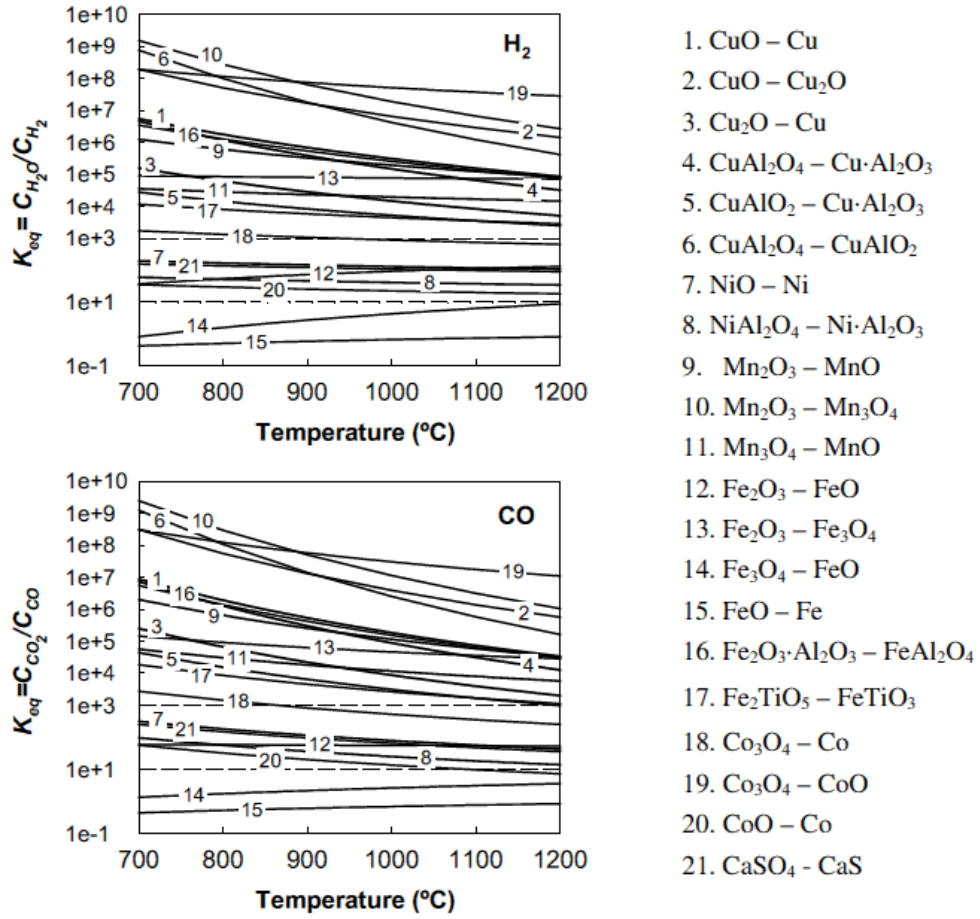


**Figure 2-1 Equilibrium constant $K_{eq}$ for the reduction of $H_2$ and CO with varying redox systems (Adánez et al., 2012)**

The limitations of CO conversion is shown to be between 0.988-0.995 and 0.929-0.969 for NiO/Ni and CoO/Co respectively between temperatures of 800-1000ºC (Jerndal, Mattisson and Lyngfelt, 2006). It can be seen in Figure 2-1 that full conversion of $H_2$ and CO can be supported by the $Co_3O_4$ /CoO system, but the oxidation to $Co_3O_4$ is not thermodynamically favourable in air at temperatures above 880ºC. The specific systems CoO/Co and Ni/NiO were initially identified as potential oxygen carriers due to their high oxygen ratio ($R_O$), which are both 0.214, compared to $Mn_3O_4$/MnO, $Fe_2O_3$/$Fe_3O_4$ that have an oxygen ratio 0.070 and 0.033 respectively. Despite its thermodynamic limitations, the nickel system was quickly identified as the most reactive oxygen carrier for methane conversion and has been therefore the most studied material in open literature. However, due to its high cost and considerable

toxicity, research has now shifted towards alternative metal oxide systems. The $CaSO_4$-CaS has been considered as a potential redox system, but encounters similar thermodynamic limitations for the conversion of $H_2$ and CO as the NiO system. CaS can also react with $CaSO_4$ which release $SO_2$ (Wang and Anthony, 2008a). The iron systems consisting of $Fe_3O_4$-FeO and FeO-Fe exhibit equilibrium constants of below 10 with CO and $H_2$, thus re-oxidation is unfavourable without increased heat requirements and can lead to agglomeration. These redox systems must potentially be avoided if considering an interconnected fluid bed reactor system and would otherwise require a special reactor, for example with the solids and oxidising air in counter flow configuration (Adánez et al., 2012).

### 2.2.3 **Heat Balance**

Heat distribution throughout the reactors is specific to the redox system involved. The oxidation of the metal oxide in the air reactor is highly exothermic, and the reduction in the fuel reactor is typically endothermic with methane and always exothermic with $H_2$ and CO. The net heating value displayed over both reactors is that of normal combustion of the fuel used. Some exceptions are the copper-based redox cycles (Cu/CuO, CuO/$Cu_2O$, $Cu_2O$/Cu) where the reaction of oxidised form with methane is exothermic ($\Delta H_r^o$ = -178, -236.6, -119.5 kJ/mol) respectively (Adánez et al., 2012). Exothermic fuel conversion can pose problems as this excess heat in the fuel reactor can cause the metallic copper particles to melt and agglomerate due to its relative low melting point. The use of a support or binder material can change the standard heats of reaction, particularly in the case of the $CuAl_2O_4$/$CuAlO_2$ redox system; as shown in Table 2-2.

**Table 2-2 Standard heat of reaction of different redox systems (Adánez et al., 2012)**

| Redox System | $\Delta H_r^o$ (kJ/mol) | | | | |
|---|---|---|---|---|---|
| | $CH_4$ | $H_2$ | CO | C | $O_2$ |
| CuO/Cu | -178.0 | -85.8 | 126.9 | -81.4 | -312.1 |
| CuO/$Cu_2O$ | -236.6 | 100.4 | -141.6 | -110.7 | -282.8 |

| | | | | | |
|---|---|---|---|---|---|
| $Cu_2O/Cu$ | -119.5 | -71.1 | -112.3 | -52.1 | -341.4 |
| $CuAl_2O_4/Cu{\cdot}Al_2O_3$ | 282.2 | 29.3 | -11.8 | 148.7 | -542.2 |
| $CuAlO_2/Cu{\cdot}Al_2O_3$ | -24.1 | -47.3 | -88.4 | -4.4 | -389.1 |
| $CuAl_2O_4/CuAlO_2$ | 588.5 | 105.9 | 64.7 | 301.9 | -695.4 |
| $Fe_2O_3/Fe_3O_4$ | 141.6 | -5.8 | -47.0 | 78.4 | -472.0 |
| $Fe_2O_3/FeO$ | 318.4 | 38.3 | -2.8 | 166.8 | -560.3 |
| $Fe_2O_3{\cdot}Al_2O_3/FeAl_2O_4$ | -62.3 | -56.8 | -98.0 | -23.5 | -370.0 |
| $Fe_2TiO_5/FeTiO_3$ | 106.5 | -14.6 | -55.8 | 60.9 | -454.4 |
| $Mn_2O_3/MnO$ | -48.0 | -53.3 | -94.4 | -16.4 | -377.1 |
| $Mn_2O_3/Mn_3O_4$ | -396.6 | -140.4 | -181.6 | -190.7 | -202.8 |
| $Mn_3O_4/MnO$ | 126.3 | -9.7 | -50.8 | 70.8 | -464.3 |
| NiO/Ni | 156.5 | -2.1 | -43.3 | 85.9 | -479.4 |
| $NiAl_2O_4/Ni{\cdot}Al_2O_3$ | 158.6 | -1.6 | -42.8 | 86.9 | -480.4 |

The majority of redox systems follow the heat distribution trends where oxidation is always exothermic and reduction is endothermic with exception of some Cu and Mn based systems. Where endothermic fuel reduction takes place, the fuel reactor is supplied heat by the transferred solids from the air reactor which is at a higher temperature from the oxidation reaction (Abad et al., 2007b). In a realistic reactor system, it is preferred to have higher heat release in the fuel reactor to facilitate the fast reaction of fuel conversion and achieve a high energetic efficiency. However, a too higher temperature (>1050ºC) can cause issues for the oxygen carrier if it has a low melting point. Operating at temperatures above this level can also affect the reactor vessel internals thus requiring careful consideration of the materials used in its construction (Adánez et al., 2012). Heat recovery mechanisms will be required to remove excess heat and should be used to optimise a steam cycle and maintain the energy balance in the system (Bolhàr-Nordenkampf et al., 2009a).

### 2.2.4 **Attrition and agglomeration**

Attrition is the wearing down of particles due to physical and chemical stress from the process cycle. It is an important consideration, as the use of oxygen carrier particles in fluidised-bed reactors, allows attrition to take place more readily. This is fundamentally due to the friction against reactor walls, other

particles and on-going physical stresses produced from the oxidation and reduction reactions. Attrition occurs at higher rates when solid fuels are used where increased solid-solid interactions occur. Within the CLC process it is common to see the rate of attrition increase significantly at the start of the looping process and then stabilise as the process continues. This is due to irregular shaped particles being fragmented and 'rounded off' to a better fluidising spherical shape. The loss in initial oxygen carrier is known as 'fines' and are characterised by the loss of particles that are less than 45μm in CFBCs (Jia et al., 2007). In the characterisation of oxygen carriers the attrition rate should be quantified to give an indication of lifetime of the carrier to be expected. The attrition rate of different particles was investigated in a specialised system developed at Chalmers University of Technology known as the jet-cup method. The-jet cup method continues to be used as part for the oxygen carrier characterisation methodology (Rydén et al., 2014b).

Agglomeration is process in which oxygen carrier particles can bond to each other. This process is highly detrimental in solid looping systems as it can cause defluidisation, which causes the fluidising gas to channel through the bed material rather than fluidising the bed itself and therefore, has a direct effect of solid circulation rate. The process of agglomeration also affects the oxygen transport capacity as there is less surface area for the reduction and oxidation reactions to take place. (Cho, Mattisson and Lyngfelt, 2006) The extent at which agglomeration occurs is dependent on the redox system, their specific melting points, its preparation method and operating conditions of the reactor. A high operating temperature may be favourable for heat transfer power-generation schemes; this should be closely monitored, should the temperature be close to that of the oxygen carrier's melting point. This is apparent in the Cu/CuO system as the temperature at which oxygen is uncoupled is close to the melting temperature of Cu. By contrast, Ni based oxygen carriers seem to be highly resistant to agglomeration (Cho, Mattisson and Lyngfelt, 2004). The use of supporting materials can increase mechanical strength and resistance to agglomeration. However, this depends on the support material and for instance, it was reported by Kidambi et al., that corundum ($\alpha Al_2O_3$) supporting hematite

($\alpha Fe_2O_3$) succumb to agglomeration between 20-40 oxidation cycles, thus lowering the oxygen transport capacity by the increase of macro-porosity within the structure of the particles and this is illustrated in Figure 2-2.

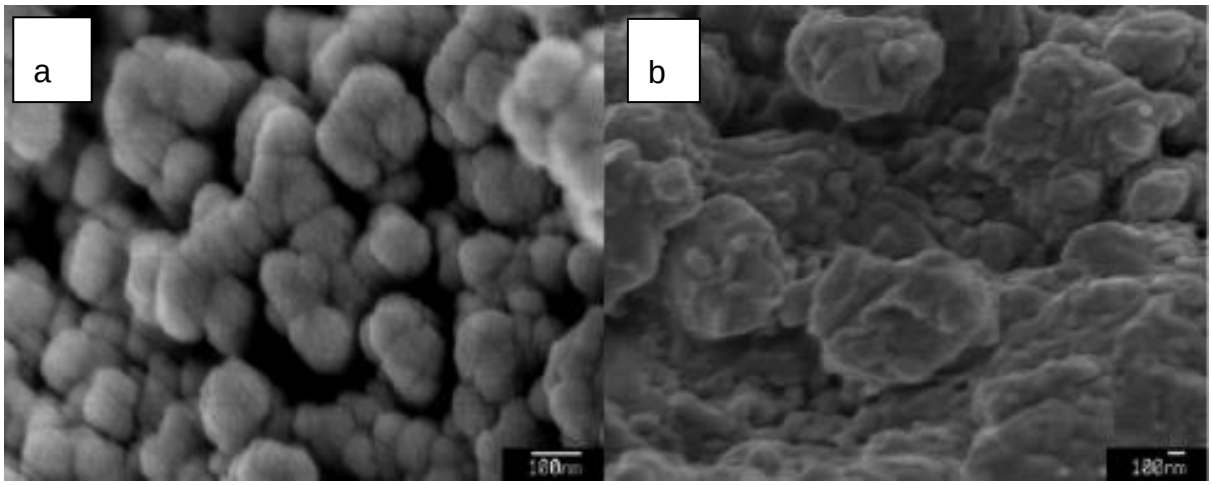


**Figure 2-2 SEM Images for 75%wt Fe2O3 particles a) as prepared b) after 50 cycles, from (Kidambi et al., 2012)**

### 2.2.5 **Economic comparison**

With respect to commercialising the CLC process it is paramount to take into account the cost of the oxygen carrier. The overall cost is due to three aspects, namely the cost for the preparation of the carrier; the cost of the raw material and the cost of the supporting/binding. The cost of the raw material is specific to the metal used. In principle nickel is a relatively expensive metal to be used as an oxygen carrier. However, it should be noted that nickel has had the most extensive testing in terms of operational time in CLC reactors due to its high reactivity (Ishida and Hongguang Jin, 1994). However, it is too expensive to be used in larger scale investigations. Copper is similar on this basis, as it too has been investigated extensively due to its favourable temperature for oxygen uncoupling (Imtiaz, Hosseini and Müller, 2013). Manganese and iron are the cheapest options to consider for the CLC process. The use of raw metal ores and wastes from other industries may allow for reductions in cost. In a recent study, the cost of oxygen carrier material was evaluated based on a theoretical

1000$MW_{th}$ chemical looping plant. There was a clear advantage to use low cost natural minerals, though there are still uncertainties in terms of their potential operational lifetime. With conservative assumptions for an ilmenite carrier lifetime ranging between 100-300h can yield an additional cost range of 1.3-4 € per tonne of $CO_2$ avoided, signifying that oxygen carrier cost can represent up to 20% of the total operators cost (Lyngfelt and Leckner, 2015).

**Table 2-3 Comparison of various oxygen carrier production techniques**

| Property | Production Technique | | | | | |
|---|---|---|---|---|---|---|
| | Mechanical Mixing | Freeze Granulation | Dry impregnation | Wet impregnation | Co-precipitation | Sol-Gel process |
| Economic Feasibility | ++ | + | - | - | + | + |
| Metal/ support Loading | ++ | ++ | -- | -- | - | - |
| Homogeneity | -- | -- | n/a | n/a | + | + |
| Attrition Resistance | - | - | + | - | - | -- |
| Fe System | ++ | ++ | + | + | ++ | ++ |
| Ni System | ++ | ++ | + | + | ++ | + |
| Cu System | -- | -- | ++ | + | - | - |

++ highly suitable + suitable – not suitable – highly not suitable n/a not applicable (Fan, 2010)

The method by which an oxygen carrier is produced can add significant costs to the overall system. Processes such as co-precipitation and wet impregnation are suitable for the quantity required for lab scale investigations. However they are probably not commercially scalable due to the wastewater produced, which cannot be released to the environment and would require specialist disposal, incurring additional costs. For the purposes of commercial deployment methods such as; mechanical mixing, spray drying and to a lesser extent freeze-dry granulation are favourable methods for producing oxygen carriers for CLC (see Table 2-3).

### 2.2.6 **Environmental Considerations**

It is paramount to assess the environmental impacts of metals used as oxygen carriers in order to safeguard the environment and to protect the operators of the installation and the local environment. At lab scale a vast range of oxygen carriers have been tested, with the appropriate safe handling procedures in place. For process commercialisation, only the more environmentally benign elements can be ultimately considered for the role. These include iron and manganese and their respective ores. Nickel and copper oxides have significant health implications. Nickel possess carcinogenic properties, while nickel and copper are toxic and can impact the surrounding natural environments. It should be noted that any oxide, could cause significant issues when dispersed as a mesh therefore, there must be specific controls on flue emissions, which could contain these oxygen carriers.

### 2.2.7 **Copper–based oxygen carriers**

Copper-based oxygen carriers have been identified as promising candidates as oxygen in both the CLC and CLOU based processes. Copper systems been shown to exhibit high reaction rates and possess a high oxygen transfer capacity, with no thermodynamic limitations such as is the case for nickel and cobalt based redox systems. Furthermore copper-based systems are less expensive, and their health and safety and environmental impacts are considered much less compared to nickel and cobalt. Early investigations were

carried out on the pure CuO system and results showed that the redox system has high rates of reactivity even at temperatures which would be considered low for chemical looping processes (Cao, Casenas and Pan, 2006). The use of lower temperature investigations safe guards against full reduction to metallic copper, which can cause agglomeration due to its low melting point (1079°C).

Copper redox systems have been combined with many different support materials to maintain stability over a large number of cycles, as pure CuO can deactivate rapidly over increasing numbers of reduction and oxidation cycles (De Diego et al., 2004). Support materials include; $Al_2O_3$, $SiO_2$, $TiO_2$, bentonite and $ZrO_2$ amongst others. When a support material is employed it is typically regarded as an inert substance, which plays no role, except to stabilise the active oxygen carrying material. If alumina is employed with the copper redox systems, interactions between the two materials are common with the formation of copper aluminates ($CuAl_2O_4$). This material has been reported to have similar reaction rates to pure CuO and can resist agglomeration (de Diego et al., 2005). Adanez et al., reported successful operation for 120h in a $10kW_{th}$ fluidised-bed reactor with a CuOγ-$Al_2O_3$ oxygen carrier and achieved full methane conversion at 800ºC (Adánez et al., 2006).

A major benefit of employing a copper redox system is fuel reduction is exothermic. Therefore, a decreased solid circulation rate is required in the fuel reactor compared to alternative redox systems, which would otherwise be required to reduce the temperature disparity between the air and fuel reactors.

The redox system CuO/$Cu_2O$ has some operational benefits; they have significantly higher melting points 1326ºC and 1232ºC respectively, than redox systems, which reduce to elemental copper. The CuO/$Cu_2O$ redox system also has the ability to liberate gaseous oxygen at temperatures above 900ºC and at lower than the equilibrium $O_2$ partial pressures as seen in Figure 2-3. This CLOU effect is limited in copper and alumina-based systems, as the $CuAl_2O_4$ and $CuAlO_2$ phases cannot release oxygen.

Copper-based oxygen carriers have been used in a large number of studies, earlier work has been reviewed in detail by Adánez et al., 2012. Recent large

scale investigations in 120kW$_{th}$ CLC reactor with gaseous fuels have been conducted by at the Technical University of Vienna (Penthor et al., 2015). Their studies concluded that their reactor their design required a greater active inventory in the fuel reactor to achieve full methane conversion. The copper and alumina-based oxygen carrier also suffered from attrition, reducing the initial CuO content of 16% to 9%.

Copper-based materials do offer great potentials as oxygen carriers in CLC and CLOU processes, but copper still remains an expensive material. The consideration of price to operational lifetime is important with respect to large-scale systems. Should suitable lifetimes become achievable, copper-based oxygen carriers can be a noteworthy choice for gaseous and low ash fuels (Fennell and Anthony, 2015).

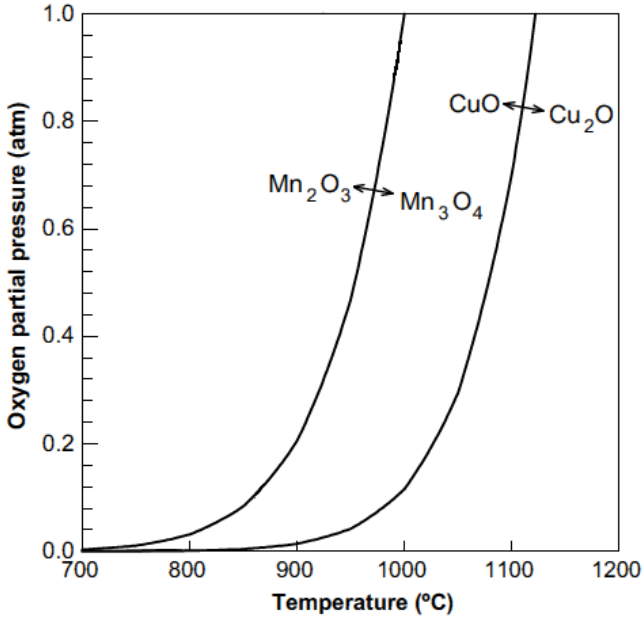


**Figure 2-3 Equilibrium oxygen concentration over the manganese and copper redox systems releasing oxygen as a function of temperature**

### 2.2.8 **Manganese-based oxygen carriers**

Research into manganese-based materials has gained increasing interest as potential oxygen carriers. Such metal oxides are considered relatively safe, with respect to handling and the environment compared to nickel and cobalt. They are also considered a cheap and abundant class of materials, though not as

cheap and available as iron, but in their favour they possess a greater oxygen carrying capacity than iron redox systems as shown in Table 2-1. In practical CLC processes the $Mn_3O_4$/MnO redox system is only considered, where the $Mn_3O_4$ phase is stable above temperatures of 800ºC. Other manganese oxide phases have issues for the CLC process where $MnO_2$ decomposes above 500ºC and $Mn_2O_3$ is only thermodynamically stable below 900ºC (Stobbe, de Boer and Geus, 1999; Zafar et al., 2007). Pure manganese oxygen carriers have shown to have relatively low reactivity with methane (Adánez et al., 2012). The majority of support material has been shown to interact with the manganese oxides, resulting in unreactive phases which are difficult to reverse (Adánez et al., 2012). Notable exceptions have been the use of $ZrO_2$ support, as reported by Abad et al., 2006 where 70h of continuous operation were achieved with completed syngas conversion. However methane conversion was limited, with unconverted methane detected at the outlet of the fuel reactor. The $Mn_3O_4$/$Mn_2O_3$ redox system has been identified thermodynamically, as a possible candidate for CLOU. The $Mn_2O_3$ phase can liberate gaseous oxygen at temperatures above 900ºC, but still has the limitation of re-oxidising $Mn_3O_4$ back to $Mn_2O_3$. The temperature required for the re-oxidation is below 800ºC at an oxygen concentration above 5% in the air reactor, and in realistic applications, operating at this temperature is not practical (Mattisson, Lyngfelt and Leion, 2009). This thermodynamic constraint can be reduced by the combination of manganese oxides with other metal oxide systems such as iron, nickel, silicon and magnesium whilst retaining its CLOU properties. The combined manganese and iron system is particularly promising due to its favourable thermodynamics (Azimi et al., 2013; Shulman et al., 2009a) and is discussed in further detail in section 2.2.10 discussing combined and mixed oxides systems.

### 2.2.9 **Iron-based oxygen carriers**

The use of iron-based oxygen carriers is attractive in the CLC process, due to their low cost, high abundance and low impact on health and safety and the environment (Abad et al., 2007a). Its use does have some limitations; the redox

system typically exhibits low methane conversion and possesses the lowest oxygen transport capacity compared to nickel, copper and manganese-based redox systems as show in Table 2-2. Iron-based oxygen carriers can operate over a range of iron oxidation states (II, III) hematite ($Fe_2O_3$) can be reduced to magnetite ($Fe_3O_4$), wursite (FeO) and elemental iron. The redox system of magnetite to hematite is preferred, as reduction to FeO and Fe with fuel yields incomplete combustion products. This would otherwise lead to increase in equilibrium concentrations of CO and $H_2$ and therefore reduce the purity of the $CO_2$ stream at the outlet of the fuel reactor (Jerndal, Mattisson and Lyngfelt, 2006). In pure iron-based systems trends show a general increase in activity with accumulative redox cycles. The intensification in reactivity has been attributed to increasing porosity of the particles with subsequent redox cycles. The heightened reactivity occurs, as there is a greater surface area for oxidation and reduction to take place, although its effect is limited. The transition from micro-pores to macro-pores occurring with increased redox cycles shows the iron system reaches a critical point and the reactivity decreases substantially when surpassing it due to then reduction surface area (De Diego et al., 2004; Ishida and Jin, 1996). The use of support materials has been employed to improve activity over increased redox cycles, with the use of alumina being the most utilised. Details of iron-based oxygen carrier investigations and their production methods up to 2012 have been reviewed in detail by Adanez et al. A number of studies have shown that the reactivity of iron-based oxygen carriers is sufficient for the conversion of CO and $H_2$ and less so for methane requiring the fuel reactor to be operated above 950ºC (Abad et al., 2007a; Adánez et al., 2004; Mattisson, Johansson and Lyngfelt, 2004). It has been reported that the use of impregnation as a means of oxygen carrier production, a process used extensively by ICB-CSIC in Zaragoza (Spain), has improved the reactivity of an iron based carrier for methane conversion to higher rates (80%) than previously reported (60%). This resulted in a decreased solids inventory required for full fuel gas conversion (Gayán et al., 2012b). To date over 1000h of combined operation have been achieved with the use of iron-based oxygen carriers in pilot-plant reactors (Fennell and Anthony, 2015).

### 2.2.10 **Combined-oxide based oxygen carriers**

The use of combined metal oxides can produce oxygen carriers, which have enhanced properties compared to the properties of a given individual metal oxide alone. These properties include; increased reactivity and stability, improved fuel conversion, improved mechanical strength, minimise cost and reduce the use of toxic materials (Adánez et al., 2012). The mixing of two or more oxides can involve physically or chemically combining materials into a single oxygen carrier, thus constituting as a new oxide material, and this can be produced through several methods and techniques (Lambert, Briault and Comte, 2011; Lambert, Delquié and Clémeneçon, 2009). The resulting final and desired product is typically achieved on final calcination of the oxygen carrier. Lambert et al., has reported positive results from $Cu_{0.95}Fe_{1.05}AlO_4$ formed in the spinel phase with high oxidation rates and increased oxygen transfer capacity. Perovskite structures are also an example of mixed oxide systems with potential benefits over a single oxide system, with some variants being suitable for CLOU processes. One promising perovskite-based material is calcium manganates and its variants. Rydén et al., operated a 0.3kW CFB with a $CaMn_{0.875}Ti_{0.125}O_{3-\delta}$ oxygen carrier and reported stable fluidisation behaviour, stable and steady gaseous oxygen release when the oxygen carrier subjected to an inert environment and more-over, complete methane conversion was achieved. The use of calcium-manganate perovskites were also used in a 10kW pilot CFB for gaseous fuels where a higher rate of methane conversion was reported than a Ni/NiO based oxygen carrier used in the same reactor unit (Källén et al., 2013; Shulman et al., 2009b). The manganese redox system ($Mn_2O_3/Mn_3O_4$) in combination with other metal oxides can still provide its CLOU properties but demonstrates enhanced thermodynamic behaviour, which can result in changes to its reaction characteristics. Candidates such as iron, nickel and calcium can be employed in order to improve the manganese system (Leion et al., 2009b; Rydén, Lyngfelt and Mattisson, 2011a; Shulman et al., 2009a). Research has indicated the combination of manganese and iron redox pairs could be a

capable coupling in an oxygen carrier system (Fossdal et al., 2011; Lambert, Delquié and Clémeneçon, 2009; Rydén et al., 2014a).

$$6(Mn,Fe)_2O_3 \leftrightarrow 4(Mn,Fe)_3O_4 + O_2 \qquad \textbf{Equation 2-5}$$

Figure 2-4 shows that from the binary phase diagram for $(Mn_yFe_{1-y})O_x$ that hematite and bixbyite $(Fe,Mn)_2O_3$ are stable, fully oxidised phases at temperatures below 950ºC.

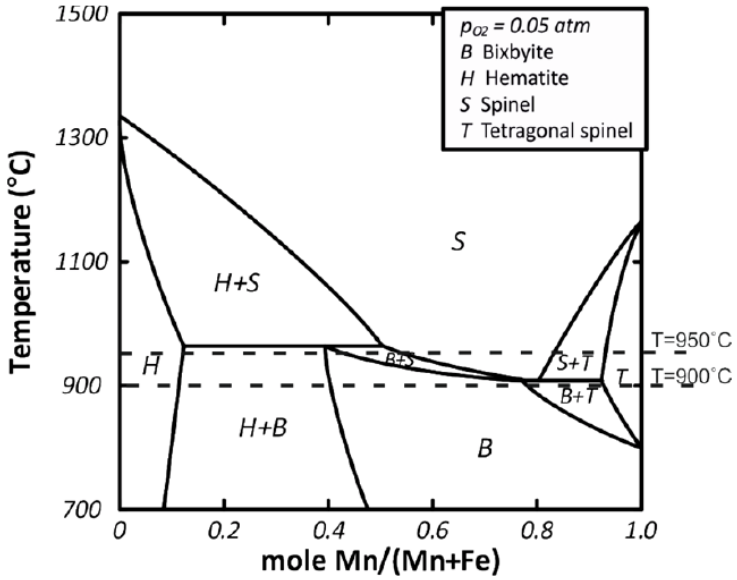


**Figure 2-4 Binary phase diagram of (MnyFe1-y)Ox in an O2 partial pressure of 0.05 atm from (Azimi et al., 2013)**

Their reduced spinel $(Fe,Mn)_3O_4$ and tetragonal spinel form hausmannite $(Mn_3O_4)$ are stable forms above 950ºC. An increase in temperature across the boundary will lead to a phase change of $(Fe,Mn)_2O_3$ to $(Fe,Mn)_3O_4$. The significance of this, is the release of gaseous oxygen equivalent to 3.3-3.4% change of mass according to Figure 2-4 (Azimi et al., 2013). Moving from a high to a low oxygen concentration environment, such as when an oxygen carrier is transferred from the air reactor to a fuel reactor can also cause the phase change. Gaseous oxygen is liberated and is consumed by the fuel, thus maintaining a low oxygen concentration and facilitating the further release of oxygen.

### 2.2.11 **Low-cost for oxygen carrier materials**

Low cost materials are attractive for use as oxygen carriers in CLC processes in particular with solid fuels. Typically in solid fuel conversion, with non-CLOU oxygen carriers, the fuel must first be gasified, which typically occurs in the fuel reactor. The solid fuel and the oxygen carrier are therefore mixed in the same reactor and there inevitably will be a loss of oxygen carrier inventory, as the oxygen carriers are carried out with the waste ash stream of the gasified solid fuel (Adánez et al., 2012). With an oxygen carrier being a major cost consideration for potential CLC plant operators, the predicted loss of oxygen carrier material produces the requirement to use as cheap and abundant materials as possible. The use of natural minerals such as ores is therefore interesting in this regard.

Ilmenite ore consisting of iron and titanium phases ($FeTiO_3$) has been used extensively as an oxygen carrier at varying scales with over 800h of combined use in pilot scale fluid bed reactors (Fennell and Anthony, 2015). Initial reactivity is typically low with ilmenite. As subsequent redox cycles progress, porosity of the particles increase, thus the reactivity improves; suggesting ilmenite particles are required to undergo an activation process. Once this has been achieved reactivity can remain stable over many cycles. The main active phase in ilmenite is pseudobrookite ($FeTiO_5$) and studies have shown the migration of iron containing phases to the surface of a particle for interactions with fuel (Adánez et al., 2010). Ilmenite has shown moderate reactivity with methane and is better suited to syngas conversion and therefore has been employed in several pilot plant studies for use with solid fuels. Results from investigations in a 100kW CFB reactor at Chalmers University of Technology have indicated positive fluidisation behaviour, good mechanical stability and achieved a $CO_2$ capture rate of 99% from the conversion of bituminous coal when operating between 940-980ºC in the fuel reactor with ilmenite (Markström, Linderholm and Lyngfelt, 2012).

Iron ore consisting mainly of hematite has been one of the first natural materials to be tested for chemical looping combustion. Early results indicated that iron

ore exhibited low reactivity towards methane conversion (Mattisson, Lyngfelt and Cho, 2001). Later investigations have qualified its suitability for use with both syngas and solid fuel conversion (Leion et al., 2009a; Leion, Mattisson and Lyngfelt, 2009a). Solid fuel conversion has been examined in a $1kW_{th}$ CLC reactor (Gu et al., 2011), where it was shown that after 10h of continuous operation with a combination of sawdust biomass and bituminous coal, there was no decrease in reactivity. Similarly to ilmenite the iron ore had to go through a number of redox cycles, to activate the particles, but after 10 cycles, stable operation was maintained.

Manganese ores have also been considered as possible candidates for oxygen carriers in chemical looping processes. In comparison to iron ores, they are more costly due to their relative scarcity as manganese ore production amounts to 1% of the global production of iron ore (Fennell and Anthony, 2015). Nonetheless, they are still far cheaper than the use of nickel and copper-based systems would be. Manganese ores will contain significant impurities, with $Mn_2O_3$ content ranging from 45% to 82%. Chalmers University of technology have conducted notable studies on the use of manganese ores for solid fuel conversion with some ore exhibiting quantifiable CLOU properties. (Arjmand et al., 2012, 2014; Rydén, Lyngfelt and Mattisson, 2011b) The use of manganese ores is not without its issues. The main component is manganese oxide based and therefore is limited by the same thermodynamic considerations. Also it is commonly reported that manganese ores often attrite causing the significant production of fines which are lost in operation (Linderholm et al., 2012; Rydén, Lyngfelt and Mattisson, 2011b). A fairly recent study has concluded the use of a manganese ore used in over 100h of continuous use in a 10kW reactor with bituminous coal, produced effectively no fines, though the details of the manganese ore used were not publicised (Sozinho et al., 2012). The mixture of manganese ores with ilmenite has also shown positive results in a $100kW_{th}$ CLC reactor with coal and wood char. The mixing of the two ores improved fuel conversion to from 84% to 92% compared to using ilmenite alone whilst the comparison of using manganese alone suggested the production of fine material was reduced (Linderholm et al., 2016).

## 2.3 **Chemical looping scale up**

Chemical looping reactors should satisfy the following criteria in order to scale up

- Suitable for achieving the required gas and solid transfer to ensure high rates of conversion of a given fuel in the fuel reactor and high rates of oxidation in the air reactor
- Ensure sufficient transfer of heat from the air reactor through the hot-solid oxygen carriers to the typical endothermic conversion of the fuel in the fuel reactor.
- Ensure a high circulation rate of oxygen carriers throughout the whole system, to maintain sufficient oxygen transfer between the two reaction environments allowing constant supply for fuel conversion.
- Minimise gas leakage between the reactor environments and therefore maintaining a high purity stream at the outlet of the fuel reactor

Fluidised-bed reactors are a well-established technology deployed throughout many industries for a variety of processes including; gasification, combustion of low-grade fuels and waste, and catalytic cracking. More recently, there has been increasing interest for uses in sustainable combustion. Techniques such as oxy-fuel fluidised-bed combustion and solid looping cycles for carbon capture are continually being researched, due to the nature of fuel variability and possibility of incorporating such systems into existing installations (Koornneef, Junginger and Faaij, 2007).

The advantage of using circulating fluidised beds for this type of process is that it allows flexibility in use of different fuel types. The majority of research within the CLC field has been done using gaseous fuels. Syngas derived from gasification process and natural gas has received the most attention, due to their clean burning nature and high product and conversion rates. Research into utilising solid fuels has now become the research trend within the field, where investigations into the conversion heavy liquid fuels are also gaining pace (Leion, Mattisson and Lyngfelt, 2008; Moldenhauer et al., 2014; Wang and Anthony, 2008b).

While several configurations of reactors have been proposed for CLC systems, for gaseous fuels, the most widely considered system is that of the dual interconnected circulating fluidised bed. In the utilisation of solid fuels such as coal or biomass, commonly proposed systems are an interconnected circulating fluidised bed and bubbling or moving/packed bed systems. In these systems a third reactor is typically linked to the fuel reactor in order to maximise fuel conversion and oxygen carrier recovery. The utilisation of loop-seal between the reactors and their specific reaction environments minimises potential leakage of reaction environments into one another, whilst also providing a possible mechanism for the control of solid circulation rate. In chemical looping reactors, the air reactor, where the oxidation of the oxygen carrier takes places is typically a pneumatic transport bed. In this type of reactor the oxygen carriers are fluidised by air through a distributor at a superficial velocity, which maximises gas-solid contact. The solids are separated from the air in a cyclone and are then transferred to the fuel reactor. Depending on its configuration and the fuel utilised, the oxygen carrier oxidised the fuel, and is returned either pneumatically or by moving/bubbling bed processes (typically under gravity) and returned back to the air reactor.

Adánez et al 2012, has reviewed several reactor configurations in detail. Their specific characteristics and applicable operating conditions are summarised in Table 2-4.

**Table 2-4 Reactor patterns and characteristics**

| Reactor system | Mode 1 | Mode 2 | Mode 3 |
|---|---|---|---|
| Operation regime | Moving/packed bed | Bubbling, turbulent or spouted fluidised bed | Fast fluidised bed |
| Gas solid flow pattern | Counter-current | Mixed/co-current | Mixed/co-current |
| Gas solid contact | Low | High | High |
| Fuel and oxygen carrier conversion | High, but may low when scaling up due to the poor mixing | May be low, due to back mixing and gas channelling | High by recirculation |
| Solid circulation rate | Low | Medium | High |
| Ash separation technique with solid fuel | Easy | Difficult | Difficult |
| Particle size, μm | 1000-3000 | Usually 100-1000, wide range is acceptable | Usually 100-600, wide range is acceptable |
| Gas velocity, m/s | >1 | 2-4 | 2-6 |
| Temperature (ºC) | <1100 | <1100 | <1100 |
| Reactor size $MW_{th}$ | +1000 | +500 | 300-600 |
| Scale up | Difficult | Easy | Easy |

In order to design an optimised reactor configuration for a fuel specific CLC process, the use of scaling and dimensionless fluidisation parameters is advantageous.

### 2.3.1 **Scaling rules with dimensionless parameters**

Investigating the fluidising regime and hydrodynamics of the gas and solids in a CLC reactor is a fundamental consideration, as this behaviour will ultimately affect the operation and optimisation of the reactor. In the design process, the

hydrodynamic behaviour of an intended fluid-bed system can be investigated at smaller scales and at ambient conditions through cold flow modelling.

The importance of developing a cold flow model is that they allow one to accurately predict the experimental conditions required in a larger scale system (Shrestha et al., 2016).

Many research groups have utilised cold flow modelling to complement the design process of larger-scaled high temperature looping systems. A cold-flow model would be typically constructed from transparent material (plastic or acrylic) that can allow one to view the internal fluidisation behaviour, patterns and particle mixing or a reactor configuration. In the case of CLC important studies include those conducted by Kronberger et al., 2005;Pröll et al., 2009b; Shuai et al., 2011 and Markström and Lyngfelt, 2012.

The philosophy of cold-flow modelling utilises non-dimensional analysis to provide scaling laws, which can accurately represent the hydrodynamic similarity between a geometrically smaller scaled cold-flow model and a corresponding larger system. The non-dimensional analysis of system similarity was adapted and developed for fluidised beds by Glicksman,(Glicksman, 1982) in which he proposed a full set of scaling laws, allowing ambient temperature modelling of systems operating at elevated temperatures. These scaling laws were simplified in a later study (Glicksman, Hyre and Farrell, 1994) in which the authors presented a relaxed set of parameters detailed in Equation 2-6. These were appropriate for both viscous and inertial dominated regions of the fluidised bed, and could accommodate a wide range of Reynolds numbers applicable to small particles at low fluidisation velocities and large particles at high fluidisation velocities, a limitation of his previously proposed scaling laws.

$$\frac{{u_0}^2}{gL}, \frac{\rho_s}{\rho_g}, \frac{u_0}{u_{mf}}, \frac{L_1}{L_2}, \frac{G_s}{\rho_s u_0}, \varphi \qquad \textbf{Equation 2-6}$$

In order to scale two systems effectively, the scaling pairs detailed in Equation 2-6 should be in agreement between the two systems. The first non-dimensional pair ($u_0^2/gL$) takes into account the velocity (m $s^{-1}$) and the

diameter of the bed (m) multiplied by the acceleration due to gravity (9.81 m $s^{-2}$). The second pair ($\rho_s/\rho_g$) are the ratio of the densities of the solids and gases deployed (kg $m^{-3}$). The third pair ($u_0/u_{mf}$) considers the superficial and minimum fluidisation velocities (m $s^{-1}$). The forth pair ($L_1/L_2$) is the comparison of the length of the risers (m). The final scaling pair, ($G_s/\rho_s u_0$) is the intended circulation rate (kg $m^{-2}$ s) over the particles density and superficial velocity. $\varphi$ is the particles sphericity.

Glicksman's scaling laws are generally regarded as the standard methodology for scaling fluidised beds and while many investigations have proven the applicability of these laws, limitations still exist. Thus for instance, as there are no reactions occurring in cold-flow systems, a reaction such as the combustion of methane and the expansion in the volume of gas cannot be accurately represented (Kronberger et al., 2005). The scaling laws do not consider inter-particle forces which can heavily affect the fluidisation behaviour. Also, it was determined that neither gas and particle wall friction effects nor the solid particle acceleration are accounted for (Pröll et al., 2009b).

### 2.3.2 **Fuel types used in CLC**

CLC is an advantageous technology due to the wide range of fuels that can be used with this approach. Early research in the field utilised gaseous fuels such as natural gas and or methane in their investigations. Research into the use of gaseous fuels has been documented from bench-scale operations through to pilot plant scale (Lyngfelt, 2011). The use of solid fossil fuels such as coal will continue to receive more attention, as CLC is potentially the cheapest combustion technology when carbon capture is required for systems firing solid fuels, with an approximate cost of £15/tonne $CO_2$ avoided based on scale-up to 1000$MW_{th}$ system (Lyngfelt and Leckner, 2015).

Notable investigations using solid fuels in pilot plant reactors above 10kWth include; Chalmers University of Technology, Ohio State University, Hamburg University of Technology and South East University and are detailed in Table 2-5 (Fennell and Anthony, 2015)

**Table 2-5 Pilot plant operation >10kWth with solid fuels adapted from (Fennell and Anthony, 2015)**

| Location | Year | Size (kW) | OC | Fuel | Fuel diameter (μm) | $P_{fuel}$ (kW) | $T_{FR}$ (ºC) | Operation length (h) | Reference |
|---|---|---|---|---|---|---|---|---|---|
| Chalmers | 2012-2014 | 100 | Ilmenite | BIT-PET | 45-BIT 80-PET | 43-130 | 915-980 | 23 | (Lyngfelt, 2013; Markström, Linderholm and Lyngfelt, 2012) |
| Chalmers | 2016 | 100 | Ilmenite Mn-Ore | BIT-WC | 45 | 50-117 | 960-970 | 18 | (Linderholm et al., 2016) |
| Chalmers | 2016 | 100 | Fe-Ore | BIT-WC | 43-103 | 59-127 | 895-960 | 26 | (Linderholm and Schmitz, 2016) |
| Hamburg | 2013 | 25 | Cu-Based | LIG | 70 | 9-26 | 900 | 22 | (Thon et al., 2013) |
| Hamburg | 2014 | 25 | Ilmenite | LIG | 70 | 9-26 | 895-940 | 21 | (Thon et al., 2014) |
| Ohio | 2013-2014 | 25 | Iron Oxide | BIT, SUB, LIG, MET | <100 | <25 | 900-1010 | 313 | (Bayham et al., 2013; Kim et al., 2013; Luo et al., 2014) |
| South-East | 2012 | 100 | Iron Ore | BIT | 1000 | 50 | 950 | 19 | (Xiao et al., 2012) |

BIT – Bituminous Coal, PET – Petcoke, WC – Wood Char, LIG – Lignite Coal, SUB-Sub-bituminous Coal, MET – Metallurgical coke

### 2.3.3 **Status of current CLC reactors**

Research in chemical looping has gained pace in the late 1990's since it had been proposed as a viable research and development option for carbon capture following the investigation conducted by (Ishida and Jin, 1996). Subsequently, significant research was being conducted globally by early 2000.

Important progress was achieved by Chalmers University of technology, which had set the benchmark for reactor design and configuration. Consequently the majority of installed reactors follow the design proposed by Anders Lyngfelt and his research group of two interconnected fluidised beds (Lyngfelt, Leckner and Mattisson, 2001), following the publication of an investigation using iron oxide and reacting it with methane in a small quartz reactor (Mattisson, Lyngfelt and Cho, 2001). Variants of the configuration are common when the reactor is designed for solid fuels. Investigations into alternate reactor configuration have been carried out, but limited to bench-scale activities (Adánez et al., 2012).

A game changing development was due to the GRACE project 10kW chemical looping combustor in 2003 (Lyngfelt et al., 2004) by a partnership involving Chalmers University, Alstom, Technical University of Vienna and the Spanish research councils' Instituto de Carboquimica (CSIC/ICB) (Anthony, 2008). The associated investigation used nickel oxide particles in a 10kW prototype CLC reactor and combusted natural gas. From the published results the research group reports more than 100h of operation with little fines loss from oxygen carrier particles. It is noted that the fines loss in the Ni/NiO particles were due to particle 'hardening' as they became optimised and adapted to the process in the preliminary phases of operation. The fuel conversion rate was high at 99.5%. The prototype was deemed to have demonstrated successful operation, as there was no gas leakage between the reactors. From the cost evaluation developed from this project for a 200$MW_{th}$ commercial unit, it was concluded that CLC had the potential to be the best options for reducing the cost of carbon capture.

Chalmers then utilised the $10kW_{th}$ installation to carry out investigations using nickel and iron based oxygen carriers with natural gas. They were the first research group to present the long term operation of the unit (>1000h), with high fuel conversion rates (98-99%) and little degradation to the integrity of nickel based oxygen carriers (Linderholm et al., 2008). Chalmers University quickly established themselves as the leaders in European CLC research. With over 190 conference and journal publications and the design and operation of a $100kW_{th}$ CLC installation designed for solid fuels, (Lyngfelt, 2013) in which approximately 70h of operations for published studies have been carried out (Linderholm and Schmitz, 2016; Linderholm et al., 2016; Lyngfelt, 2013; Markström, Linderholm and Lyngfelt, 2012).

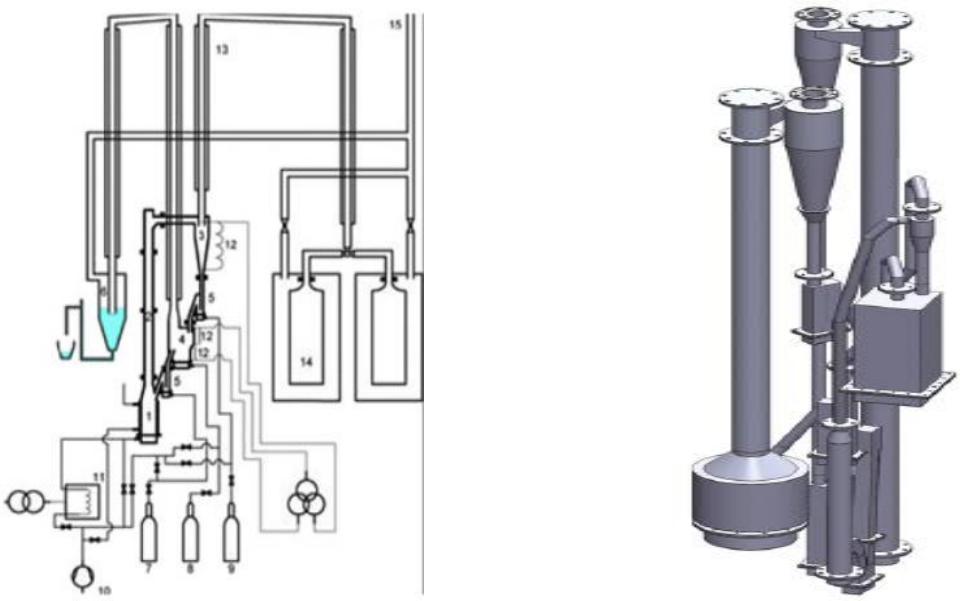

**Figure 2-5 (Left) 10kW for gaseous fuels (Right) 100kW for solid fuels at Chalmers**

ICB-CSIC subsequently built a similar 10 kW reactor to the initial reactor at Chalmers University and investigated the use of copper oxide (CuO) as an oxygen carrier. The results concluded that the use of copper oxide could facilitate long operation in a CLC reactor, with complete conversion of methane.

It was determined that fuel to oxygen carrier ratio and the temperature in the reactor were the most important factors in determining fuel conversion (Adánez et al., 2006). The research group has also modified this installation for solid fuel. They have been prolific in extensive testing of nickel and copper systems, but have also researched the use of ilmenite with several types of fuels. The 10kW installation has been used to conduct chemical looping oxygen uncoupling (CLOU) and steam reforming chemical looping combustion (SR-CLC) (Abad et al., 2012; Gayán et al., 2012b). In recent developments, CSIC have completed the commissioning and preliminary testing phases of their newly constructed 50kW pilot plant for solid fuels. The system consists of two interconnected CFBs, carbon stripper for ash removal and a double loop-seal for fine solid inventory control of the fuel reactor. This unit is designed to be utilised for CLC and CLOU investigations. Preliminary investigations have used bituminous coal with an ilmenite oxygen carrier in CLC mode and yielded positive results with capture efficiencies of approximately 95%. Figure 2-6 (Left) schematic view (Right) image of 50kW CLC pilot plant ICB-CSIC from (Adánez et al., 2014)shows the installation and its scheme as described above (Adánez et al., 2014).

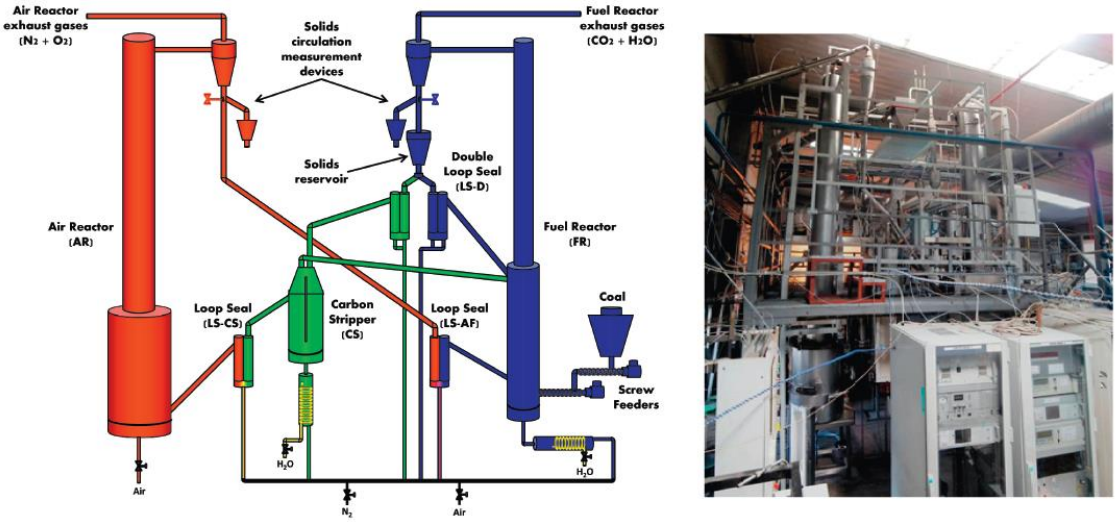


**Figure 2-6 (Left) schematic view (Right) image of 50kW CLC pilot plant ICB-CSIC from (Adánez et al., 2014)**

Table 2-6 lists the details of CLC pilot scale reactors larger than 10kW$_{th}$. The largest CLC installation in Europe for gaseous fuels is the 120kW$_{th}$ installation at Technical University of Vienna as shown in Figure 2-7 TUV 120kW CLC pilot plant for gaseous fuels from (Penthor et al., 2015). The pilot plant, which comprises a dual circulating fluidised bed (DCFB) has been successfully operated for more than 90 hours with nickel based oxides using supports such as $Al_2O_3$, $TiO_2$ and MgO. The particular investigation (Bolhàr-Nordenkampf et al., 2009b) reported high fuel conversion rates, though this decreases when the fuel to oxygen carrier ratio and fuel reactor temperature is increased. The results were comparable to those published by Chalmers University, when conducting a similar study using the same oxygen carriers. The research group also investigated the use of natural substances for potential oxygen carriers. They concluded the use of ilmenite was better suited for syngas conversion, compared to $CH_4$. This was moderately improved by the addition of naturally occurring olivine, (Pröll et al., 2009a). Investigations since have utilised a wide range of oxygen carriers, including ilmenite, copper and iron based materials. More recently the uses of perovskite materials were evaluated with methane and syngas, reporting near-complete conversion (Mattisson et al., 2014).

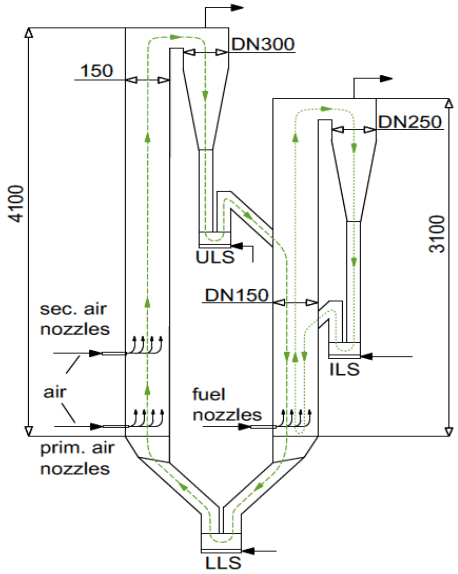


**Figure 2-7 TUV 120kW CLC pilot plant for gaseous fuels from (Penthor et al., 2015)**

**Table 2-6 Summary of chemical looping units larger than 10kW$_{th}$**

| Location | Unit Size kW$_{th}$ | Configuration | Fuel | OC Tested | Operational Time (hours) | Year data published |
|---|---|---|---|---|---|---|
| CHALMERS - Sweden | 10 | Interconnected CFB-BFB | Nat Gas[a] Coal, Petcoke[b] | NiO, $Fe_2O_3$ [a], Ilmenite[b] | 1350[a] 90[b] | 2004[a] 2008[b] |
| CHALMERS - Sweden | 100 | Interconnected CFB-BFB with carbon stripper | Coal | Ilmentite | 23 | 2012 |
| ICB-CSIC - Spain | 10 | Interconnected CFB-BFB | $CH_4$ | CuO | 200 | 2006 |
| IFP TOTAL – France | 15 | 3 - Interconnected BFB-BFB | $CH_4$ | NiO | n/a | 2010 |
| Vienna UT – Austria | 120 | Dual CFB | $CH_4$/ Syngas | Ilmenite NiO | 390 | 2009 |
| Hamburg UT | 25 | Interconnected CFB-BFB | Coal | Ilmenite CuO | 48 | 2013/ 2014 |
| South-east China | 10 | Interconnected CFB-BFB | Biomass | $Fe_2O_3$ | 30 | 2009 |
| South-east China | 100 | Interconnected CFB-BFB | Coal | Iron Ore | 19 | 2012 |
| Ohio State USA | 25 | CDCL Interconnected CFB-BFB | Coal | $Fe_2O_3$ | 313 | 2013/ 2014 |
| ALSTOM – France | 15 | Interconnected CFB-BFB | Nat gas. | NiO | 100 | 2009 |
| KIER Phase 1 Korea | 50 | Interconnected CFB-BFB | Nat gas | NiO | 53 | 2010 |
| KIER Phase 2 Korea | 50 | Dual CFB | Syngas | NiO | 52 | 2010 |
| Jiatong China | 10 | Pressurised 0.3MPa | Coke oven gas | $Fe_2O_3$/CuO – $MgAl_2O_4$ | 15 | 2010 |
| DARMSTADT UTD - Germany | 1MW | Interconnected CFB-BFB | Coal | Ilmenite | 6 | 2012 |

Adapted from data in; (Adánez et al., 2012; Anthony, 2008; Fennell and Anthony, 2015; Lyngfelt, 2011; Markström, Linderholm and Lyngfelt, 2012; Orth, Ströhle and Epple, 2012)
[a] Primary Test
[b] Secondary Test (Installation may have been retrofitted for specific fuel)

### 2.3.4 **Large scale development**

The Technical University of Darmstadt and Alstom have recently operated the largest dual interconnected fluidised bed for chemical looping. The installation is rated at 1MW, but is also multi-purpose, and can facilitate operation in calcium looping mode. The dimensions of the facility are detailed in Table 2-7 Dimensions of 1MWth CLC facility at the Technical University of Damstadt from (Ströhle, Orth and Epple, 2014).

**Table 2-7 Dimensions of 1$MW_{th}$ CLC facility at the Technical University of Damstadt from (Ströhle, Orth and Epple, 2014)**

| Dimensions | Fuel Reactor | Air Reactor |
|---|---|---|
| Height (m) | 8.66 | 11.35 |
| Inner diameter (m) | 0.59 | 0.40 |
| Outer diameter (m) | 1.30 | 1.00 |

A recent experimental campaign utilised ilmenite as an oxygen carrier to convert a Russian hard coal. They report a 50% $CO_2$ capture efficiency and the oxygen demand for the full conversion of gasified fuel was approximately 25%. Comparisons with results from modelling studies suggested similar capture efficiencies based on the design (Ohlemüller et al., 2015). The absence of a carbon-stripper caused unconverted char to be transported to the air reactor, and it was also suggested that a taller CFB system would allow for greater residence time thus improved capture efficiency (Ohlemüller et al., 2016).

Alstom and DOE/NETL are currently constructing a 3$MW_{th}$ chemical looping facility in Windsor Connecticut. The facility is being designed as a CLC system for solid fuel conversion with use of a $CaS/CaSO_4$ oxygen carrier. The facility is due to be fully constructed by the end of 2016. Subsequent successful operation will contribute to high fidelity techno-economic assessments for a proposed 550$MW_e$ CLC facility based on the scale up of the 1MW design (Chiu and Andrus, 2014).

# 3 Development of iron and manganese ore-based oxygen carriers

This chapter describes the use of Canadian iron ore and Brazilian manganese ore as oxygen carriers for the conversion of gaseous fuels. Here the preparation methods for the oxygen carriers and experimental procedure for assessing their suitability are detailed there in. The investigation and its results aims to satisfy objective 2a defined in the PhD aims and objectives.

The investigation was conducted at Chalmers University of Technology. The results described in this chapter have been peer-reviewed and published as an article in Applied Energy.

S.K. Haider, G. Azimi, L. Duan, E.J. Anthony, K. Patchigolla, J.E. Oakey, H. Leion, T. Mattisson, A. Lyngfelt (2016) 'Enhancing properties of iron and manganese ores as oxygen carriers for chemical looping processes by dry impregnation' *Applied Energy* (163) pp 41-50

http://dx.doi.org/10.1016/j.apenergy.2015.10.142

## 3.1 **Scope**

Based upon the literature review conducted in chapter 2, a key gap has been identified as the requirement for low cost materials for the use as oxygen carriers in the CLC process.

Iron ore (mainly $Fe_2O_3$) is one of the cheapest and readily available materials to be considered as oxygen carrier candidate. While it's relatively low cost, abundance and low environmental impact are favourable properties; the iron system has one of the lowest oxygen carrying capacities ($R_O$ 0.33), furthermore its tendency towards methane conversion is typically low.

Manganese ores (mainly $Mn_2O_3$) have also been considered as a low-cost material for chemical looping. Some manganese ores possess the ability to be utilised in CLOU processes, but have difficulties in re-oxidation, as this typically has to occur at temperatures below 800ºC, and the rate-kinetics at this temperature are slow at an oxygen concentration of 5%. Furthermore,

manganese ores have been shown to have low resistance to attrition and are typically ‘soft’ in comparison to iron ores, causing their use to be supplemented with additional make up material in fluid-bed operations, due to elutriated loses.

The use of ores as oxygen carries typically exhibit reduced fuel conversion compared to synthetically produced oxygen carriers, due to the range of impurities contained within the material at the source of extraction. Combining the two active phases of iron and manganese can have positive use for both materials. Where the studies conducted by (Azimi et al., 2013, 2015; Larring et al., 2015a, 2015b) have discussed numerous benefits in combing the two systems, yielding higher fuel conversion the ability to exhibit CLOU properties up to 2%.

The investigation presented in this chapter comprises on an experimental series in which ores of manganese and iron from Brazil and Canada are modified by impregnation. Evaluation of these modified ores as low-cost oxygen carriers for the CLC process are performed in a lab-scale fluidised-bed reactor. Their reactivity towards gaseous fuels ($CH_4$ and syngas ($CO/H_2$ 50%/50%)) and the conversion of these fuels to combustion products is assessed as a function of temperature. In particular, this work seeks to evaluate these oxygen carriers for their CLOU potential for solid fuels by determining the potential gaseous oxygen release in an inert environment to simulate low oxygen partial pressures found in a fuel reactor. Lastly, this study characterises the produced oxygen carriers and their unmodified ore precursors to determine potential improvements in physical and mechanical properties, which could lead to a greater oxygen carrier particle life span and thus evaluate the efficacy of improving ores with the impregnation method.

### 3.1.1 **Impregnation background**

The Impregnation methods can successfully combine an active phase of a metal oxide onto an inert support material. The technique involves introducing a metal salt solution onto a porous inert support material. This salt solution is first dehydrated to remove the aqueous component and is then thermally treated to decompose the salt component, and yield the required loading of the active

metal oxide. The support material is used to increase the mechanical strength of the oxygen carrier particle, in turn increasing the longevity of carrier particles. Several research groups have used the impregnation technique in investigations involving the screening of different supports for active phase materials, and their potential as suitable oxygen carriers have been discussed in detail (Abad et al., 2007a; Mattisson et al., 2007; Sedor, Hossain and de Lasa, 2008) Research investigating the use of the impregnation technique to improve the chemical reactivity and mechanical properties of ores, and the general concept of improving ores for oxygen carrier materials has however received limited attention. Gu et al., reports on the use of a $1kW_{th}$ interconnected fluidised-bed reactor for solid fuels with a modified iron ore. Dolomite/cement was added to the iron ore by means of mechanical mixing and extrusion. Extruded oxygen carriers once sintered positively enhanced the iron ores ability to covert coal. (Xu et al., 2014) has discussed the addition of varying ratios of copper oxide to manganese ore, and found a substantial increase in the conversion of CO even at temperatures as low as 600$^{\circ}$C.

## 3.2 **Methodology**

### 3.2.1 **Particle preparation**

Canadian iron ore was supplied by U.S. Steel Canada and Brazilian manganese ore was supplied by Mineracao Buritirama. The ores were tested in this work, as a base case scenario and were used as supports to prepare the modified oxygen carriers. The method of dry-impregnation was selected here, as it allows the active material to be deposited within the pores of the support material. The impregnation was achieved by using two different nitrate salt solutions, to treat the iron and manganese ores separately. The description of the oxygen carriers tested, and the analysis of the iron and manganese ores, as conducted by ALS Scandinavia AB, is given in Table 3-1and Table 3-2 respectively.

**Table 3-1 Oxygen Carriers Samples**

| Designation | Major component | Final Impregnated Material (%) |
|---|---|---|
| Fe100 | Canadian Iron Ore (100%) | N/A |
| Mn100 | Brazilian Manganese Ore (100%) | N/A |
| FeMn33 | Canadian Iron Ore (67%) | $Mn_2O_3$ (33%) |
| MnFe33 | Brazilian Manganese Ore (67%) | $Fe_2O_3$ (33%) |

The ores were initially heated (calcined) in a high-temperature furnace at 950$^{o}$C for a period of 24 h, to ensure complete oxidation. The samples were then crushed and sieved to a size range of 125-180μm.

The aim of the impregnation method is to achieve uniformity with respect to the dispersion of the nitrate solution on the substrate, or in this case the support material. An estimation of the pore volume of the ores is therefore a requirement to know, as in can relate to how much solution can be absorbed by the ores. The pore volume was estimated by the uptake of water into the sample. This was achieved by adding a measured volume of water to the sample by pipette. This could then relate to the possible amount of nitrate solution that could be absorbed. This was estimated to be 29 ml and 39 ml per 100 g of iron and manganese ore respectively. Using this technique, it was important to add the solution in a manner that one can avoid over saturating the ores, which causes non-uniform dispersion of the active material loading.

For the case of iron ore, an aqueous solution of $Mn(NO_3)_2$ was prepared by dissolving 78.9 g of $Mn(NO_3).4H_2O$ in 20 ml of deionised water to produce a volume with a concentration of 1.315 g/ml and a corresponding molarity of 5.23 M. A volume of 12 ml of this $Mn(NO_3)_2$ solution was pipetted onto a 42 g sample of iron ore. The sample was then heated in a furnace at 220$^{o}$C for 24 h, to decompose manganese (II) nitrate to manganese dioxide ($MnO_2$). The sample was then oxidised at 950$^{o}$C for 24 h to ensure the production of the fully oxidised state of the both the ore support ($Fe_2O_3$) and impregnated metal oxide

($Mn_2O_3$) (Gallagher and Schrey, 1971). The process was then repeated twice more until a desired theoretical 2:1 molar ratio of ore to impregnated metal oxide was achieved. A similar process was used for the preparation of the impregnated manganese ore. 122.1 g of hydrated Iron (III) nitrate ($(Fe(NO_3)_3).H_2O$ was dissolved in water to make a 136ml aqueous solution with a corresponding molarity of 3.7 M and 0.8 g/ml concentration. 13 ml of this aqueous Iron (III) nitrate ($Fe(NO_3)_3$) solution was used as the salt to impregnate a 34 g sample of the manganese ore support. Following the impregnation step, the sample was placed in a furnace at 250$^{\circ}$C to promote thermal decomposition to $Fe_2O_3$ (Wieczerok-Ciurowa, K., Kozak, 1999).

**Table 3-2 Composition analyses of ores**

| Ore Origin | Supplier | Major Component | % Total solids (TS) |
|---|---|---|---|
| Canadian Iron Ore | U.S. Steel Canada | $Fe_2O_3$ | 87 |
| | | CaO | 7 |
| | | MgO | 2 |
| | | MnO | 2 |
| | | $SiO_2$ | <1 |
| | | $K_2O$ | <1 |
| | | $Al_2O_3$ | <1 |
| | | $Na_2O$ | <1 |
| | | $P_2O_5$ | <1 |
| | | $TiO_2$ | <1 |
| Brazilian Manganese Ore | Mineracao Buritirama | MnO | 72 |
| | | $Fe_2O_3$ | 9 |
| | | $Al_2O_3$ | 7 |
| | | $SiO_2$ | 6 |
| | | $K_2O$ | 2 |
| | | CaO, | <1 |
| | | MgO | <1 |
| | | $Na_2O$ | <1 |
| | | $P_2O_5$ | <1 |
| | | $TiO_2$ | <1 |

### 3.2.2 **Experimental Setup**

Tests were conducted in a bench-scale quartz fluidised-bed reactor, heated by an external vertical furnace as shown in Figure 3-1. The reactor length is 820 mm, with a diameter of 22 mm. The reactor has a sintered porous quartz plate, acting as a gas distributor located 370 mm from the base. Simulating the different reaction environments of the AR and FR was achieved by subjecting the oxygen carriers to alternating oxidation (5% $O_2$ by volume) and reduction ($CH_4$ or $CO/H_2$ 50%/50% by volume) cycles within the same reactor vessel. $N_2$ was used as a sweeping gas in between gas phases, and for inert periods to investigate any possible gaseous oxygen release.

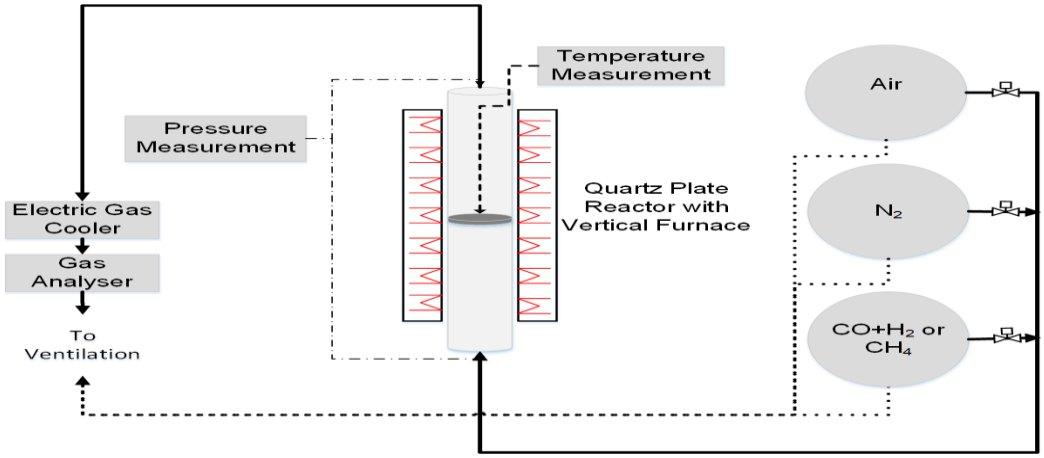


**Figure 3-1 Overview of laboratory-scale fluidised-bed system**

Temperature measurements were made above (25 mm) and below (5 mm) the sintered porous plate by K type chromel-alumel thermocouples. The differential pressure was measured above and below the bed by a Honeywell pressure transducer, which has a measurement frequency of 20 Hz. This measurement provided an indication of fluidisation regime, or de-fluidisation. The resultant flue gas was cooled using an electric cooler achieved by steam condensation. The flue gas was then analysed though a Rosemount NGA-2000 gas analyser which measured the volumetric flow-rate and gas concentration on a dry basis. The gas species measured were $O_2$, CO, $CO_2$ and $CH_4$.

### 3.2.3 **Experimental Conditions**

A sample of oxygen carrier (10 g) was placed on the distributor plate of the quartz reactor. The reactor was then heated up to the first required temperature of 800°C, at an approximate heating rate of 15°C/ min, whilst in an oxidising atmosphere (5% $O_2$ in $N_2$ balance). This 5% $O_2$ composition was selected to assess the oxygen carrier's ability to oxidise in an oxygen deficient environment as compared to Air. A 5% oxygen concentration corresponds to outlet concentrations of an air reactor for a realistic CLC unit (Arjmand et al., 2011). Following the stabilisation of the reactor temperature, the particles were exposed to a $N_2$ sweeping phase for 60s, to ensure the residual oxygen for the oxidation phase had been fully purged from the system. The particles were then exposed to the reducing environment for 20s with methane to assess their fuel conversion ability. Another 60 s period of inert sweeping gas was then passed through the system to purge any combustible gases, before the oxidising step was repeated. The potential for gaseous oxygen release was assessed, by exposing oxidised oxygen carriers to extended inert periods (360 s) of $N_2$ gas. These reduction/oxidation and extended inert cycles were conducted three times at a given temperature. The temperature was then increased by increments of 50°C and three reduction/oxidation and inert cycles were conducted at 850, 900, 950 and 1000°C. The reduction/oxidation cycles were then repeated at temperature increments of 50°C decreasing from 1000-800°C to determine if the oxygen carrier sample's fuel conversion ability is affected with subsequent cycle numbers. Experiments using syngas ($CO/H_2$, 50%/50%) followed a similar procedure to that of methane. The oxygen carriers were exposed to a 20s reduction period with syngas. Due to the high reactivity of the syngas mixture only 1 g of oxygen carrier was used in a bed of 9 g of silica sand. The sand was considered to be an inert bed make-up material and played no role in the reaction chemistry of the oxygen carriers. Table 3-3 lists the reaction conditions and gases involved which the oxygen carriers are exposed to. In all environments, an aggregative fluidising regime was employed. The flow rates were selected to correspond approximately to a gas velocity ($U$) of 5,

8 and 11 times the minimum fluidisation velocity ($U_{mf}$) for reduction, inert and oxidation steps respectively.

**Table 3-3 Experimental gaseous conditions**

| Condition | Gas Composition (% volume) | Time (s) | Gas Flow Rate (ml/min) | Temperatures assessed (°C) |
|---|---|---|---|---|
| Oxidation | $O_2/N_2$ (5%/95%) | 1200 | 900 | 800, 850, 900, 950,1000 |
| Inert | $N_2$ (100%) | 360 | 600 | |
| Reduction | $CH_4$ (100%) | 20 | 450 | |
| Reduction | $CO/H_2$ (50%/50%) | 20 | 450 | |

### 3.2.4 **Oxygen Carrier Characterisation**

The force required to fracture the oxygen carrier particles (crushing strength) was measured using a load cell (Shimpo FGN-5) mounted on a base. Particles of a larger size fraction than those used in the reaction investigation (180-250 μm) were assessed. The particles are placed on the stage, subjected to force until the particles fracture, and the force required to do so is measured. A mean (determined from 30 samples) was used to determine the overall crushing strength. Attrition resistance is measured by the jet cup method as described by (Rydén et al., 2014b). The BET surface area of the oxygen carriers was measured by the nitrogen absorption method in a Micromeritics ASAP 2020 instrument. X-ray diffraction crystallography (XRD) by Siemens D5005 (20-70°θ) and scanning electron microscope (SEM) Philips XL30 with energy-dispersive X-ray (EDX) spectroscopy analysis by Oxford Instruments Swift-ED and analysed by Aztex systems software were utilised to further characterise the physical properties of the particles.

### 3.2.5 **Data Evaluation**

Fuel conversion is quantified by the amount of gaseous fuel introduced to the oxygen carrier sample that is converted to carbon containing combustion products in the outlet stream. Its measure is an indication of the oxygen carrier's reactivity toward the gaseous fuels. The gas conversion γ is calculated using Equation 3-1 and Equation 3-2 for methane and syngas, respectively, where $P_i$ denotes the partial pressure of the gaseous component. In Equation 3-2, the $H_2$ component of syngas is not taken into account when quantifying gas yield. The conversion of $H_2$ is assumed to be complete due to the rapid kinetic rate of reaction (Hallberg et al., 2013).

$$\gamma_{CH_4} = \frac{P_{CO_2}}{P_{CO_2} + P_{CO} + P_{CH_4}} \qquad \textbf{Equation 3-1}$$

$$\gamma_{syn} = \frac{P_{CO_2}}{P_{CO_2} + P_{CO}} \qquad \textbf{Equation 3-2}$$

The degree of oxygen carrier conversion $\omega_i$ is defined in Equation 3-3, where $m_{ox}$ is the mass of the fully oxidised oxygen carrier material and $m_i$ is the mass of the oxygen carrier at time *i*.

$$\omega_i = \frac{m_i}{m_{ox}} \qquad \textbf{Equation 3-3}$$

Mass based conversion for fuel reduction periods is defined in Equation 3-4 and Equation 3-5 for methane and syngas, respectively. Oxygen carrier conversion $\omega_i$ is calculated as a function of time $t_i$. $m_{ox}$ is the mass of the fully oxidised sample, $n_{out}$ is the total molar flow of dry gas entering the analyser. $M_o$ is the molar mass of oxygen. $p_{tot}$ is the total partial pressure and $p_{i,out}$ is the partial pressure of component *i*. It should be noted that the $H_2$ partial pressure was not

specifically measured in the experimental scheme, and instead calculated by assuming equilibrium observing the water gas shift reaction.

$$\omega_i = \omega_{i-1} - \int_{t_{i-1}}^{t_i} \frac{n_{out} M_o}{m_{ox} P_{tot}} \left(4p_{CO_{2,out}} + 3p_{CO_{out}} + 2p_{O_{2,out}} - p_{H_{2,out}}\right) dt \qquad \textbf{Equation 3-4}$$

$$\omega_i = \omega_{i-1} - \int_{t_{i-1}}^{t_i} \frac{n_{out} M_o}{m_{ox} P_{tot}} \left(2p_{CO_{2,out}} + p_{CO_{out}} + 2p_{O_{2,out}} - p_{H_{2,out}}\right) dt \qquad \textbf{Equation 3-5}$$

## 3.3 **Results and Discussion**

### 3.3.1 **Particle Characterisation**

Table 3-4 Physical Properties of Oxygen Carriers shows the values generated by investigations of crushing strength, attrition resistance and surface area. It can be seen that the effect of impregnation of the ores positively influences their physical properties. As crushing strength and attrition resistance are non-standardised tests, the results should be assessed in comparison to other samples in the same experimental series. The results of impregnation of the manganese ores increased the crushing strength by 36% though this substantial increase is not seen in the impregnated iron ore, which exhibits a minimal improvement. The increase in overall mechanical strength is validated by the increase in attrition resistance. There was a notable decrease in weight percentage loss per hour in the impregnated ores, in comparison to their unmodified precursors. Surface area was measured by BET analysis and was shown to increase in the impregnated ores in comparison to the unmodified ores.

**Table 3-4 Physical Properties of Oxygen Carriers**

| Oxygen Carrier | Crushing Strength (N) | Attrition Rate (wt% loss/h) | BET Surface area ($m^2$/g) (Fresh) |
|---|---|---|---|
| Fe100 | 1.8 | 4.3 | 0.4 |
| FeMn33 | 1.9 | 2.7 | 2.5 |
| Mn100 | 1.1 | 4.5 | 1.8 |
| MnFe33 | 1.5 | 3.1 | 2.4 |

SEM and EDX analysis was conducted for impregnated FeMn33 and MnFe33 samples and is shown in Figure 3-2 and Figure 3-3. The sample was mounted in an epoxy resin and then cut across the mould to exhibit a typical particle's cross-sectional area. In Figure 3-2 it can be seen that there is significant loading on the outside of the particle. The iron ore had limited porosity compared to the manganese ore. In this instance, the impregnation technique led to a coating on the outside of the iron ore particles, as opposed to penetrating pores. It is considered, that the increased surface area in the impregnated iron ore is largely due to porosity of the impregnated material. It can be seen in Figure 3-3 that the MnFe33 particles have a greater degree of uniform dispersion of impregnated iron oxide.

The XRD spectra for the fresh samples of the two impregnated ores are shown in Figure 3-4 and Figure 3-5. The differentiation between peaks corresponding to manganese and iron can be problematic due to their close proximity in periodicity. Furthermore, ores tend to have complex spectra due to containing other minerals and considered impurities. The major phases seen are bixbyite (cubic) and hematite (hexagonal-rhombic) in both spectra. In the MnFe33 sample there is evidence of the formation of the non-active phase, Jacobsite, in the cubic arrangement, which is a possible indication of its reduced reactivity.

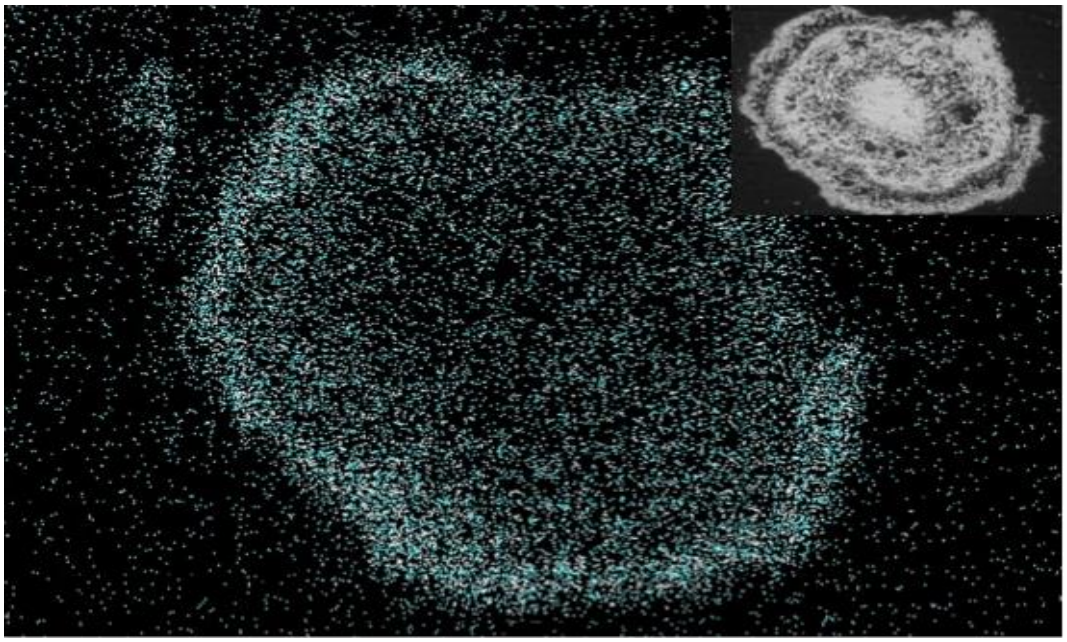

**Figure 3-2 Manganese elemental mapping by EDX of FeMn33 particle (particle size 125-180 µm)**

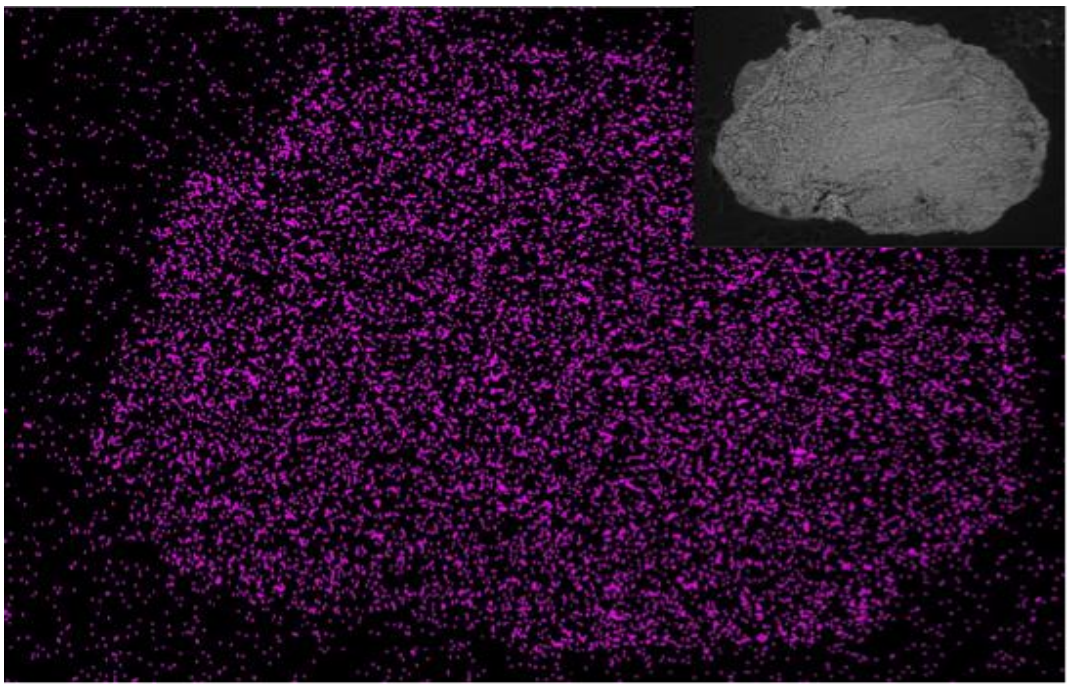

**Figure 3-3 Iron elemental mapping by EDX of MnFe33 particle (particle size 125-180 µm)**

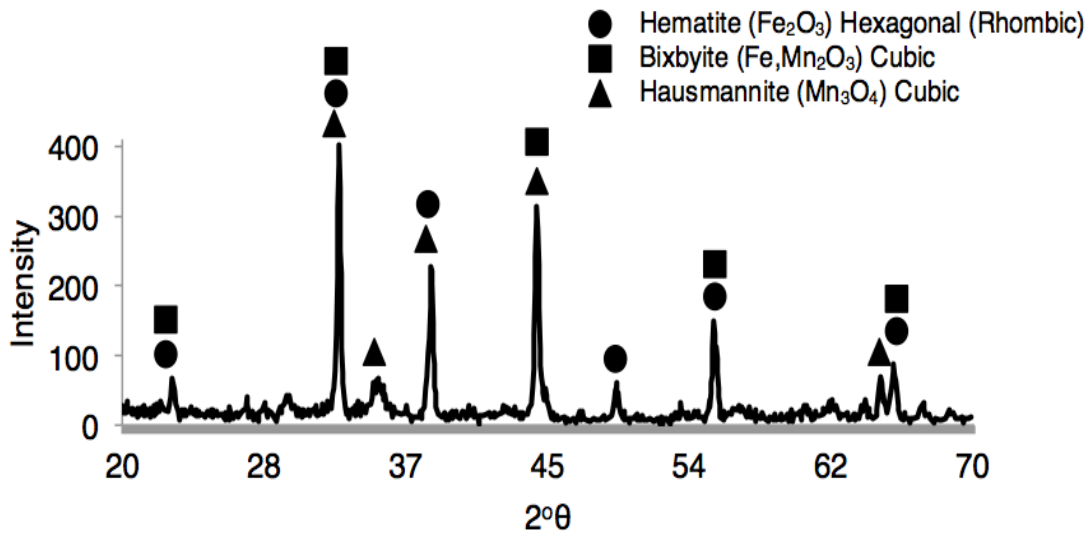


**Figure 3-4 X-ray diffraction spectra for FeMn33**

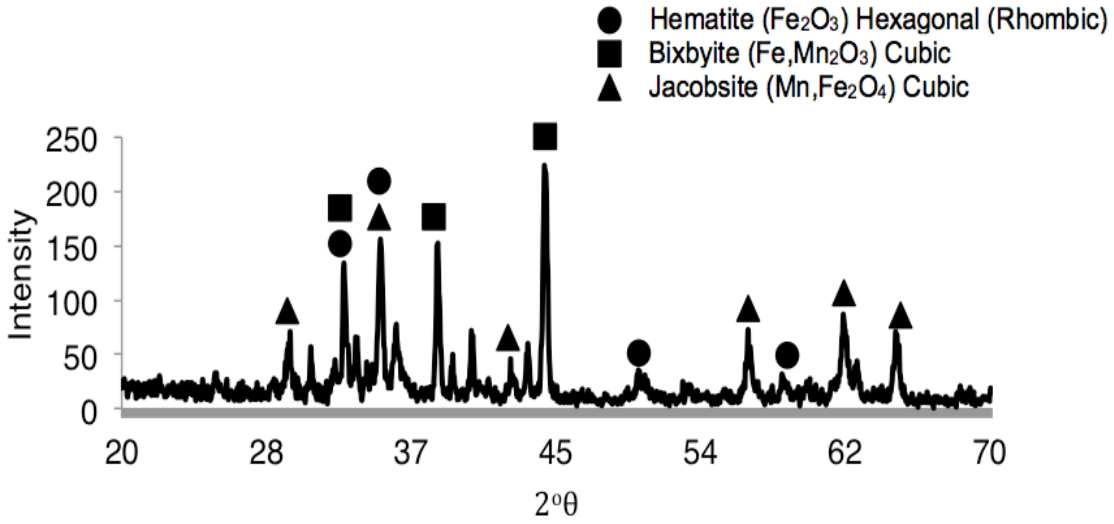


**Figure 3-5 X-ray diffraction spectra for MnFe33**

### 3.3.2 **Oxygen Release**

The prepared samples were investigated for potential oxygen release during fuel conversion experiments. Figure 3-6 gives the oxygen concentration as a function of oxygen carrier conversion or reducibility at low-oxygen partial pressure. Conversion yields corresponding to $\omega = 1$ denotes the oxygen carrier is fully oxidised. Extended Inert cycles were conducted for a length of 360 seconds in the presence of $N_2$ gas as shown in Figure 3-7, which depicts oxygen release at low partial pressure as a function of time. As shown in Figure 3-6 the samples varied considerably, though it should be noted, the extent to which all samples released oxygen was limited. Fe100 showed a limited but detectable release of gaseous oxygen. The Canadian iron ore has impurities of CaO (8% TS) and MgO (3% TS), calcium have featured as supports in perovskite structured materials, which have been demonstrated to exhibit CLOU behaviour (de Diego et al., 2014). The content of magnesium oxide in a hematite-based sample has been shown to increase its oxygen carrying capacity and could contribute to this CLOU behaviour (Miller, Siriwardane and Poston, 2015). Mn100 and MnFe33 can be considered to release no gaseous oxygen under inert conditions at 950$^{\circ}$C and MnFe33 with a manganese ore content of 66%, was not expected to release gaseous oxygen, as this is governed by the phase change of bixbyite ($Fe,Mn_2O_3$) to spinel ($Mn,Fe_3O_4$). At temperatures above 950$^{\circ}$C, the spinel phase for a manganese content ratio of 66% is stable as per the phase diagram discussed by (Azimi et al., 2013) FeMn33 exhibits significant oxygen release compared to the pure iron ore system (Fe100), which is composed of a hematite phase. With a manganese content of 33%, the FeMn33 sample contains both hematite and bixbyite phases. At a temperature of 950$^{\circ}$C, there is a phase boundary with hematite + spinel and hematite + bixbyite phases. The oxygen release exhibited by FeMn33 is attributed to the shift in phase from bixbyite to spinel at this temperature. A small increase in temperature will drive the reaction to form the spinel phase and thus release oxygen more readily. FeMn33 releases oxygen for the entire inert period (360 seconds). This is evident in Figure 3-7, and shows the release is consistent at 0.2% by the end of the inert period.

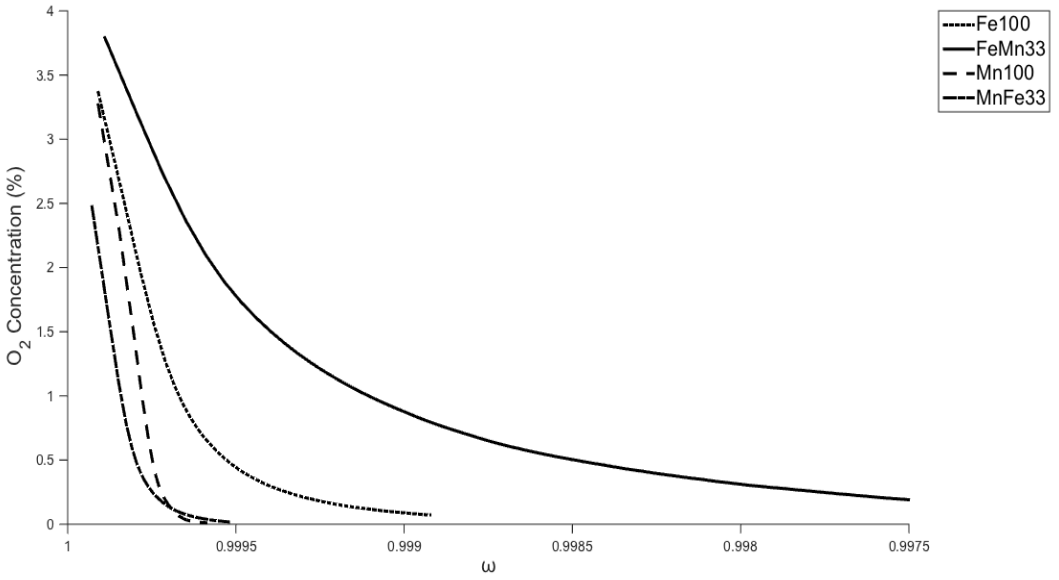


**Figure 3-6 Oxygen carrier conversion vs. oxygen concentration for inert period at 950°C**

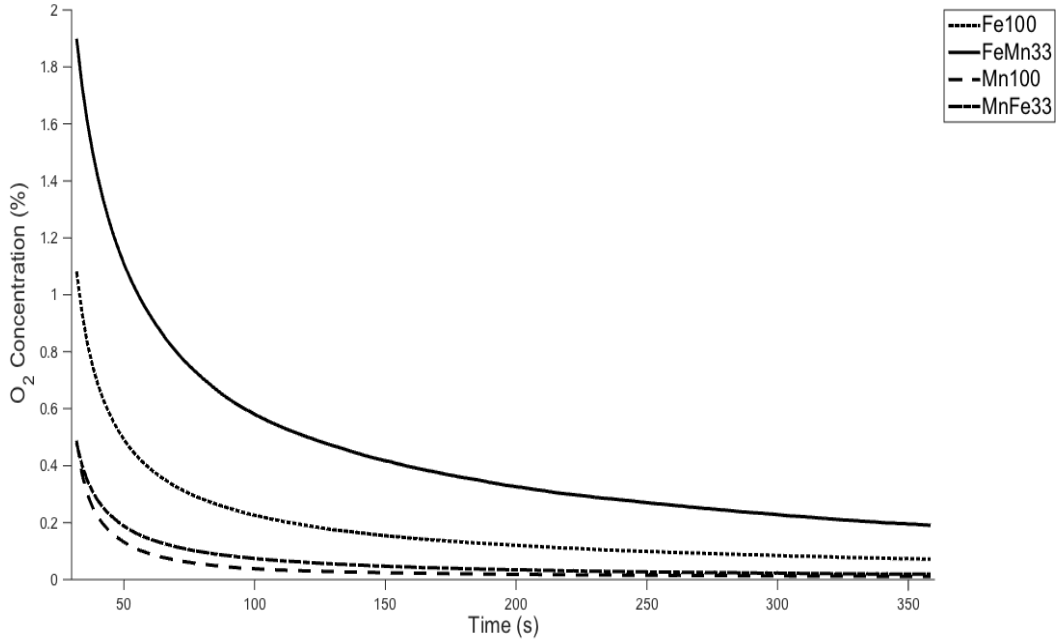


**Figure 3-7 Oxygen release during inert period (360s) at 950°C**

### 3.3.3 **Syngas conversion**

Initial tests investigating the fuel conversion of syngas ($CO/H_2$ 50%/50%) utilised a full bed (10 g) of oxygen carrier. Due to the high reactivity of the syngas fuel with the investigated oxygen carriers, it was difficult to assess the extent of oxygen carrier conversion due to CO being fully converted to $CO_2$ by the full bed of oxygen carrier. It was, therefore necessary to limit the amount of oxygen carrier to be assessed and it was judged to be suitable to utilise 1 g of oxygen carrier particles, in a bed of 9 g of silica sand. The gas conversion γ as a function of mass-based oxygen carrier conversion ω is shown in Figure 3-8 and Figure 3-9 at 950°C and 850°C, respectively. At 950°C, FeMn33 marginally outperformed the iron ore system (Fe100) though, both samples were fully reduced and successfully converted the syngas to combustion products. The manganese-based ores exhibited limited performance in comparison. The pure manganese ore (Mn100) demonstrated greater extent of syngas conversion than the impregnated ore (MnFe33), this is evident from Mn100 producing a greater yield in combustion products while the mass based conversion indicating a greater reduction potential than MnFe33. It should be noted, neither sample fully converted the CO to $CO_2$, and the extent of conversion was limited to 65% and 45% for Mn100 and MnFe33, respectively, based on outlet concentration (dry basis) measured by the gas analyser.

Syngas conversion at a temperature of 850°C is shown in Figure 3-9. As discussed in the experimental procedure, samples were subjected to fuel cycles from 800-1000-800°C. In Figure 3-9 samples denoting a suffix [A] refers to the gas conversion as a function of mass-based conversion at 850°C, but with the decreasing temperature step, occurring subsequently after being exposed to the maximum temperature of 1000°C. The rationale of this procedure was to investigate performance, with increasing cycle numbers. The [A] samples would have been subjected to 19 reduction and oxidation cycles up to this point. The iron-based samples show a clear increase in conversion with cycle numbers, with the impregnated iron ore FeMn33 outperforming its pure ore counterpart. It has been previously discussed that iron-based systems require a number of activation cycles before they achieve stabilised performance. In the iron system,

the porous nature of the sample increases, thus increasing reaction surface area with further oxidation and reduction cycles, although this expansion has limited benefit. Over an increased number of cycles, the micro-pores develop in size and become macro-pores, thus decreasing the surface area and oxygen carrying capacity, and can eventually lead to the oxygen carrier particle disintegrating. Both Mn-based samples exhibit a decline in reactivity and syngas conversion with increased cycle numbers. MnFe33 showed a significant decrease in reactivity, at 850°C. At this temperature the bixbyite phase formation is prevalent and requires a high rate of kinetics to drive the phase change.

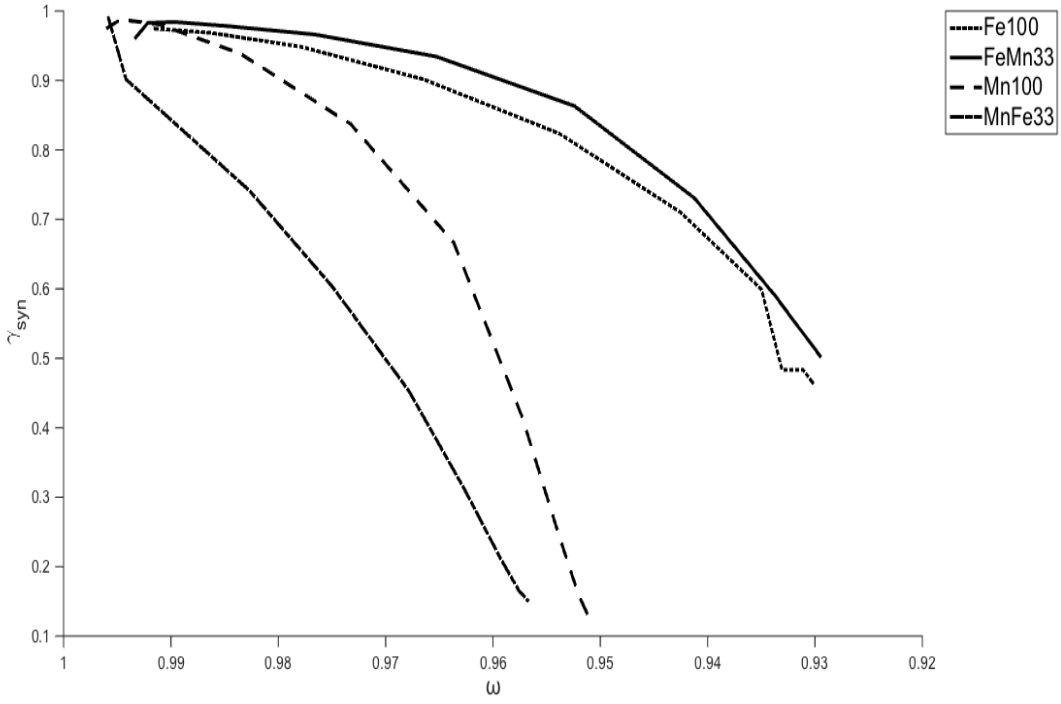


**Figure 3-8 Oxygen carrier conversion vs. gas yield for reduction with syngas at 950°C**

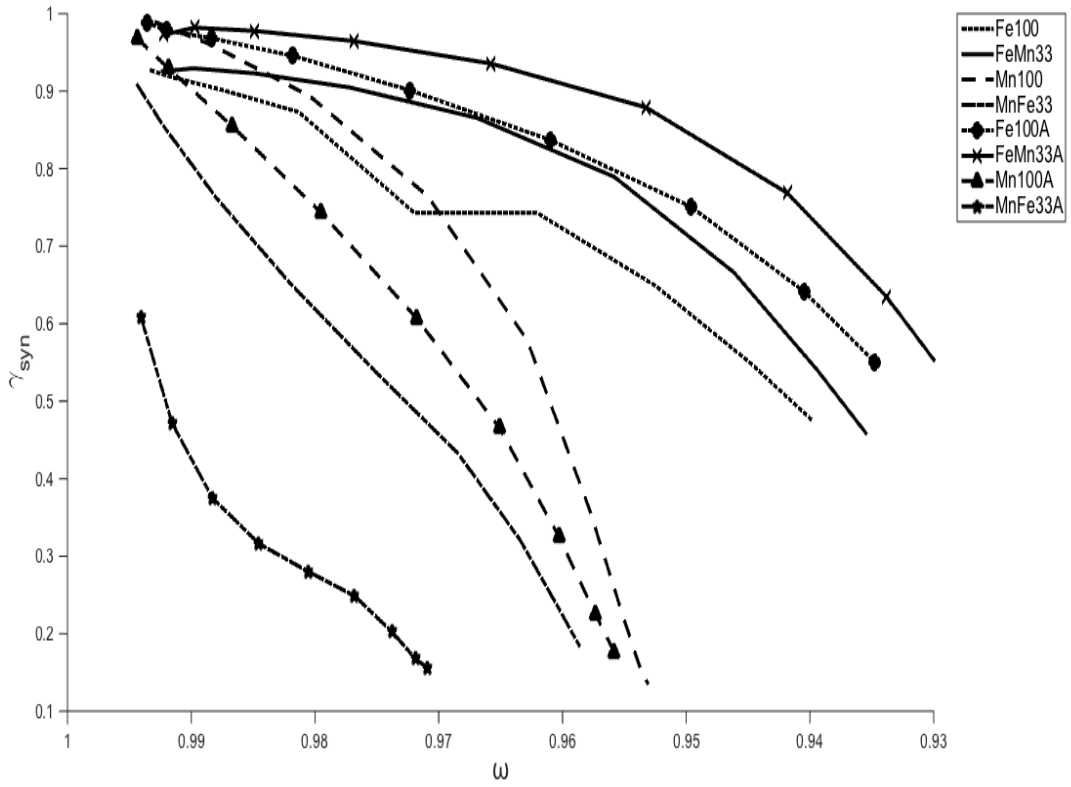


**Figure 3-9 Oxygen carrier conversion vs. gas yield for reduction with syngas at 850°C**

The average syngas conversion versus the range of exposure temperatures is shown in Figure 3-10. This figure shows that the average syngas conversion of all oxygen carrier samples increases with temperature between 850-1000°C. The samples denoted [A], depicted with corresponding markers, are the values of syngas conversion of the oxygen carrier samples, when decreasing the temperature from 1000 to 800°C. The iron ore based oxygen carriers exhibit boosted average syngas conversion, due to the preconditioning associated with being exposed to the maximum temperature of 1000°C and the effect of further oxidation and reduction cycle numbers. The opposite affect is seen in the manganese ore based oxygen carriers, where average syngas conversion decreases. In both manganese ore based oxygen carriers, that syngas conversion is higher at 800°C than at 850°C. Given that the oxidation cycles are

conducted at the same temperature as reduction with syngas, the enhanced conversion seen at a lower temperature is due to a greater degree of oxidation occurring at a favourable lower temperature of 800°C, which facilitates the required phase change of Hausmannite/Spinel to Bixbyite.

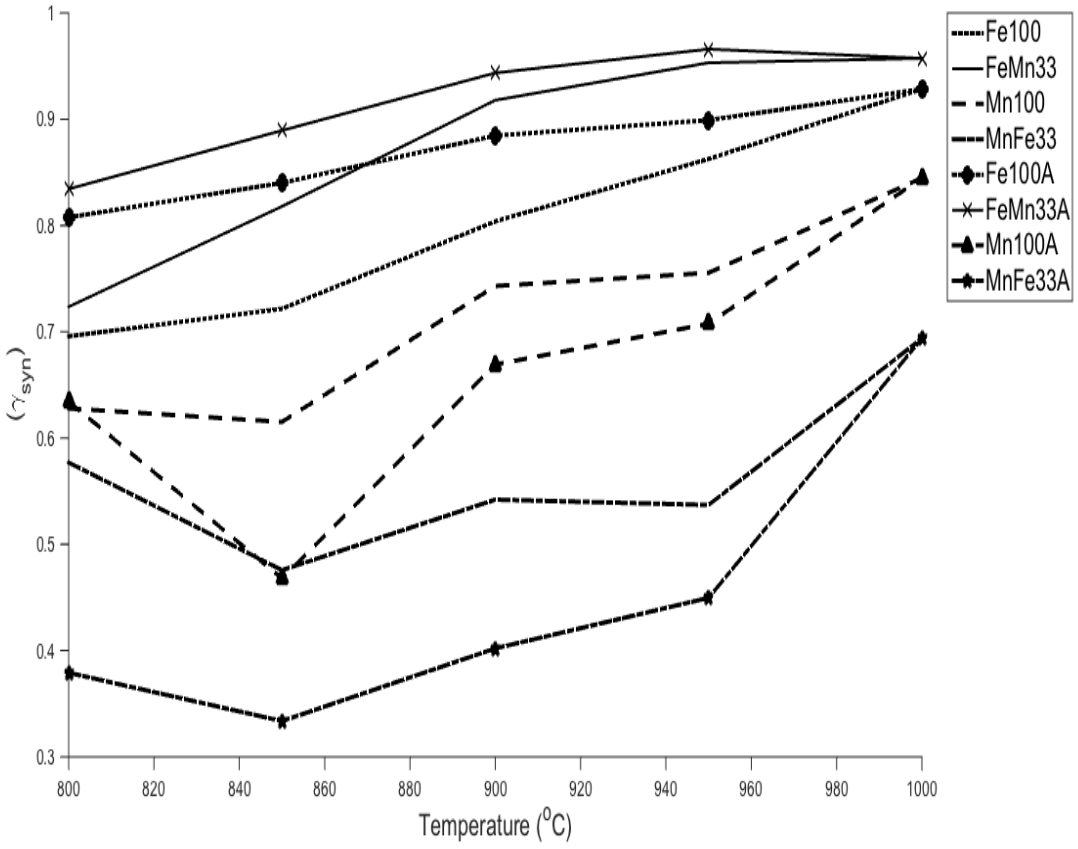


**Figure 3-10 Average Syngas Conversion at 800 – 1000°C showing the effect of increasing cycle numbers**

### 3.3.4 **Methane Conversion**

Figure 3-11 and Figure 3-12 show the gas conversion of methane as a function of mass-based oxygen carrier conversion at 950°C and 850°C, respectively. At 950°C, the range of samples exhibited comparable conversion and reducibility. However, it should be mentioned that the conversion rates for methane at this temperature were of the order of 30-40%. The manganese ore (Mn100) converted methane to a greater extent than the other samples. Both Fe100 and FeMn33 samples showed very similar extents of conversion. Therefore, it is suggested that conversion of methane is not dependent on a gaseous oxygen-methane reaction. At a temperature of 850°C methane conversion becomes progressively limited with conversion rates reduced to below 20%. The increased performance with accumulating cycle numbers was not observed. The increase in micro-pore volume is directly related to the extent of reduction of the oxygen carrier. It is clear that reduction is significantly hindered at this temperature with methane as a reducing gas, and will therefore, exhibit a lower than expected reactivity.

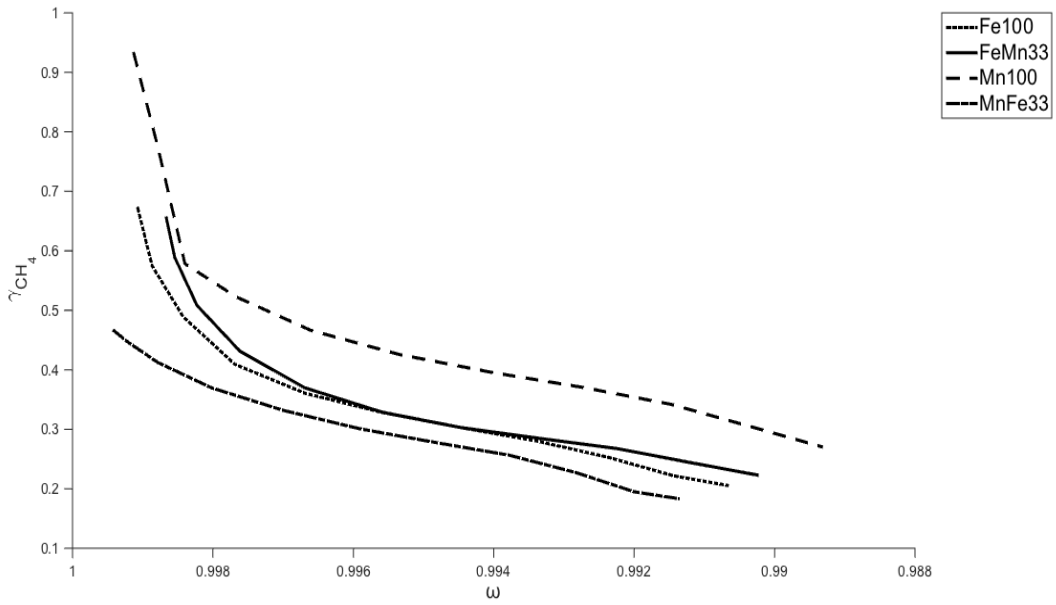


**Figure 3-11 Oxygen carrier conversion vs. gas yield for reduction with $CH_4$ at 950°C**

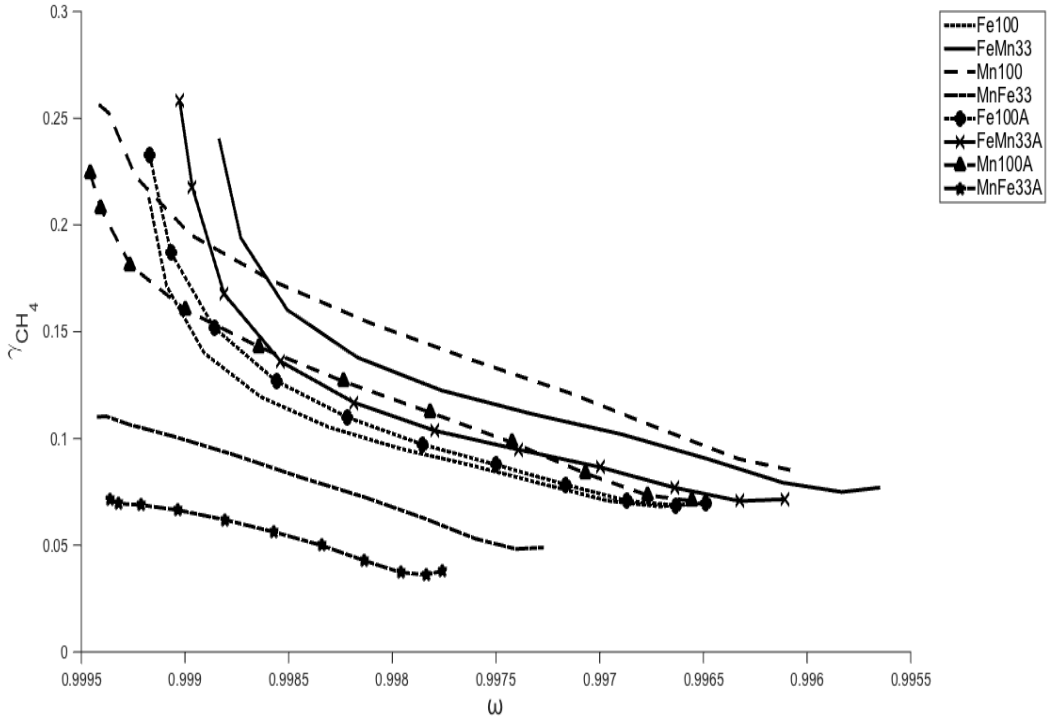


**Figure 3-12 Oxygen carrier conversion vs. gas yield for reduction with $CH_4$ at 850°C**

Average methane conversion against the range of temperatures examined, is shown in Figure 3-13. The average conversion of methane increases with temperature; but the effect of increased oxidation and reduction cycles, and exposure to the maximum reaction temperature of 1000°C does not bear the same influence in reactions with $CH_4$ as it does in comparison to reactions with syngas. This is most evident in iron ore based carriers, where no significant influence is demonstrated. Although it is evident, manganese ore based samples exhibit a decrease in methane conversation with increasing cycle number. The unmodified manganese ore still averaged a greater methane conversion compared to the other oxygen carrier samples examined.

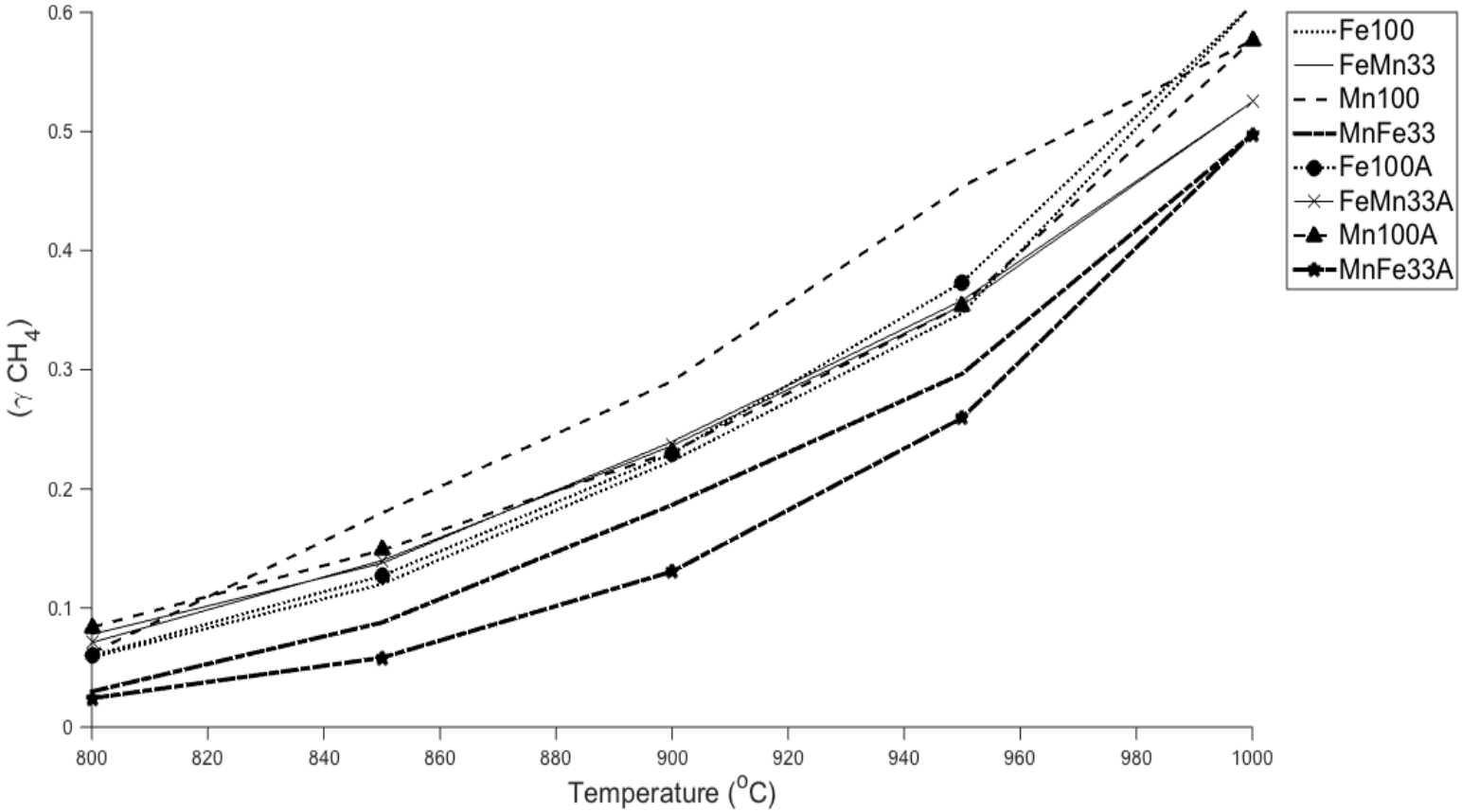


**Figure 3-13 Average Methane Conversion at 800 – 1000°C showing the effect increasing redox cycle numbers**

## 3.4 **Conclusions**

This study investigates the use of the impregnation method to improve the properties of natural metal ores, in order to produce a suitable oxygen carrier for CLC and CLOU processes. The results from this investigation satisfy the PhD aims 2 and objective 2a detailed in chapter 1. The major findings and conclusions that can be drawn from the investigations are:

The impregnation process positively affected the performance indicators for mechanical strength, with enhancements in attrition resistance and crushing strength. Optical characterisation and surface area by BET $N_2$ absorption also suggests the porosity of the impregnated material increases.

The manganese impregnated iron ore, was the only sample to exhibit notable CLOU behaviour with oxygen release of 0.2% at the end of the extended inert cycles. This oxygen release could advance the utilisation of solid fuels in CLC processes. This sample also has the greatest tendency towards syngas conversion, in comparison with the other samples examined. The effect of increasing cycles number positively influenced the yield of combustion products in iron ore based samples. This behaviour was not observed in the manganese ore based samples, and the effect of increased cycle numbers reduced the ability for gaseous fuel conversion. The conversion of syngas to combustion products by manganese ore based oxygen carriers was not significantly influenced by faster kinetics with higher temperature. Unmodified manganese ores showed increased $CH_4$ conversion compared to the other ores tested at 950°C, though this after an increased number of cycles, its conversion rate decreased, signifying problematic use in long term operation.

# 4 Development of copper-based oxygen carriers

This chapter describes the methods for potentially scalable production with copper as the oxygen carrier and low-cost materials as supports. The investigation here, studies gaseous fuel conversion with the copper-based oxygen carriers, as detailed below in order to satisfy the PhD aims and objectives 2b and 2c outlined in chapter 1.

The experimental study was conducted in a lab-scale fluidised bed provided by Dr Stuart Scott at the department of engineering in Cambridge University. The results described in this chapter are intended to be submitted as an article for publication in a peer-reviewed journal such as Fuel.

## 4.1 **Scope**

Copper-based materials as have been studied as potential oxygen carriers for the chemical looping process in great detail (Abad et al., 2007a; De Diego et al., 2004; Donat et al., 2015; Gayán et al., 2012a; Sim et al., 2012). Copper-based systems have favourable redox characteristics, where both the oxidation and reduction reactions are exothermic, and they also possess a high oxygen transfer capacity ($R_o$ 0.201-0.112). Furthermore copper systems can decompose to a lower metal oxide liberating gaseous oxygen in the so called CLOU process (Imtiaz, Hosseini and Müller, 2013). Their use in the conversion of solid fuels is largely due to the fact that such gaseous oxygen release can enhance the oxidation of the char. The gaseous oxygen produced from CLOU can avoid the requirement of the char needing to be gasified into a synthesis gas for combustion in conventional CLC processes.

Examples of the benefits provided by the CLOU properties of a copper-based system are demonstrated by the fact the rate of conversion of a solid fuel, for example petroleum coke, can be increased by a factor of 80 (Leion, Mattisson and Lyngfelt, 2009b) compared to conventional solid fuel CLC. This faster rate of conversion can reduce the requirement of the solids inventory and total reactor volume for a given fuel-feeding rate and hence reduce the associated capital and operational costs of a CLC process. It was calculated that the amount of oxygen carrier per $MW_{th}$ of input fuel could be reduced to

approximately 135kg with a CuO oxygen carrier. By contrast, one would require approximately 1200kg per $MW_{th}$ of fuel input for $Fe_2O_3$ operating in conventional CLC processes (Eyring et al., 2011). Like all oxygen carriers in the fluidised-bed process, these carriers are subjected to mechanical and chemical stresses. In the case of CuO based oxygen carriers, the copper oxide component is far more costly than some alternatives, for example they are likely to cost about 10 times more than a comparable iron oxide carrier (Adánez et al., 2012). It is therefore imperative that the inventory losses associated with attrition are minimised. Attrition due to both mechanical and chemical stresses can be significantly reduced by the appropriate choice of a support material for the active phase, as well as by the choice of the method of preparation of the oxygen carrier. However, all methods of oxygen carrier preparation must be scalable in order to produce the quantities required in full-scale operation. Also, the material utilised as a support should be of relative low cost to ensure the overall cost of produced oxygen carrier is minimised.

The investigation presented in this chapter consists of an experimental study, in which CuO as the active phase is produced as an oxygen carrier in varying ratios with a low-cost support material, consisting of CaO, derived from a natural limestone and an alumina-based cement. Two different production methods are presented here, and are assessed for their feasibility of producing the oxygen carriers at scale. The characterisation of the produced oxygen carriers are assessed and determined for their suitability in a CLC process. The oxygen carriers are then investigated for their efficacy for gaseous fuel conversion. This is assessed in a cyclic redox investigation with CO as a reducing gas in a lab scale fluid-bed reactor. The oxygen carriers showing greater suitability were then further investigated for their reactivity and conversion of $CH_4$.

## 4.2 **Methodology**

### 4.2.1 **Particle Preparation**

Two different methods, both based on the principle of mechanical mixing were used to produce copper-based oxygen carriers, the main steps of each are

described below. The support materials for the oxygen carriers produced are CaO, which is derived from the calcination of limestone from Longcliff (UK) and an alumina-based cement traded as ‘Alpha-bond 300’ sourced from Almatis gmbh (Germany). The CuO was obtained from Johnson Matthey (UK) The series of oxygen carriers have varying weight ratio of CuO with either the CaO or alumina-based cement as the supporting material. The composition of the support materials is given in Table 4-1.

**Table 4-1 Properties of reagents used in oxygen carrier preparation**

| | CuO Johnsson Matthey | Alumina-based cement (Almatis) ‘Alpha-bond 300’ | Longcliff Limestone |
|---|---|---|---|
| Composition | CuO (min~98%) | $Al_2O_3$ (min~88%)<br>CaO (max~0.1%)<br>$Na_2O$ (max~0.5%)<br>$SiO_2$ (max~0.3%) | $CaCO_3$ (min~98%) |
| Particle size (as received) | 120μm (100% passing)<br>70μm (20% passing) | 90μm (max~30%)<br>50μm (min~4%)<br>50μm (max~8%) | 600μm (100% passing)<br>425μm (85-95% passing)<br>300μm (60-85% passing)<br>212μm (30-50% passing)<br>150μm (10-20% passing)<br>45μm (min~4%) |

### 4.2.2 **Ball mill production method**

The ball mill method was used solely for the production of alumina-based cement (referred to Al300 from here) supported oxygen carriers. This production method of oxygen carriers with CaO as a support was considered too hazardous to be handled in our laboratory due to the exothermic reaction of water with CaO.

Prior to the manufacture of the oxygen carriers, it was important that the materials used in their production were below particle diameter of 10μm. To this end, the ball mill was primarily utilised to further crush the constituent material. The ball mill apparatus (produced by Ortho-Alesa), is shown in Figure 4-1 consists of a variable speed controlled rubberised rollers, on which a 10L internally baffled mill drum is rotated to an operator defined rpm.

**Figure 4-1 Ortho-Alesa ball mill; (left) milling ball bearings, (right) ball mill**

Inside the mill drum were 1kg of 9mm stainless steel ball bearings, which serve to crush and grind the required material added to the mill drum. Approximately 1kg of material was added to the mill drum with the 1kg ball bearings for optimum grinding. The ball mill was operated for 24h at 100 rpm. The PSD analysis (Malvern Mastersizer 2000) of Copper (II) oxide material provides an example of the final product size range obtained from the initial stage of the production process, after the grinding process in Figure 4-2. It can be seen the bulk of the resultant product has a particle size diameter of 10μm or less.

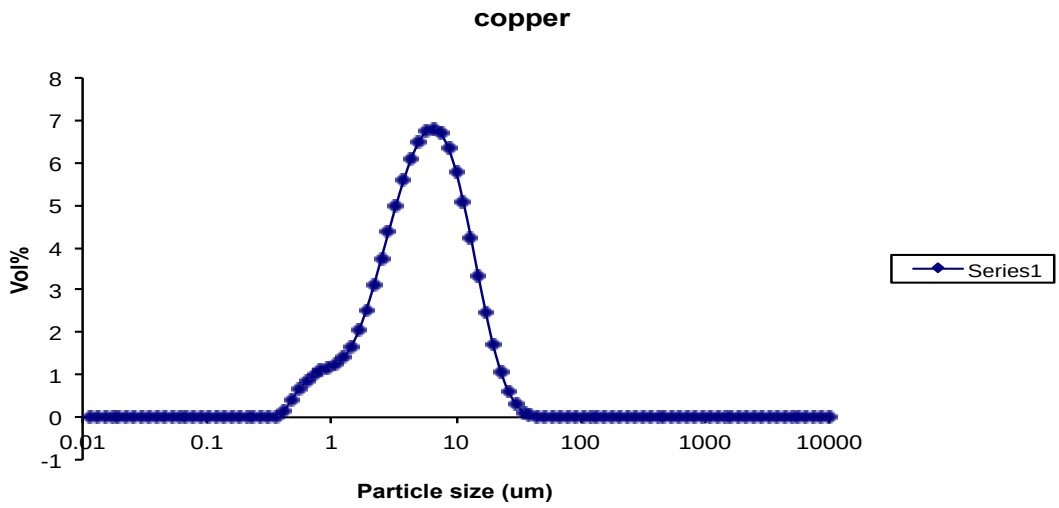


**Figure 4-2 Particle size distribution of CuO after 24h of ball mill operation**

The fine powders (<20μm) of CuO and Al300 were weighed to the desired %wt ratio (60:40 600g CuO and 400g Al300). The mixture of powders was then added to the mill drum with the ball bearings and rotated in the ball mill for 1h to promote a uniform powdered mixture. The mixture was then passed through a 4mm screening sieve to remove the stainless steel ball bearings and the powdered mixture was introduced back into the mil drum. At this stage, deionised water was added to the powder mixture though a fine spray nozzle bottle intermittently, while the drum was rotated for 1h at 40 rpm. The addition of water is a critical stage, and must be limited to avoid over-saturating the particles. Typical volumes for addition were around 200 mL per 1000g of mixed particles. The 'wet' particles were then screened through a 1mm screened sieve to promote mixed granules.

This powder was dried at 200$^{o}$C in an oven and screened for the required size range. The desired size range was then transferred to alumina ceramic trays for sintering in a high temperature furnace at 900$^{o}$C for 5 hours. After the sintering process, the material was screened again to ensure a suitable size range. The typical yield in terms size range of particles is shown in Table 4-2.

**Table 4-2 Typical product yield from 1kg of CuO + Al300**

| Size Range | Yield |
|---|---|
| 212-355μm | 20% |
| 125-180μm | 30% |
| 90-125μm | 20% |
| <90μm | 30% |

A 60:40 wt% (CuO to Al300) oxygen carrier was produced using the ball mill method for use in the pilot chemical looping reactor in a single reactor CLOU investigation. The investigation and its results are detailed in chapter 5.

### 4.2.3 **Pelletisation Method**

The second method of producing oxygen carriers explored here was a pelletisation method, which utilises a table-top TGM granulator manufactured by Glatt. The granulator is consists of a mixing vessel, in which high-shear rotating blades are mounted horizontally and vertically these are designated the agitator and chopper respectively. The granulator unit and its internal rotating blades are shown in Figure 4-3. The fine powdered reagents produced from the milling process of the ball mill (described above) are weighed to their desired quantities. They are then transferred to the mixing vessel. The rpm of the agitator and the chopper are set to 500 and 2500 respectively. Water is then added to the powdered mixture. Water is introduced through a pressurised spray nozzle system and can be added or halted at discretion. The water spray is added for 10s at intervals of 60s. After each minute the process is then halted to visually inspect the mixture to ensure no over saturation and to the grain size is increasing. The effect of over-saturation in a short period of time would lead to larger than desired sized particles.


**Figure 4-3 (left) Glatt TGM Granulator (right) 4 litre vessel with blades i) agitator, ii) chopper**

When Al300 is the support material, approximately 150-200ml of water is added per kg of powdered mixture. When CaO is the support material, the

addition of water, promotes $Ca(OH)_2$ formation and is exothermic, and a greater quantity of water to is required to form the pelletised oxygen carriers due to the loss of water as steam. This phenomenon varies strongly with the wt% ratio of CaO used as a support. The typical quantity of water added was between 300-500 ml per kg of powdered material. The formed particles were then transferred to an alumina tray for air-drying at 200°C. The particles were then sintered at 900°C in a high temperature furnace for 4h. Following the sintering step the pelletised oxygen carriers were screened to the desired size range of 355-425µm.

The pelletisation technique, for the production of combined oxygen carriers yields particles, which are effectively spherical, making them suitable for fluidised-bed operation. The size range of oxygen carrier is dictated by a combination of time in the granulator, and quantities of water added. With the correct management of water addition and time, one batch can typically produce 60% the required size range. The SEM image and the photo of various oxygen carrier products are shown in Figure 4-4. Pelletised oxygen carriers are investigated in a lab-scale fluidised-bed study for the conversion of gaseous fuels (CO and $CH_4$).


**Figure 4-4 Oxygen Carriers produced by pelletisation method: (left) SEM image of multiple oxygen carriers, (right) range of produced samples**

### 4.2.4 **Oxygen carrier characterisation**

The produced oxygen carriers were characterised by X-ray diffraction crystallography (XRD) by means of a Siemens D5005 (10-90°θ) and by scanning electron microscope (SEM) Philips XL30 with Schottky Field Emission Gun (SFEG) mode for high-resolution imaging. The SEM was also coupled with energy-dispersive X-ray (EDX) spectroscopy analysis by Oxford Instruments Swift-ED and analysed by Aztex systems software. The crushing strength of the particles were determined using the technique utilising the Shimpo FGN-5 load cell, described in chapter 3, which is applicable for particles in a size range between 325-425 μm.

### 4.2.5 **Lab-scale experimental setup**

The investigation into gaseous fuel conversion was conducted in a quartz fluid bed reactor (FBR) heated by an external furnace as shown in Figure 4-5. The reactor length measured 550mm tall with an internal diameter of 24mm. The distribution plate consisted of sintered porous quartz and was located 10mm from the bottom of the reactor. FBR could utilise mixtures of $N_2$ and Air, $N_2$, CO 10% in $N_2$ balance and 5% $CH_4$ in $N_2$ balance, all supplied from gas cylinders from BOC Ltd using three Bronkhorst (EL-Flow) series mass flow controllers to control the flow rate. A portion of the exhaust gases from the FBR were sampled continuously by a means of a pump using an approximate flow rate of 0.5L/min through a 6.25mm o.d stainless steel tube inserted 10mm into the top of the quartz reactor. A particle filter protected the down-stream analysis equipment and a moisture trap with a $CaCl_2$ drying agent, ensured the gas sample was dry. The sampled gas was analysed at a frequency of 1Hz by an ABB EL3020 series multi gas analyser, which measured the gas flows of CO, $CO_2$, $CH_4$ (0-20%vol) and $O_2$ (0-25%). Temperature measurements were made by a K-type thermocouple inserted into the fluid-bed reactor. The differential pressure was measured above and below the bed to ensure the bed was fluidised throughout the investigations.

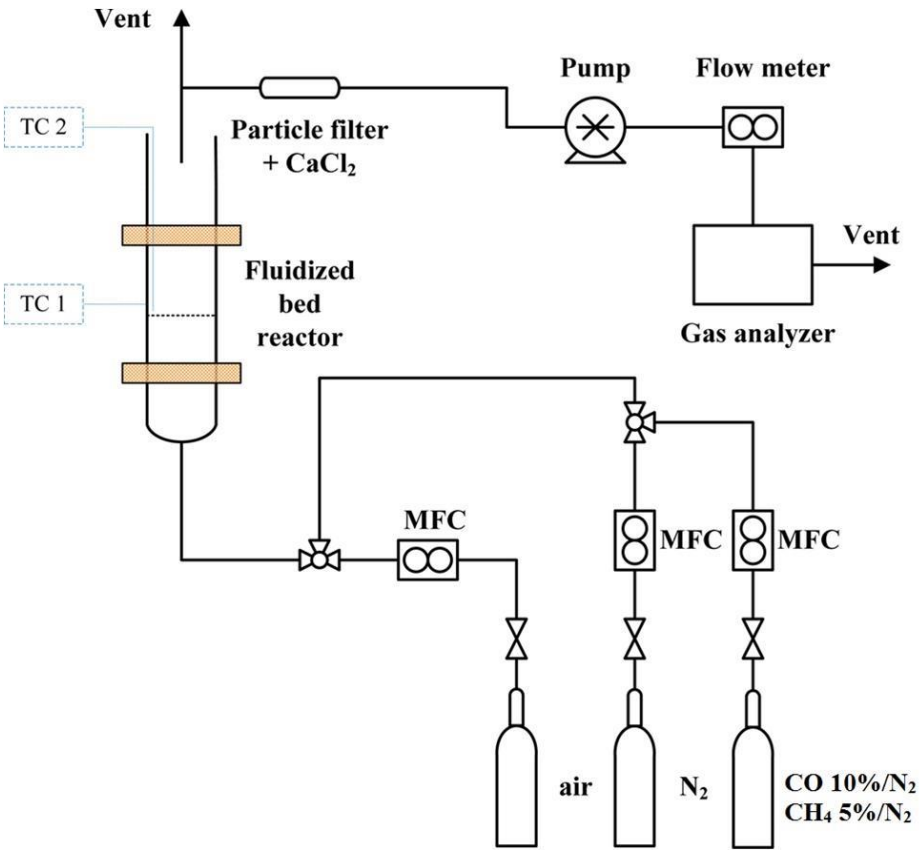


**Figure 4-5 Simplified scheme of fluid bed reactor for redox investigation**

### 4.2.6 **Experimental conditions**

The experimental setup described above, was used to investigate the cyclic performance of oxygen carriers with varying ratios of CuO as the active phase supported by either CaO or Al300 support materials. The oxygen carriers were fluidised in a bubbling regime and were subjected to 25 redox cycles. All investigations were conducted at 950°C. As both the oxidation and reduction reactions of $CuO/Cu_2O$ are exothermic, the oxygen carrier was diluted with silica sand (325-450µm from Sigma Aldrich) in order to help control the bed temperature. In the investigation approximately 1.5g of oxygen carrier was used together with 13.5g of silica sand. The oxygen carriers, their compositions and properties are shown in Table 4-4. A blank cycle was conducted with sand only for calibration of the analyser and to determine whether there were any side reactions of the reactor material with the oxidation and reduction gases. Each redox cycle consisted of 4 stages; 1)

Inert stage with $N_2$ for a period of 300 s, 2) reduction stage with CO 10% in $N_2$ balance or $CH_4$ 5% in $N_2$ balance for a period of 60s, 3) sweeping stage with $N_2$ for 60s, 4) oxidation stage with air 20% with $N_2$ balance for 360s. The air in the oxidation stage was diluted with nitrogen to give a corresponding $O_2$ concentration of 5%. The inlet gas flows were maintained at a combined 30ml/s measured at standard conditions (20°C and 1atm) for all the gaseous reaction environments. This corresponded to a ratio of superficial fluidising gas velocity ($U_0$) to minimum fluidisation velocity ($U_{mf}$) of approximately 4 that ensures a vigorously bubbling bed. The gaseous operating conditions are listed in Table 4-3.

**Table 4-3 Experimental conditions, gases and flow rates**

| Condition | Gas composition | Time (s) | Gas flow rate (L/min) | Temperature ($^{o}$C) |
|---|---|---|---|---|
| Inert | $N_2$ | 300 | 1.8 | 950 |
| Reduction | CO 10%/$N_2$<br>$CH_4$ 5%/$N_2$ | 60 | 1.8 | |
| Inert | $N_2$ | 60 | 1.8 | |
| Oxidation | Air 20%/$N_2$ | 360 | Air 0.45<br>$N_2$ 1.35 | |

### 4.2.7 **Data evaluation**

The degree of oxygen carrier conversion ($X$) in this investigation is defined in Equation 4-1 and is used to describe the extent to which the oxygen carrier can be reduced. ($m_t$) is the mass of the sample at a given time ($i$), ($m_{red}$) is the mass of the fully reduced sample and ($m_{ox}$) is the mass of the fully oxidised sample.

$$X = \frac{m_i - m_{red}}{m_{ox} - m_{red}} \qquad \textbf{Equation 4-1}$$

($X$) is used to determine the mass based conversion for fuel reduction periods and is defined for $CH_4$ and CO in Equation 4-2 and Equation 4-3 respectively. ($P_{i,out}$) is the concentration of the gaseous species leaving the reactor, ($n_{tot,in}$) is the total number of gaseous moles entering the reactor in mol/s, ($M_{CuO}$) is the molecular weight of CuO in g/mol. ($a_{oc}$) is the mass fraction of active metal oxide in the oxygen carrier and ($m_{oc}$) is the mass of the oxygen carrier sample. The yield of gas conversion ($\gamma$) calculated from the equations 3-1 and 3-2 described in chapter 3 for $CH_4$ and CO respectively.

$$X_i = X_{i-1} - \int_{t_{i-1}}^{t_i} \frac{n_{tot,in} \cdot M_{CuO}}{m_{OC} \cdot a_{OC}} \cdot \left(4P_{CO_{2,out}} + 3P_{CO_{out}} + 2P_{O_{2,out}}\right) dt \qquad \textbf{Equation 4-2}$$

$$X_i = X_{i-1} - \int_{t_{i-1}}^{t_i} \frac{n_{tot,in} \cdot M_{CuO}}{m_{OC} \cdot a_{OC}} \cdot \left(2P_{CO_{2,out}} + P_{CO_{out}} + 2P_{O_{2,out}}\right) dt \qquad \textbf{Equation 4-3}$$

## 4.3 **Results and discussion**

### 4.3.1 **Particle characterisation**

Table 4-4 shows the crushing strength, bulk density and the major crystalline phases seen in the fresh pelletised oxygen carriers. The crushing strength is positively improved with greater support composition in the oxygen carrier. The average crushing strength of thirty pure CuO particles was 0.43 N, in comparison to the cases of the oxygen carriers containing the lowest percentage of support material, the crushing strength had improved by a minimum of 280%.

**Table 4-4 Oxygen carrier characterisation properties**

| Oxygen carrier name | Crushing strength (N) | Bulk Density ($kg/m^3$) | Major crystalline phases |
|---|---|---|---|
| Cu25Al75 | 1.55 | 1680 | Bohmite, Tenorite |
| Cu50Al50 | 1.27 | 2680 | Corundum, Tenorite |
| Cu75Al25 | 1.23 | 3510 | Corundum, Tenorite |
| Cu25Ca75 | 1.63 | 2220 | Portlandite, Tenorite |
| Cu50Ca50 | 1.50 | 2219 | Portlandite, Tenorite |
| Cu75Ca25 | 1.31 | 3320 | Portlandite, Tenorite, $Ca_2CuO_3$ (orthorhombic) |

The major crystalline phases of the produced oxygen carrier particles were determined by XRD spectrometry. Their diffraction spectra are shown in Figure 4-6 and Figure 4-7 for Al300 and CaO supports respectively. There are no significant differences between phases seen in the diffraction spectra, with exceptions in Cu25Al75 where the presence of Bohmite was identified and Cu75Ca25 where $Ca_2CuO_3$ was identified.

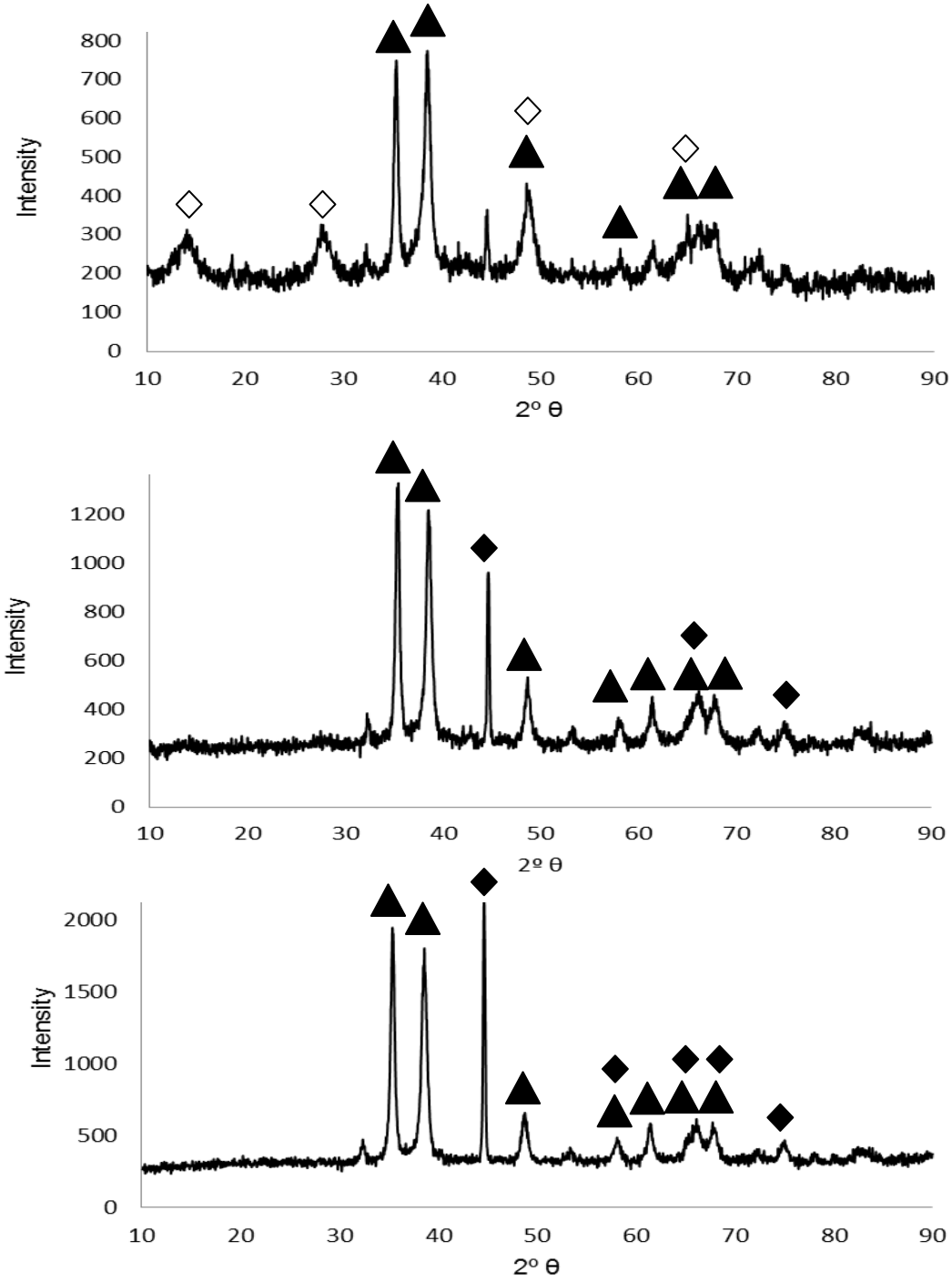


**Figure 4-6 XRD spectra of alumina supported oxygen carriers (Top)-Cu25Al75 (Centre)-Cu50Al50 (Bottom)-Cu75Al25 ▲-CuO (Tenorite) ♦- $Al_2O_3$(Corundum) ◊-$AlHO_2$ (Bohmite)**

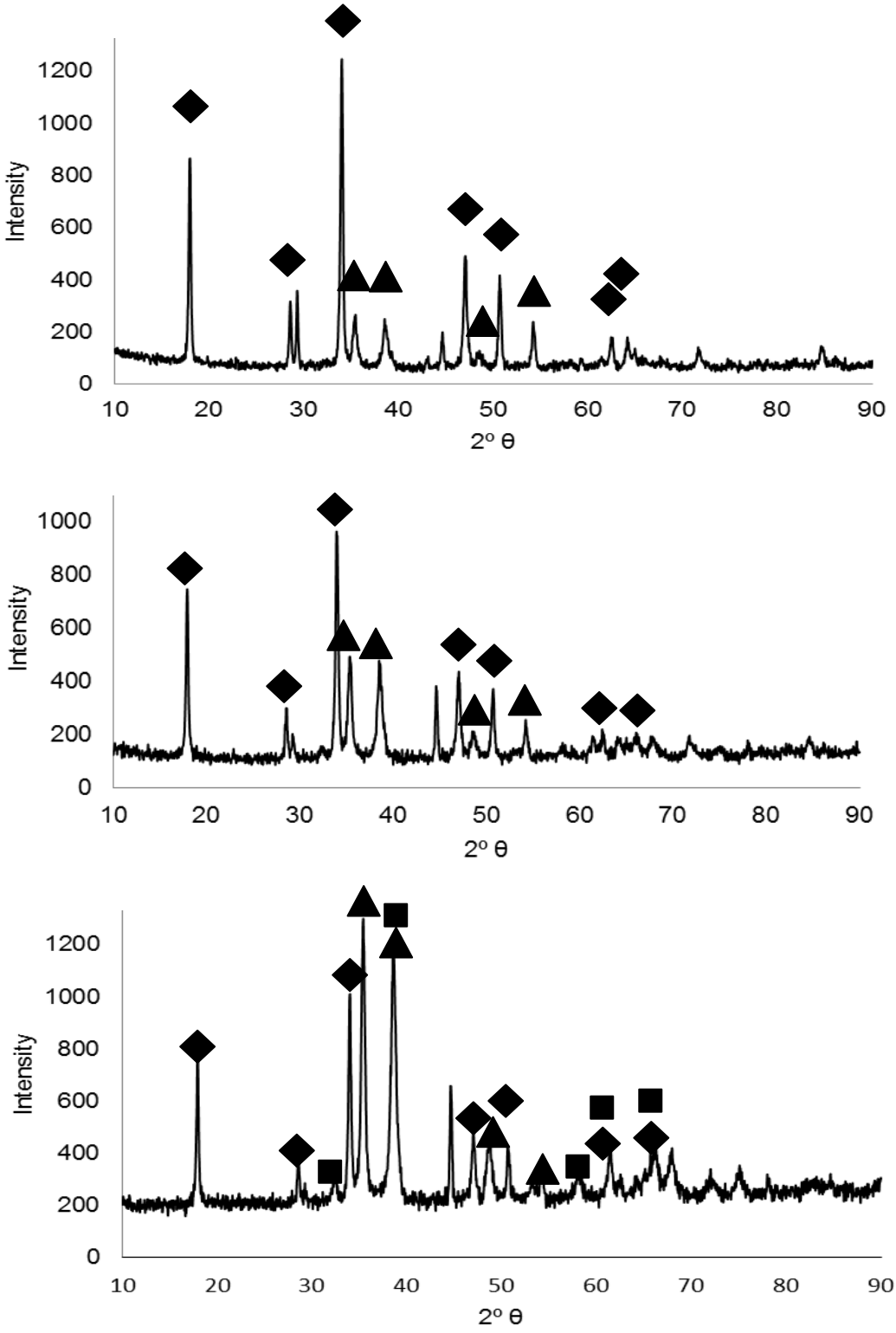


**Figure 4-7 XRD spectra for Ca-supported oxygen carriers (Top)-Cu25Ca75 (Centre)-Cu50Ca50 (Bottom)-Cu75Ca25 ▲-CuO (Tenorite) ♦-$CaH_2O_2$ (Portlandite) ■-$Ca_2CuO_3$**

The fresh produced particles were assessed under SEM in SFEG mode for high-resolution imaging. To investigate the internal composition of the oxygen carriers, the particles were first mounted in an epoxy-resin. This resin mould was then ground back as to reveal the cross sectional area of the particles. The resin moulds were then assessed under SEM with EDX analysis. This allowed one to examine the uniformity of support material and copper (II) oxide within.

The oxygen carriers containing the Al300 support are shown in Figure 4-8, Figure 4-9 and Figure 4-10. The increase in composition ratio of CuO to Al300 is quite evident from these figures. The non-uniformity of the elemental distribution within the particles shows that the CuO tends to be localised to specific areas within a given particle. This appears to be due to the specific component particle sizes originally involved in forming the oxygen carrier particle. This is also observed in the oxygen carrier particles containing CaO as a support (Figure 4-11, Figure 4-12 and Figure 4-13).

The comparison in morphology of the 25% CuO containing oxygen carriers clearly shows a difference in support material structure. In Cu25Al75 it appears the Al300 supports is formed of smaller particles and are compacted together with the CuO to form the oxygen carrier. In contrast, to the production of the Cu25Al75 oxygen carrier, the formation of the support appears to be uniform with a greater distribution of the active CuO and is likely a contributing factor for its increased crushing strength over the Al300 supported particles. The pelletisation method favours the use of CaO as a supporting material. It can be seen that the Ca-based supported oxygen carriers appear to be more spherical than the Al300 based particles and can result in more favourable fluidisation properties and less attrition due to reduced fragmentation and ‘rounding’ of the particles occurring during fluidising operation due to the removal of asperities on the particles.

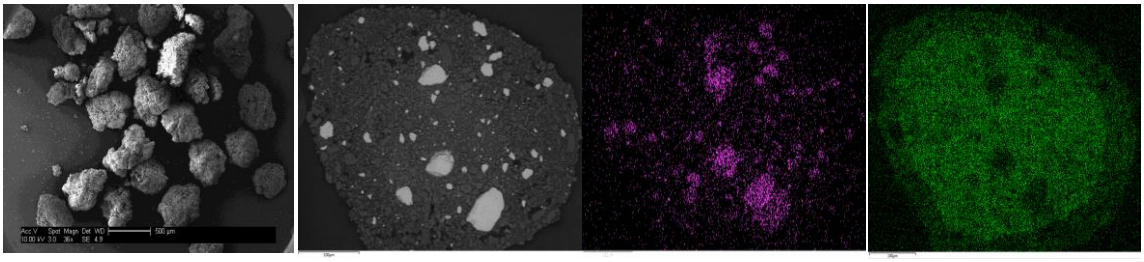

i) ii) iii) iv)

**Figure 4-8 Cu25Al75 i) High resolution SFEG image (scale 500µm), ii) Global particle view EDX, iii) Cu elemental mapping EDX, iv) Al elemental mapping EDX**

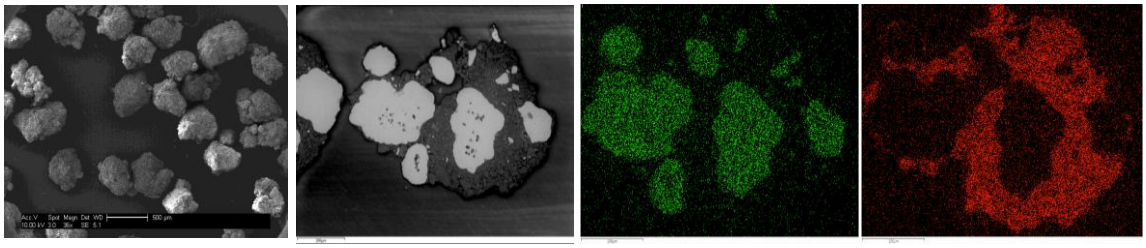

i) ii) iii) iv)

**Figure 4-9 Cu50Al50 i) High resolution SFEG image (scale 500µm), ii) Global particle view EDX, iii) Cu elemental mapping EDX, iv) Al elemental mapping EDX**

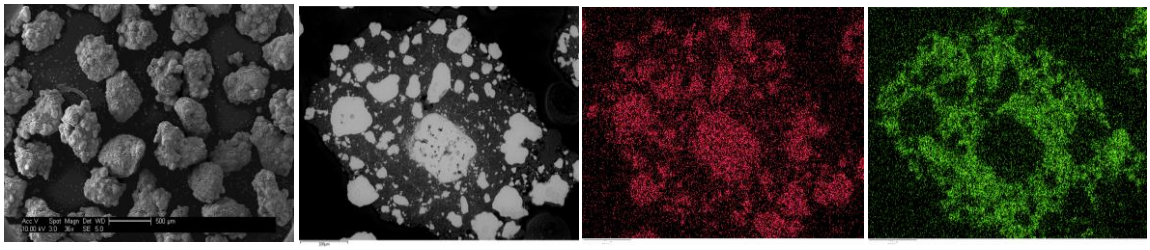

i) ii) iii) iv)

**Figure 4-10 Cu75Al25 i) High resolution SFEG image (scale 500µm), ii) Global particle view EDX, iii) Cu elemental mapping EDX, iv) Al elemental mapping EDX**

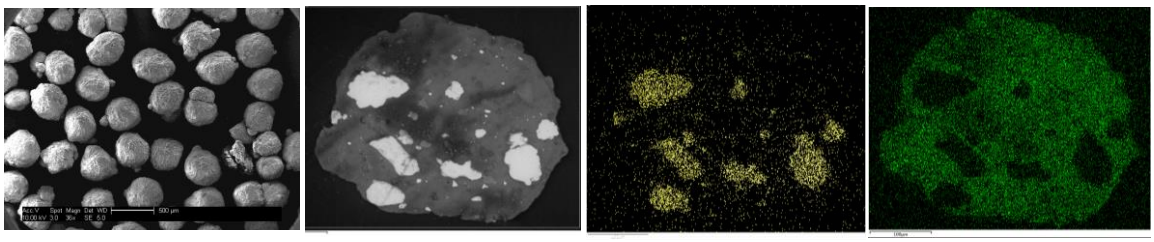

i) ii) iii) iv)

**Figure 4-11 Cu25Ca75 i) High resolution SFEG image (scale 500µm), ii) Global particle view EDX, iii) Cu elemental mapping EDX, iv) Ca elemental mapping EDX**

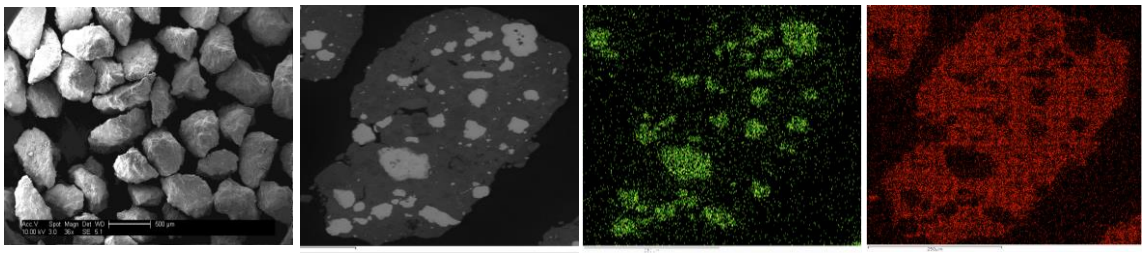

i) ii) iii) iv)

**Figure 4-12 Cu5OCa50 i) High resolution SFEG image (scale 500µm), ii) Global particle view EDX, iii) Cu elemental mapping EDX, iv) Ca elemental mapping EDX**

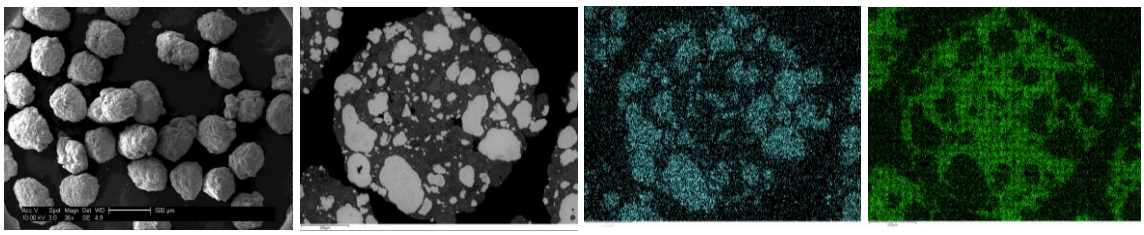

i) ii) iii) iv)

**Figure 4-13 Cu75Ca25 i) High resolution SFEG image (scale 500µm), ii) Global particle view EDX, iii) Cu elemental mapping EDX, iv) Ca elemental mapping EDX**

### 4.3.2 **Carbon monoxide conversion**

The cyclic redox behaviour of the CuO-supported oxygen carriers were assessed in a fluidised bed with twenty-five alternating oxidation ($O_2$ 5%), reduction (CO 10%) and inert cycles at a temperature of 950°C. The CO conversion ($\gamma_{CO}$) as a function of oxygen carrier conversion in the reduction stage ($X_{red,CuO\text{-}Cu}$) is shown in Figure 4-14 for Al300 supported oxygen carriers. In all of the investigations, the reduction step was sufficiently fast to ensure that the CO was consumed by the oxygen carrier and thereby successfully reducing the active phase CuO to Cu. This is confirmed by all the oxygen carriers reaching a ($X_{red,CuO\text{-}Cu}$) of >0.9. For each specific oxygen carrier, the shape of the curve changes in relation to the increased activation or deactivation with accumulating redox cycles. The general trend is followed throughout the investigation where the increased content of active CuO gives an increased CO conversion yield. The general shapes of the curves for each of the oxygen carriers become increasingly horizontal, with a CO conversion yield near to 1. This indicates greater conversion of CO to $CO_2$ with increased CuO content. In cycle 1 of Cu75Al25 it can be inferred that the entire CO entering the fluid bed in the reduction period was converted to $CO_2$. All of the Al300 supported oxygen carriers follow a trend where-by the primary redox cycle exhibits the greatest CO conversion. As the accumulation of redox cycles occur, the gas yield produced, reduces. In Cu25Al75 there is little significance in the difference between he curves in cycle 12 and 25, but both show decreased gas yield compared to the first cycle. It can be observed in the curves of Cu50Al50 and Cu75Al25 that there is a greater difference between cycle 12 and 25, which results in a reduced CO conversion yield. Cu25Al75 was the only particle to not suffer from agglomeration. Due to the full reduction to elemental Cu, in all of the Al300 supported oxygen carriers, the particles with 50% CuO and higher suffered significant agglomeration. High-resolution SEM images of the morphology comparison between Al300 supported fresh prepared particles and those undergone redox investigations are shown in Figure 4-15, Figure 4-16 and Figure 4-17.

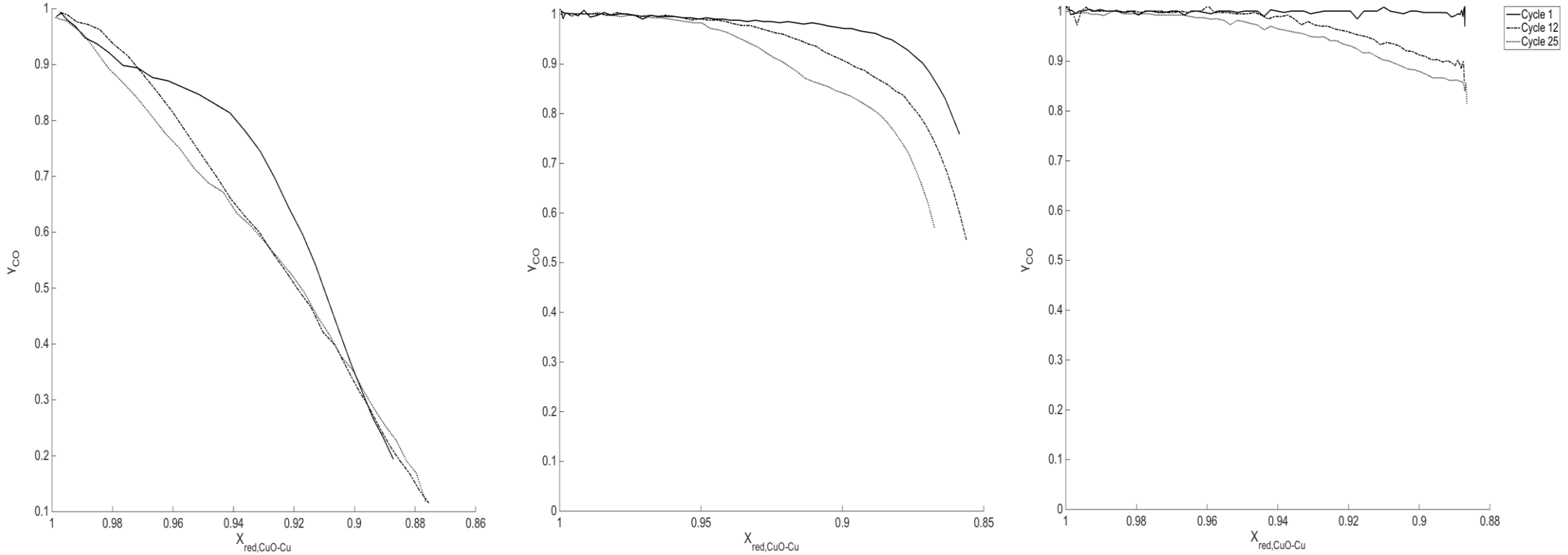


**Figure 4-14 Redox cyclic behaviour over 25 cycles assessed by oxygen carrier conversion against the conversion of CO to $CO_2$ (Left) Cu25Al75, (Centre) Cu50Al50, (Right) Cu75Al25**

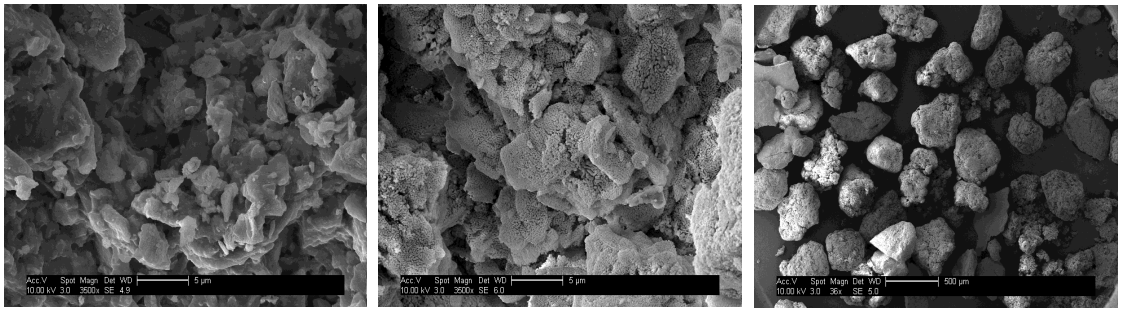

**Figure 4-15 High resolution SEM images showing morphology of Cu25Al75 (left) Fresh produced 5µm, (centre) After 25 redox cycles with CO 5µm (right), Multiple particles after 24 redox cycles with CO 500µm**

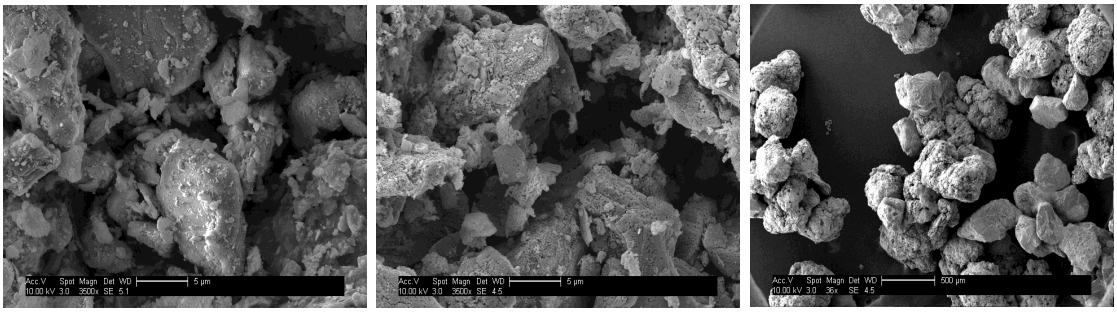

**Figure 4-16 High resolution SEM images showing morphology of Cu50Al50 (left) Fresh produced 5µm, (centre) After 25 redox cycles with CO 5µm (right), Multiple particles after 24 redox cycles with CO 500µm**

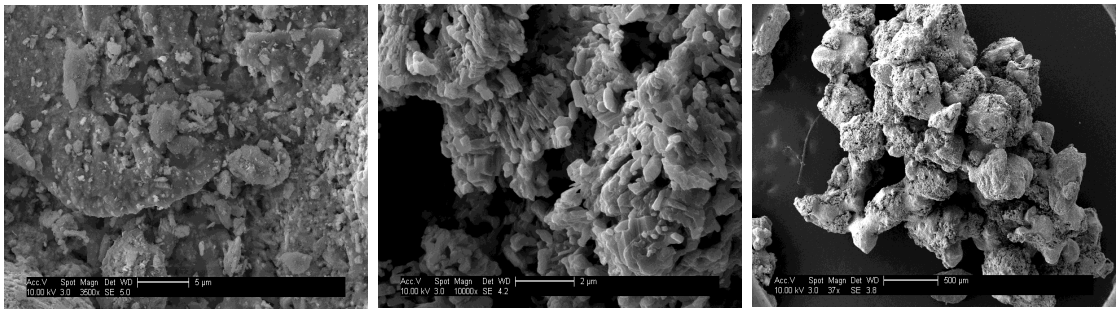

**Figure 4-17 High resolution SEM images showing morphology of Cu75Al25 (left) Fresh produced 5µm, (centre) After 25 redox cycles with CO 5µm (right), Multiple particles after 24 redox cycles with CO 500µm**

The SEM images of the Cu50Al50 and Cu75Al75 taken at 500µm of multiple particles show the extent of the agglomeration of the particles. It is clearly more severe in the oxygen carriers with a higher CuO content. The agglomeration would be detrimental in a circulating fluid bed process. The general comparison in the morphology between the fresh particles and those subjected to the redox cycles shows increased pore size. The decrease in the ability to convert fuel with increasing redox cycles may have been due to particle agglomeration. However, there was little decrease in CO conversion over the redox cycles in Cu25Al75, which did not agglomerate. Fine particulates were recovered at the filter inlet and are an indication of attrition of the oxygen carriers. Cu25Al75 attrite the most with losses of 7.7%. Cu50Al50 and Cu75Al25 had losses of 2.7% and 0.25% respectively.

The cyclic redox behaviour of CaO supported oxygen carriers is shown in Figure 4-18. The CaO supported oxygen carriers follow the same trend as the AL300 supported oxygen carriers where the extent of fuel conversion appears largely due to the ratio of active CuO present in the oxygen carrier. In Cu25Ca75 and Cu50Ca50, the effect of increased fuel conversion with accumulating redox cycles is not as evident as it is in the Al300 supported oxygen carriers. The Cu25Ca75 oxygen carrier improves in reducibility and yield of gas conversion with an in increase redox cycle number. In Cu50Ca50 there is a negligible difference in both reducibility of the oxygen carrier and gas conversion between different cycles. In the Cu75Ca25 oxygen carrier, the effect of subsequent redox cycles is apparent, where ability to convert CO to $CO_2$ is reduced when compared to the $1^{st}$ and $12^{th}$ redox cycles. This oxygen carrier is also subject to severe agglomeration as can be seen in Figure 4-21, whereas agglomeration was observed in the other CaO-supported oxygen carriers, this did not occur to the same extent and did not cause de-fluidisation during the test period.

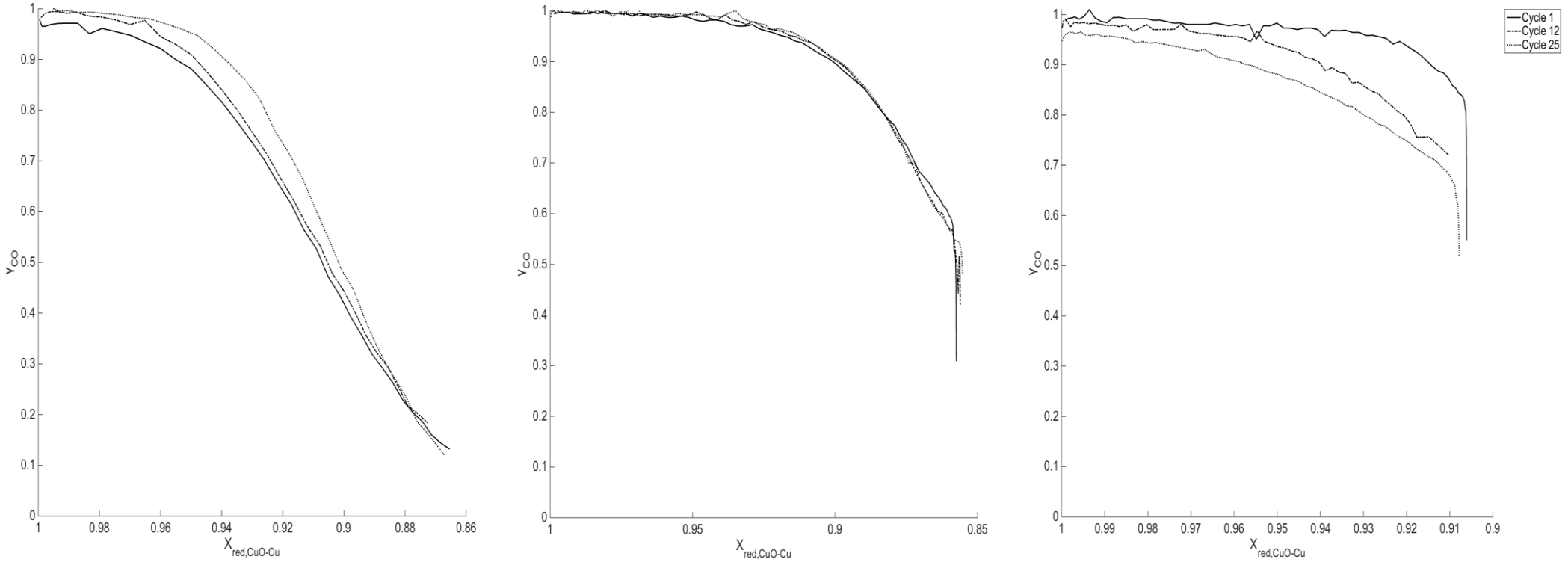


**Figure 4-18 Redox cyclic behaviour over 25 cycles assessed by oxygen carrier conversion against the conversion of CO to $CO_2$ (Left) Cu25Ca75, (Centre) Cu50Ca50, (Right) Cu75Ca25**

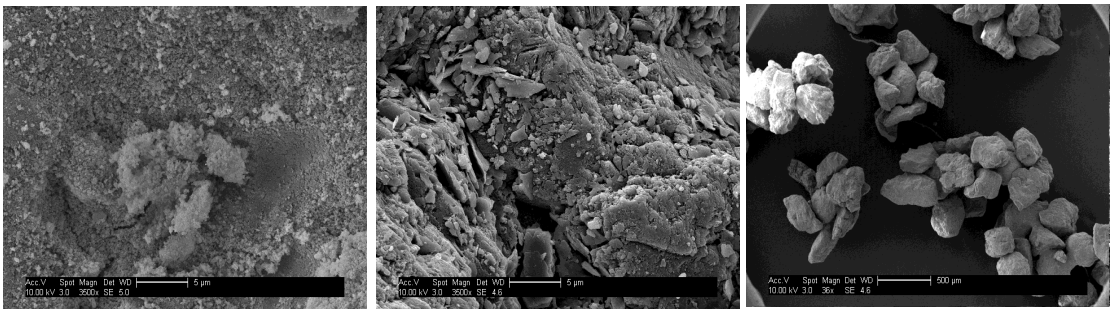

**Figure 4-19 High resolution SEM images showing morphology of Cu25Ca75 (left) Fresh produced 5µm, (centre) After 25 redox cycles with CO 5µm (right), Multiple particles after 24 redox cycles with CO 500µm**

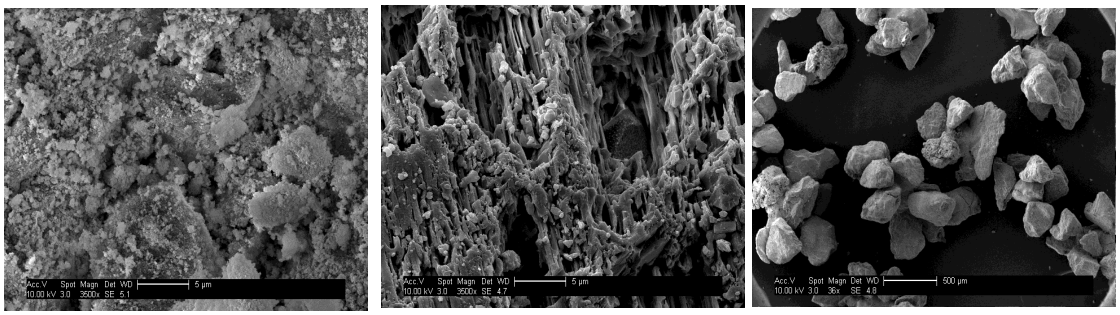

**Figure 4-20 High resolution SEM images showing morphology of Cu50Ca50 (left) Fresh produced 5µm, (centre) After 25 redox cycles with CO 5µm (right), Multiple particles after 24 redox cycles with CO 500µm**

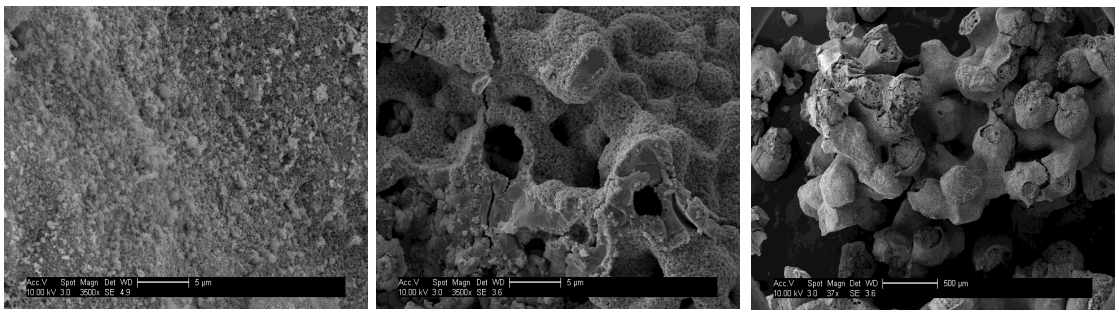

**Figure 4-21 High resolution SEM images showing morphology of Cu75Ca25 (left) Fresh produced 5µm, (centre) After 25 redox cycles with CO 5µm (right), Multiple particles after 24 redox cycles with CO 500µm**

The changes in pore structure and morphology are shown in Figure 4-19, Figure 4-20 and Figure 4-21 for the CaO-supported oxygen carriers. The effect of the accumulative redox cycles is significant. It can be observed in all the CaO-supported oxygen carriers that there is an increase in porosity, where the micro-pores in the fresh samples developed into macro-pores in the used particles. This effect can initially give rise to greater gas diffusion in the oxygen carrier, allowing a greater surface area for gas conversion to take place. However, the formation of the macro-pores eventually leads to a reduction in surface area, and thus a reduced conversion rate, as seen in the Cu75Ca25 oxygen carrier. The CaO-supported oxygen carriers exhibited no attrition, as measured from the fines collected at the particulate filter.

### 4.3.3 **Methane conversion**

Cu25Al75 and Cu25Ca75 were chosen as the most suitable oxygen carriers for a redox investigation with methane as the reducing gas, following the cyclic experiments for the conversion of CO. These oxygen carriers showed minimal agglomeration. The redox behaviour of the two oxygen carriers with methane is shown in Figure 4-22. It is observed that Cu25Al75 was reduced further and yielded a higher conversion of methane in comparison to Cu25Ca75. The methane conversion yield for Cu25Ca75 was minimal and ranged between 15-25%. The curve shows that the reducibility of this oxygen carrier from CuO to Cu was also limited. The Cu25Al25 oxygen carrier conversion to Cu was greater in extent in comparison to Cu25Ca75 (approximately 50%). The reduction was not complete but allowed enhanced conversion of methane over the reduction period. Similarly to the reduction with CO, Cu25Al75 showed a decrease in its performance for reducibility and methane conversion with accumulating redox cycles. This was not observed in Cu25Ca75, where the effect of increasing redox cycles improves these properties, as can be seen with the comparison of the higher methane conversion yield between the 25$^{th}$ and 1$^{st}$ redox cycle.

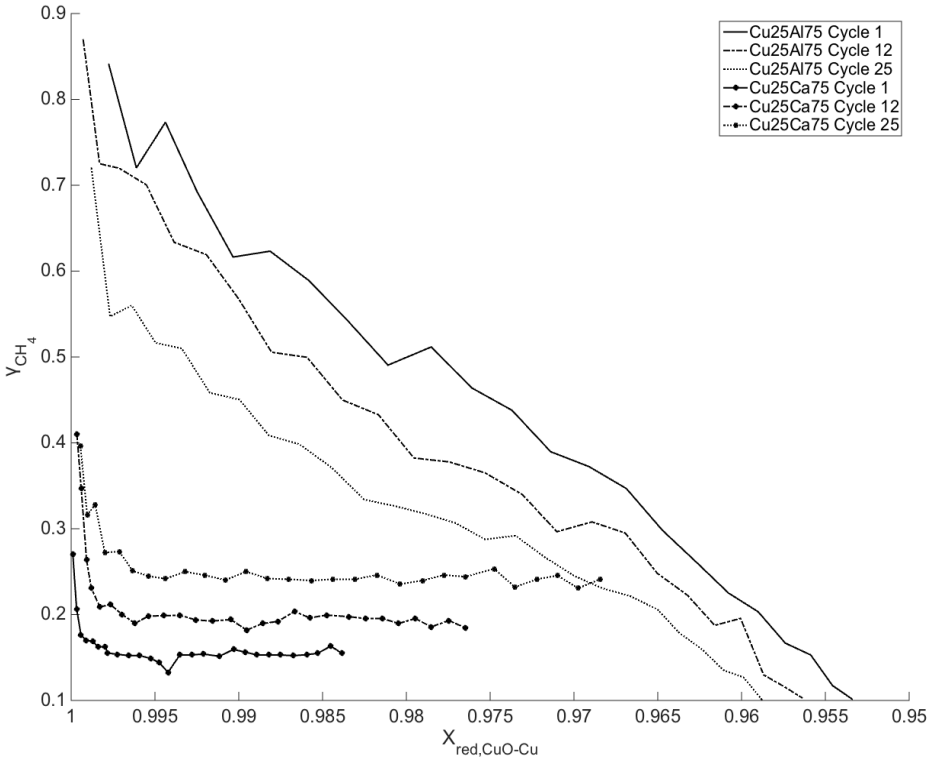


**Figure 4-22 Redox cyclic behaviour of Cu25Al75 and Cu25Ca75 over 25 cycles assessed by oxygen carrier conversion against the conversion of $CH_4$ to $CO_2$**

## 4.4 **Conclusions**

This series of experiments investigates the use oxygen carriers for gaseous fuel conversion produced by the scalable pelletisation method utilising low cost support materials. Copper (II) oxide in varying ratios was combined with either alumina-based cement, or CaO derived from limestone as support material in order to investigate the possible mechanical and chemical improvements. Utilising the ball mill method is only feasible for producing oxygen carriers with the alumina-based supports. Particles produced using this method were not included in the experimental investigation but instead used in the pilot plant investigations. The pelletisation method was suitable for the use of both support materials. The oxygen carriers containing a greater ratio of support material were found to have an enhanced crushing strength. Oxygen carriers comprising

of a 1:4 ratio of support to active CuO, increased their crushing strength by a minimum of 280% compared to a pure pelletised CuO. Elemental analysis showed the distribution of CuO and support material in an oxygen carrier particle, was fairly uniform, but is highly dependent on the size ranges of the materials used in the production stage.

In the fluidised-bed investigations, all oxygen carriers exhibited a high CO conversion yield and were fully reducible from CuO to Cu. In the Al300-supported oxygen carriers the initial redox cycle, had the greatest fuel and oxygen carrier conversion. The general trend saw the decline in conversion as accumulating redox cycles were performed. In the CaO-supported oxygen carriers, this trend was not observed except for Cu75Ca25. This leads to the conclusion that the deactivation over increasing redox cycle numbers is more likely due to the deactivation of the CuO active material as well as its interaction with the Al300 support. All but one of the oxygen carriers suffered agglomeration, and the agglomeration was as expected more evident in carriers with higher ratios of CuO. Oxygen carrier Cu25Al75, which did not suffer from agglomeration, showed the greatest attrition, with a loss of approximately 8% of its initial mass throughout the 25 redox-cycle investigation. The reduction with methane produced a decreased reducibility of the oxygen carriers and gas conversion was limited to 15-25% and 50% for Cu25Ca75 and Cu25Al75 respectively. Cu25Ca75 demonstrated improved conversion, where Cu25Al75 experienced a decrease in conversion with increasing redox cycles, although its oxygen carrier and fuel conversion was consistently greater than Cu25Ca25.

The method of pelletising oxygen carriers with low-cost support material should be quite scalable. The increased crushing strength and sphericity of CaO-based oxygen carriers show that the pelletisation method may be better suited to producing oxygen carriers containing CaO compared to Al300. While the fluid-bed investigations showed that, the chemical interactions between the two materials did not reduce the agglomeration that typically occurs with CuO oxygen carriers. The findings of this work, satisfies the PhD aims and objectives 2b and 2c outlined in chapter 1.

# 5 Development of Cranfield PACT CLC

This chapter introduces the Cranfield PACT facility chemical looping reactor. The design philosophy, configuration and supporting ancillaries are discussed. A component of this research project was to install and commission the reactor and subsequently perform preliminary investigations utilising a synthetically produced oxygen carrier for the purpose of converting gaseous fuels.

## 5.1 **Pilot-plant reactor design**

The Cranfield PACT chemical looping reactor comprises of two identical interconnected circulating fluidised beds (CFB) known as the air and fuel reactors (AR & FR). The riser height of each reactor measures 7.3m tall with an inner diameter of 0.1m. The two reactors lead to a primary and secondary cyclone, each with an inner diameter of 0.17m and 0.085m respectively, which separate the solids from the fluidising gas. The solids are then transported by gravity through a return leg (down-comer) with an inner diameter of 0.04m. In the CLC process, the reaction environments are designed to remain separated, which is achieved by a loop-seal (LS) for each reactor. They also allow an element of control with respect to the quantity of solids transferred. The loop-seals are fluidised with gas in order to transfer the solids to the following reactor. The reactor is constructed in 310-grade stainless steel and is insulated with FibreFrax ceramic wool. The gas distributers in both risers consist of 12 standpipes intended for high gas velocities and a pneumatic flow regime. Figure 5-1 shows a diagram of the 50kW (input) chemical looping reactor, and magnified images of the standpipes in each riser and loop-seal design.

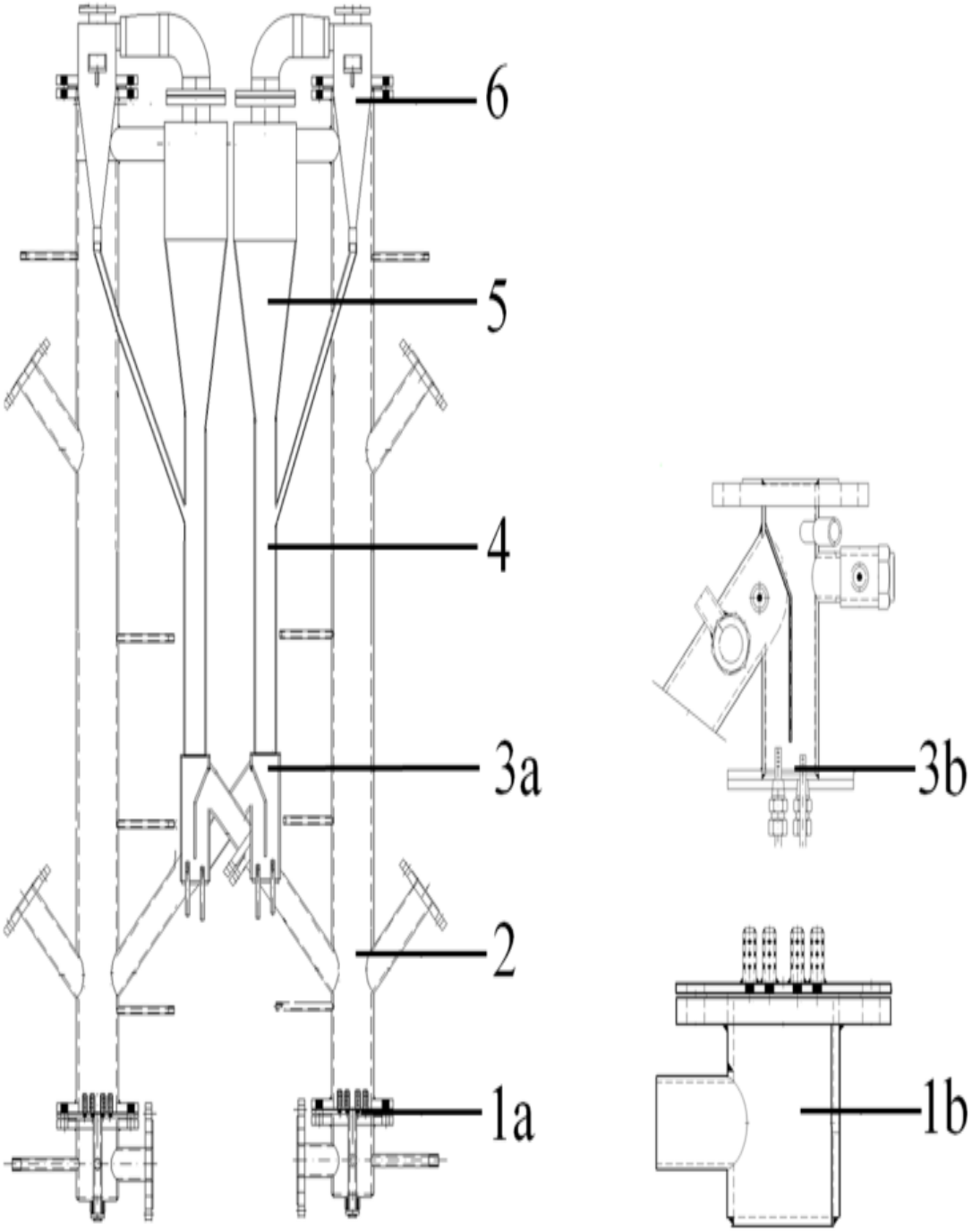


**Figure 5-1 Cranfield dual interconnected CFB design (not to scale) – 1a Distributer nozzles, 1b Wind box and Magnified distributer nozzles, 2 Main riser, 3a Loop-seal, 3b Loop-seal distributer nozzles, 4 Return leg, 5 Primary cyclone, 6 Secondary cyclone**

The heating of both reactors is achieved by trace-heating elements, which are surface mounted to the walls of the reactor, cyclone, return-legs and loop-seals. Each of the elements is rated at 2.2 kW, with each meter section of the CFB risers having two elements mounted to it. Sixteen, single-phase trace-heating controllers, each equipped with a Carel IR33 temperature control unit manages power delivery. Each trace-heating controller manages three trace-heating elements with online analysis of reactor temperature through reactor surface mounted (K-type) thermocouples.

The reactors are supplied gases through a multi-gas manifold equipped with mass-flow controllers with a supply range of 400-100L/min dependent on the specific gas. In the case of the fuel reactor, the gases available include $CO_2$, $N_2$, air and natural gas. The loop-seals are fluidised with $N_2$ and $CO_2$. In the LS following the AR cyclone the inlet is fluidised with air and the outlet is fluidised with $CO_2$. In the loop-seal following the FR cyclone the inlet is fluidised with $CO_2$ and the outlet with $N_2$. This configuration of fluidising gas supply is designed to ensure minimal dilution of gases at the outlet of the cyclones. In addition to the trace heating, the fluidising gases are pre-heated prior to entry into the two wind-boxes of the CFB reactors, in order to improve the reactor's temperature profiles. This is achieved by means of a 12kW and 9kW gas pre-heaters for the air and fuel reactor gases respectively.

The outlets of the primary cyclones from the two reactors are connected to a particulate filtration system. The system consists of two ceramic candle filters, designed to filter particles out below 2µm. The operational strategy of incorporating two filters is employed so, should elutriation of the bed material occur, one filter can be used until its capacity is reacted and then switched over to the second, while the other is emptied.

With the case of utilising natural gas as fuel for conversion in the reactor, any un-burnt natural gas from the process must be combusted prior to venting to the environment. This is achieved through a flare and is inter-connected to the outlet streams from both the air and fuel reactors.

The internal temperatures of the main CFB, return-leg and loop-seals are monitored using (K-type) thermocouples in each of the main riser sections of the CFB they are located approximately every 0.3m up the length of the riser in order to give a comprehensive analysis of the temperature distribution through-out the reactor. Internal pressures of the system are analysed by GMUD MP-S MR-1 pressure transducers from GMH Greisinger. Pressure outlet tapings are located in the wind-box, dense-bed, transition zones, freeboard, cyclone inlet and inlet and outlet of both loop-seals.

Gas composition was analysed at the outlet of each of the cyclones. A trace-heated line ensured the outlet gas stream remained in the gas phase until a condenser unit, from which the dry gas was analysed. Analysis was conducted through two ADC 3000 multi-channel gas analysers, and measure $CO_2$, CO, $CH_4$, $O_2$ and $SO_2$. A gas safety detection system is installed which triggers an alarm should it detect harmful gases such as CO.

The continuous online monitoring of temperature, pressure and gas composition is achieved through a purpose built software utility (LabVIEW) and recorded by a compact-Rio data acquisition system both from National Instruments.

Photographs of the reactor and its ancillaries during their installation can be found in appendix A.

## 5.2 **Operation strategy analysis**

A simplified process flow diagram of the 50kWt PACT CLC facility is shown in Figure 5-2. The CLC system is constructed in a configuration of two interconnected CFBs. This design was chosen due to the relative maturity of CFB technology and its applicability towards fuel flexibility and particulate and emissions control. The height of the CFB riser promotes long residence times and improved gas-solid mixing. Dual CFBs are also relatively easier to scale-up to larger systems compared to bubbling and moving bed variants (Adánez et al., 2012).

### 5.2.1 **Operational Constraints**

The inherent difficulty in the design of the system with respect to operation is the control of solid circulation between the two reactors. Assuming no requirement for the additional make-up oxygen carrier material, maintaining stable and balanced operation requires the solid flow transferred from the AR to the FR (m2 in Figure 5-2) to be equal to the solids flow transferred from the FR to the AR (m1 in Figure 5-2). The difficulty in controlling this arises from the two different reactions occurring in the AR and FR. The transfer of solids would be determined by the temperatures in the reactors, specific particle properties (size, density and sphericity), and the fluidising gas properties such as density and viscosity.

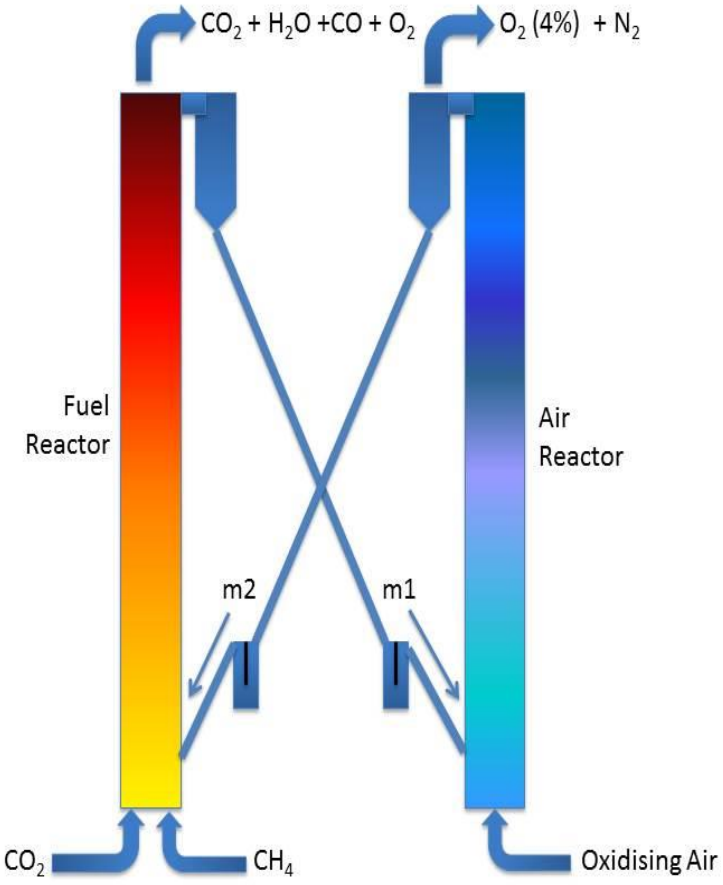


**Figure 5-2 Simplified flowchart of PACT CLC reactor**

In order to determine the best strategy to operate the PACT CLC system, a heat and mass balance has been conducted. The calculations considering the reactions of chemical looping with oxygen uncoupling with methane as the fuel gas and a copper-based oxygen carrier (60%CuO and 40% $Al_2O_3$) was used with the following assumptions:

- Formation of combustion products $CO_2$ and $H_2O$ is stoichiometric with respect to the input fuel and therefore complete.
- All $O_2$ is consumed in the fuel reactor
- The heat carried by the oxygen carrier support is not taken into account as it is inert and considered equal in terms of mass in and out
- The particle size distributions in the two columns are assumed to be the same, even though the particle size may in fact change during the oxidation/reduction reactions as well as changing with time due to attrition

The difficulty in operation is explained by an understanding of the basic heat and mass balance of the system. With the pre-set conditions of 50kW input of electrical heating and heat of combustion of methane, a mass flow rate of 5.03$Nm^3$/h of methane and 47.6 $Nm^3$/h of air are ideally required. In a hypothetical scenario assuming a bed temperature of 800ºC and 4% excess air, the corresponding gas velocity to be expected in the AR is 5.48m/s. Taking into account of the differences in density of the flue gases in the AR (majority $N_2$) and in FR ($CO_2$ and $H_2O$) it is estimated that an additional 22.74 $Nm^3$/h of $CO_2$ is required in order to balance the solid transfer between the two reactors. It would be ideal to recycle the flue gas from the FR, but in real operation of the system we can simply supply the additional required $CO_2$ in order to operate equivalent fluidisation conditions.

An additional advantage to recycling of the $CO_2$ in this system is to decrease the equilibrium partial pressure of oxygen in the fuel reactor. This further enhances the CLOU effect, in the release of gaseous oxygen from the copper-based oxygen carrier. With respect to the conversion ratio of the oxygen carrier, a

circulation rate of 120 kg/h to 240 kg/h is required for conversion ratio of 1 and 0.5 respectively.

In the first case the system as a whole (AR+FR) was considered in the heat and mass balance calculations. The Input streams were air and methane, while the exit streams consisted of 4%/vol $O_2$, $N_2$, $CO_2$, $H_2O$. The bed temperature was set at 900°C. It was calculated that approximately 30kJs$^{-1}$ of heat is required to be removed from the system as a whole.

In the second case, the heat and mass balance of the AR and FR were treated separately. It was calculated that without $CO_2$ recycle, the FR will require removal of 7.89 kJs$^{-1}$ of heat. This can be somewhat reduced as it is possible to supply $CO_2$ at room temperature. It was calculated that 12.1 kJs$^{-1}$ of heat would be required to heat up the $CO_2$, which could be facilitated by the reactors external heaters.

The situation for the AR is not so simple, due the reactor experiencing the strong exothermic reaction of oxidation of the oxygen carrier, it was calculated that approximately 22 kJs$^{-1}$ of heat must be removed. The dissipation of heat through the reactor walls can only account for 1 kJs$^{-1}$ heat loss due to the two surrounding adiabatic furnaces. In the current configuration, there is no available heat surface from which to extract heat. The comparisons between the heat balance of the system as a whole and individual reactors are supportive and shows an error percentage of 1% calculated for the heat required for dissipation.

### 5.2.2 **Feasible operation strategies**

With the consideration of the operational limitations discussed previously and the mandatory safe operation, the CLC reactor will be required to decrease its thermal input to 20 kW. With this quantity of heat input, the heat released during operation will be limited and manageable.

The alternative strategy is to increase the transfer of solids from the AR to the FR in order carry excess heat from the AR to the FR. In principle this strategy could be potentially deployable, but there are some limitations. This method of

operation requires there to be a difference in temperatures between the two reactors. The fuel reactor must be operated above 900ºC in order for the CLOU process to occur which is determined by the FR's oxygen partial pressure. If the AR is operated at elevated temperatures above 900ºC, this is a risk to the copper-based oxygen carrier due to its low melting point, and can agglomerate (Cho, Mattisson and Lyngfelt, 2004). Additionally, the system is limited physically through the maximum carrying capacity of the fluidised gas. Hypothetically, if the duel bed systems were operated at conditions where the fluidising gas carrying capacity was saturated, the facility would have to manage 839 kg/h of circulating solids, which is a vast handling requirement. This is also excessive considering 600 kg/h of the circulating solids are surplus to the requirements of fuel conversion. If the target of 100ºC temperature variation is between reactors sought, the excess solids can only transfer the maximum of 6kW of heat to the FR, which is insufficient.

## 5.3 **PACT facility commissioning**

A commissioning program was conducted on the PACT CLC reactor in order to have the reactor operating and responsive. A significant issue in reactor start-up is that the capacity of the preheating system is not sufficient for a simple heating strategy. Several adjustments have been made; the addition of a methane lines into the wind box in each riser to heat the system by combustion from the heat of the flue gas. In order to achieve this strategy, the system must reach an ignition temperature of 725ºC. Further modifications that were required include the changing the electrical heater and gas pre-heater control units to permit the maximum output, increasing the thickness of the insulation, and adding extra preheater elements.

Following this work a detailed start-up and shut down procedure was developed (appendix B). The ignition test was successful and the pressure and temperature profiles are shown in Figure 5-3 and Figure 5-4.

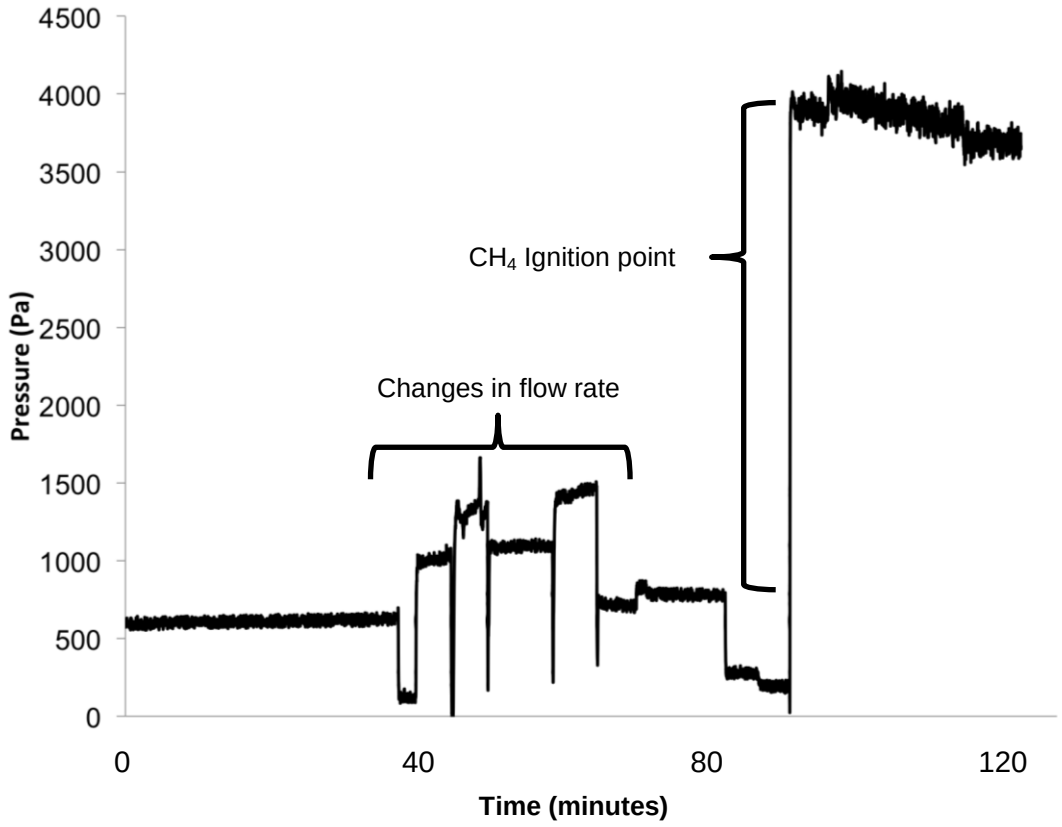


**Figure 5-3 Wind box pressure at ignition during commissioning test**

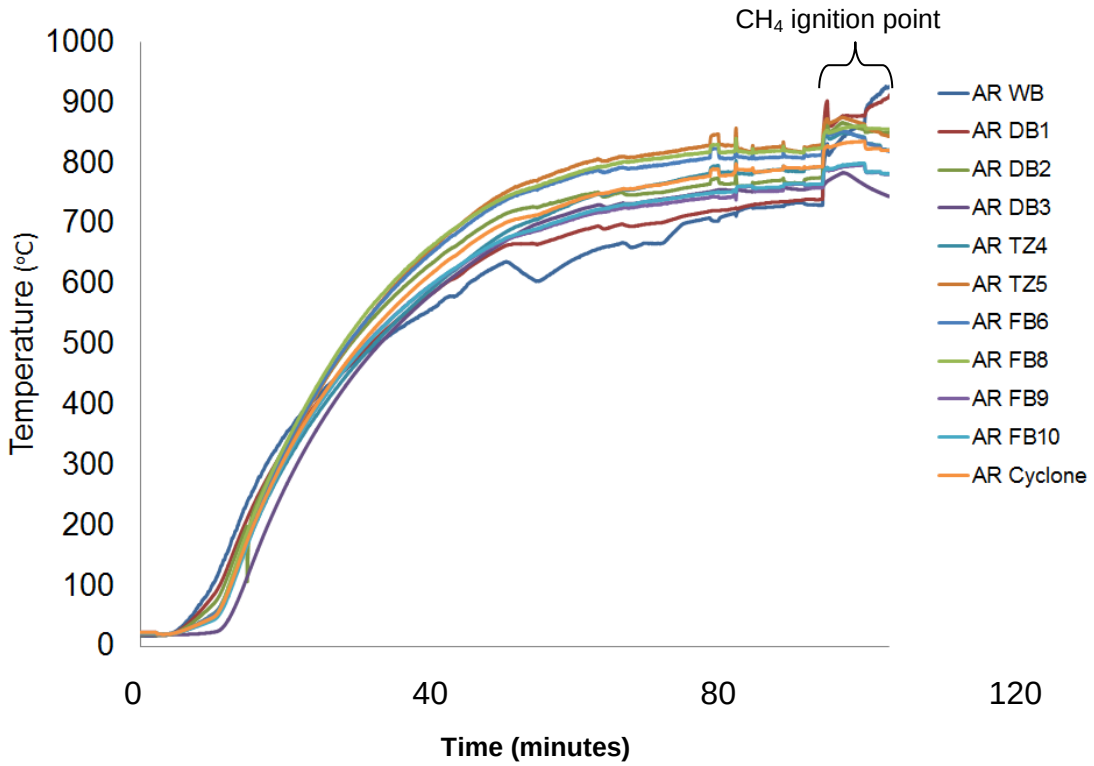


**Figure 5-4 Air reactor temperature profile at ignition during commissioning test**

A commissioning test utilising a single reactor operating as a bubbling-bed was conducted using oxygen carrier (60%CuO40%$Al_2O_3$) and sand mixture (0.5kg oxygen carrier with 4.5 kg sand) as the bed inventory.

To conduct the redox cycles a strategy of switching between oxidising and reducing atmospheres were attempted and the gas analysis results of this test are shown in Figure 5-5.

The redox phases and conditions are shown in Table 5-1. Oxidation phase was performed with air as oxidising gas. Following an undefined period of oxidation, the gaseous conditions in the system were switched to the inert gas phase, with $CO_2$ in order to purge the system of any oxidising gas. This was performed for 120s. Following the inert/purge gas phase, $CH_4$ was injected into the system with $CO_2$ for the reduction step.

**Table 5-1 Gas conditions for bubbling-bed commissioning test**

| Gas | $Q_{gas}$ *L/min* | $U_{gas}$ *m/s* | Cycle Phase |
|---|---|---|---|
| Air/$CH_4$ | 120/5 | 1.10 | Start-up/ Ignition |
| Air | 120 | 1.05 | Oxidation |
| $CO_2$ | 120 | 1.05 | Purge/ Inert |
| $CO_2$/$CH_4$ | 130 | 1.13 | Reduction |

The multi gas analysis of the commissioning test shows inconsequential impact with respect to the conversion of methane by the oxygen carrier due to the volumes of gas and the small quantity of oxygen carrier. However, it can be seen in the mass based conversion of the oxygen carrier that, it proceeded to become fully reduced in the reduction phase (methods on the calculation of fuel and OC conversion are detailed in Chapter 3). From physical and visual inspection, the mechanical strength of oxygen carrier after reaction had improved and XRD spectra shows no interaction with the support (appendix C).

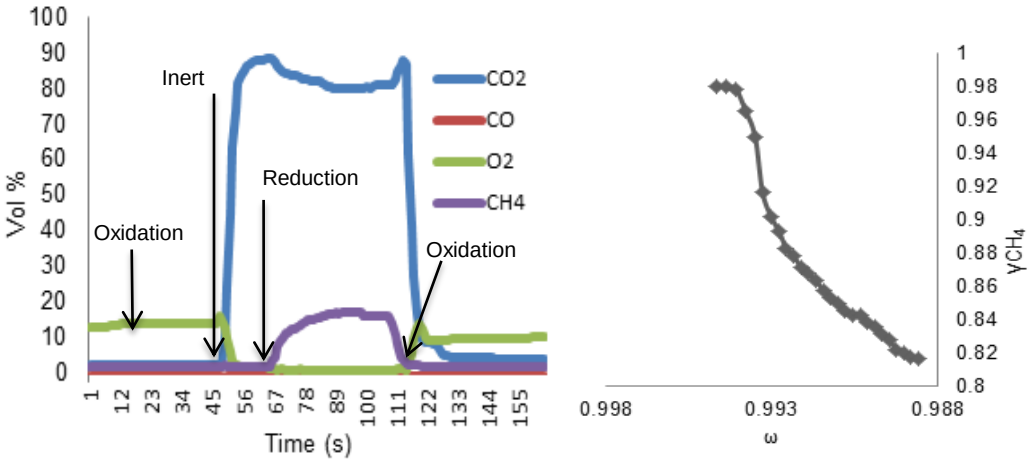


**Figure 5-5 (Left) Gas analysis during one reactor operation (Bed temperature: 850-880 °C) / (Right) Mass-based conversion of oxygen carrier and conversion of $CH_4$**

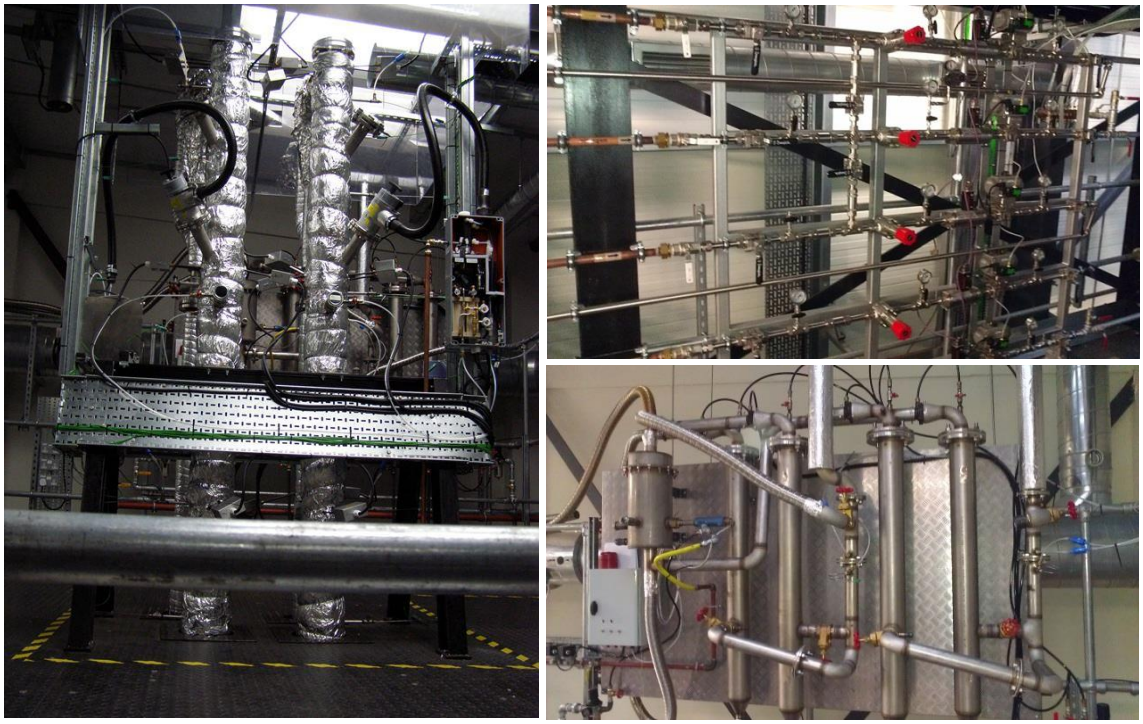

**Figure 5-6 Installed PACT CLC facility (Left) Top of risers of dual CFB (Top Right) Multi-gas supply manifold (Bottom Right) Particulate filter system and flare**

Figure 5-6 shows the commissioned PACT CLC reactor system. The commissioning of the system in a configuration of a single bubbling bed mode presents some operation issues. Maintaining a stable bed temperature is difficult and requires fine control of the ignition of methane. In principle, getting the reactor up to operating temperature can be achieved, but the introduction of cold bed material, decreases the reactor temperature significantly. In order to achieve the required temperature, in the current configuration solids have to be added in small quantities, (<250g) in a single delivery. As a result of these difficulties, a feed hopper mechanism was designed for the supply and make up of bed material (appendix A).

## 5.4 **Operation of PACT CLC in CLOU with Cu-based oxygen carrier**

Following the commissioning phase, the reactor had been operated for a total time of 30 hours under hot conditions. Two methane lines were used to aid temperature control in addition to the electrical heaters, which helped maintain appropriate temperatures. Inert bed material (molochite) was first introduced into the system to validate the control of solid transfer between the two beds. It had become apparent from the hot circulation tests with molochite, that the separation efficiency of the cyclones was not adequate. It was deemed necessary to modify the inlet aperture of the cyclone as to reduce its area and increase the velocity fluidising gas and thereby enhancing the cyclonic effect (Appendix A).

As a consequence of these required modifications, a single bed test was conducted to investigate the behaviour oxygen release of copper-based oxygen carriers. The investigation utilised 7kg oxygen carrier (60%CuO/40%$Al_2O_3$) produced by the ball mill method (detailed in chapter 4) was gradually loaded into the system to test the oxygen releasing performance in inert atmosphere for 30 minutes in bubbling bed mode.

An obvious oxygen releasing stage was observed, as is shown below in Figure 5-7. The figure shows clear oxygen uncoupling (CLOU) behaviour from the copper-based oxygen carrier when heated in the inert ($CO_2$) atmosphere. However, these tests also showed that the oxygen carrier particles prepared using the ball mill were not robust enough to survive the fluidised-bed conditions for extended periods. During operation considerable elutriation was observed confirmed from the loss of pressure head in above the gas distributor and wind-box and build in pressure down-stream. Furthermore, some agglomeration took place at 950$^{o}$C, which indicates the operating condition for the produced copper-based oxygen carrier is quite narrow in terms of temperature. The agglomerated particles and damage to the gas distributor are shown in Figure 5-8. The agglomeration of copper-based particles is a risk inherent to its low

melting point. The heating strategy of feeding fuel and air into the wind-box will have caused the agglomeration occurrence to happen more readily.

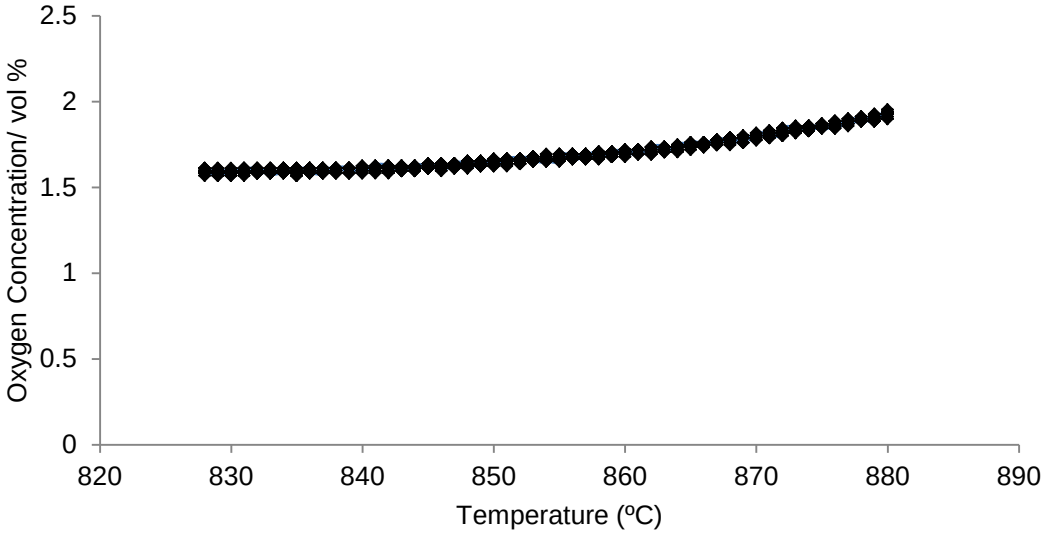


**Figure 5-7 Oxygen releasing with the temperature (total duration: 30mins)**

**Figure 5-8 Agglomerated copper-based oxygen carriers fused to the gas distributor**

# 6 Hydrodynamic investigation in a cold-flow model for CLC

This chapter describes the investigation for the hydrodynamic study of a representative cold-flow model of the Cranfield PACT facility CLC reactor. The aim of the investigation is to better understand the operational strategies required for dual-CFB operation. As discussed previously, a limitation of this design is that the circulation rate of solids between the two reactors is determined by pneumatic transport. Studying the systems hydrodynamics can aid the development of a better comprehensive strategy towards operation and optimisation of the corresponding PACT CLC reactor. The investigation and results detailed in this chapter aim to satisfy the PhD objectives 1a and 1b.

The investigation and results described in this chapter have been accepted for publication as a journal article in Energy Technology.

Haider, S.K., Duan, L., Patchigolla, K., Anthony, E.J. (2016) 'A hydrodynamic study of a fast-bed dual CFB for chemical looping combustion' *Energy Technology* (Revised version accepted 26/04/2016)

## 6.1 **Cold-flow model design**

The use of hydrodynamic modelling for the scale up of fluidised-bed reactors, can allow the investigators to predict and formulate operational strategies, which can be implemented in a corresponding hot-operated reactor.

Classically, cold-flow model (CFM) reactors are developed using scaling criteria and typically are reduced in size compared to the larger reactors, which they aim to simulate. The advantage to producing smaller scaled systems lies within the cost saved for the production and operation of the model. The scaling criterion for non-dimensionless parameters allows one to directly correlate the results from a small-scale system operated at ambient conditions to a larger scaled system operated at reaction conditions. A CFM can be produced from a transparent material (acrylic or plastic) in order to allow for ease of view of the fluidisation behaviour occurring inside the system. The CFM described in this

investigation is not reduced in size, but instead is of 1:1 scale to the Cranfield PACT CLC reactor and sharing the same dimensions for the wind-box, gas distributor, cyclone, return legs and loop-seals (details described in chapter 5). The major difference between the two systems is there are no additional off-take flanges, view-ports or secondary cyclone as is present on the CLC reactor. The return leg on the CFM is constructed from a re-enforced flexible tube; with an ID of 0.04 m. Components of the CFM are shown in Figure 6-1. The intention is to operate the facility as a dual fast-bed reactor. Considering this mode of operation, the decision to build the CFM at a 1:1 scale to the CLC reactor is beneficial. A 1:1 scaled system can reduce the possible gas/particle wall friction effects which may have be unavoidable should the model be decreased in scale. This approach of like for like scaling has been successfully employed previously by Bischi et al.

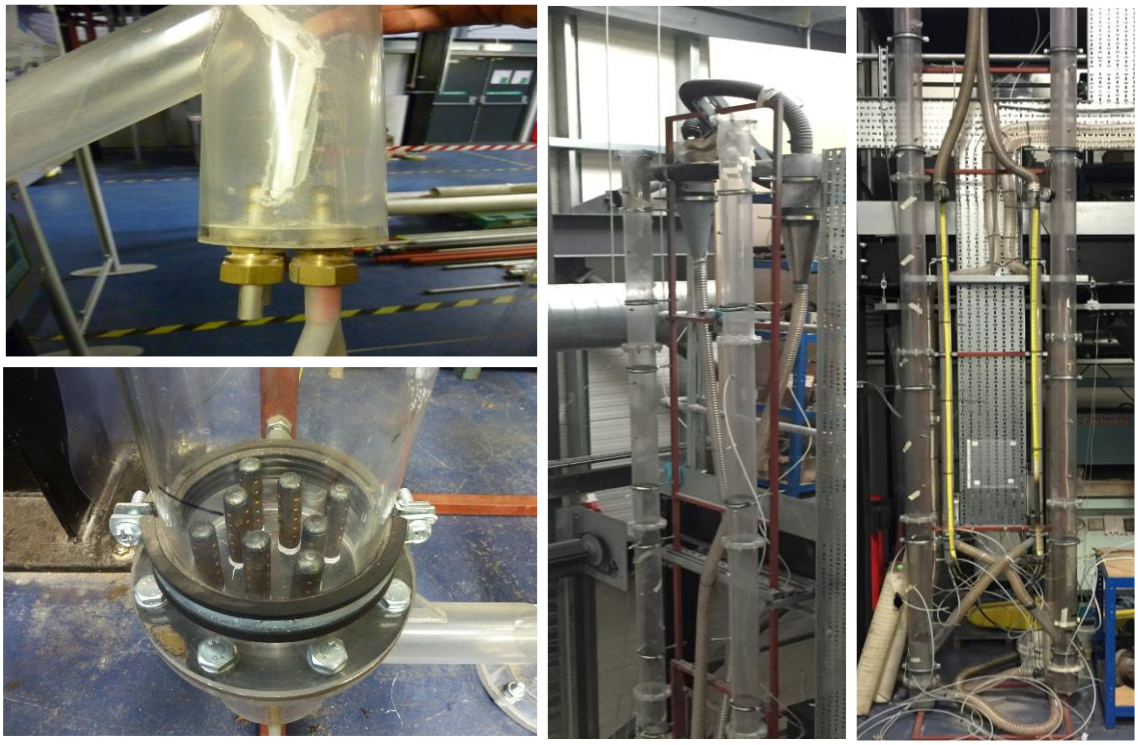

**Figure 6-1 Components of CFM (bottom left) gas distributor (top left) loop-seal (centre) Top of CFB risers and cyclones (right) Lower section of CFB and return legs and loop-seals**

## 6.2 **Methodology**

When utilising a 1:1 scaled CMF for the scale up of fluid beds, the necessary criteria of dimensionless parameters requires accurate scaling in order to allow the data to be transferable towards the corresponding reactor. At this scale, the choice of fluidising gas and the intended flow rates required determines that compressed air is the only viable option with respect to laboratory constraints. With the dimensions of the CFM fixed and air considered as the fluidising gas, the scaling parameters dictate (Equation 2-6) that particle diameter and density must be scaled to satisfy Glicksman scaling laws. In this case two different particles were chosen as bed material; molochite ceramic particles from Imerys supplied by Castree Kilns and Metallic iron particles (FE100) from William Rowland UK were determined to be suitable bed materials for use in the investigation. The operational conditions of the CLC reactor and the CFM are shown in Table 6-1. It is clear that the molochite particles share a similar density (1400 kg/m$^3$) to the oxygen carriers to be utilised in the CLC reactor (1800 kg/m$^3$). While the FE100 particles are far denser (5818 kg/m$^3$). According to the scaling laws, the FE100 show suitable similarity to the dimensionless parameters from the CLC reactor as shown in Table 6-2. The scaling laws have been implemented in such a way that complete equality was not reached, but the simplified scaling laws shown in Table 6-2 were applied using the conditions from Table 6-1 it was possible to obtain sufficient dynamic similarity and maintain reliability. This serves to allow one to utilise the CFM to control solid flow, determine how much can be transferred in a certain time and how to avoid leakage. Then using the scaling criteria one can determine the circulation rate ($G_s$) in the CLC reactor. The $G_s$ of the CLC unit was calculated from the solids required, based on 20kW operational input heat as a base case requirement for the operation of the CFM. In the modelling of CLC reactors the AR and FR have different operational requirements. In the system described here, the only feasible operational strategy requires the balance of solids transferred between both reactors that could be achieved through CO2 recycle in the FR. As a consequence the AR and FR are treated with the same conditions in this study.

**Table 6-1 Operational conditions of CLC vs CFM**

| Condition | CLC Unit | CFM with FE100 | CFM with molochite |
|---|---|---|---|
| Temperature (K) | 1123 | 293 | 293 |
| Solid density, $\rho_s$ (kg/m$^3$) | 1800 | 5818 | 1400 |
| Gas density, $\rho_g$ (kg/m$^3$) | 0.314 | 1.202 | 1.202 |
| Gas viscosity, μ (Pa·s) | 4.50*10$^{-5}$ | 1.82*10$^{-5}$ | 1.82*10$^{-5}$ |
| Particle diameter, dp (×10$^{-6}$ m) | 300 | 60 | 519 |
| $U_{mf}$ (m×s$^{-1}$) | 0.03 | 0.01 | 0.16 |
| Pressure (atm) | 1 | 1 | 1 |
| Inner diameter, D (m) | 0.1 | 0.1 | 0.1 |
| Fluidisation velocity, $U_0$ (m×s$^{-1}$) | 2 | 2 | 2 |
| $U_{mf}/(gD)^{0.5}$ | 0.031 | 0.01 | 0.161 |
| $Fr=(U_0-U_{mf})/(gD)^{0.5}$ | 1.99 | 2.01 | 1.86 |
| $G_s$ (kg/m$^2$/s) | 3.3 | 2.56 | 10.7 |
| dp/D (×10$^3$) | 3.000 | 0.6 | 5.19 |
| $\rho_g/\rho_s$ (×10$^4$) | 1.7 | 2.1 | 8.6 |
| $Re=\rho_g U_0 dp/\mu$ | 4.2 | 7.1 | 68.5 |
| $Ar=\rho_g\times(\rho_s-\rho_g)\times g\times(dp^3)/\mu^2$ | 22 | 45 | 6961 |

**Table 6-2** CFM similarity with Glicksman scaling laws

| Condition | CLC Unit | CFM with FE100 | CFM with molochite |
|---|---|---|---|
| $U_0/ U_{mf}$ | 66 | 206 | 143 |
| $\rho_s/ \rho_g$ | 5733 | 4840 | 1165 |
| $U^2_0/(gL)$ | 4.08 | 4.08 | 4.08 |
| $G_s/(\rho_s U_0)$ | 9.17x10$^{-4}$ | 9.17x10$^{-4}$ | 9.17x10$^{-4}$ |

### 6.2.1 **Experimental procedures**

The pressure of the CFM was measured over the course of the investigation. Points of measurements were located in the wind-box, loop-seal outlet, dense bed, transition zones, and the length of the riser in the free board zones. Twenty GMH-Greisinger GMUD MP-S MR-1 model transducers were used to measure

these pressures. The points of measurement are often interchanged throughout the course of the investigation, and the heights at which they are located relative to their height above the wind-box distributor are detailed in the following results section (6.3). The pressure data allowed the determination of minimum fluidisation velocity ($U_{mf}$), transport velocity/fast fluidisation ($U_{tr}$) and the density profiles in both of the CFB risers. The solid circulation rate ($G_s$, kg/m$^2$/s) was calculated at varying static bed heights and fluidising gas velocities. It was measured during stable fluidisation behaviour subsequently halting the fluidising gas to the loop-seals. The bed height of the accumulated solids in the return leg above the loop-seal was measured over a given period of time.

Reactor to reactor bypass leakage was determined by introducing $CO_2$ as a trace gas to the inlet of the fuel reactor loop-seal and measuring any corresponding trace $CO_2$ at the outlet of the fuel-reactor cyclone, which was measured by a pre-calibrated ADC MGA 3000 multi-gas analyser with a $CO_2$ range of 0-40%. The $CO_2$ leakage ratio ($LR_{CO2}$) is defined as Equation 6-1. $P_{CO2}$ is the measured $CO_2$ at analysis point (vol%), $Q_{riser}$ is the flow rate the riser (L/m), $Q_{LS}$ is the flow rate of $CO_2$ in the loop seal (L/m). These indicators were used as to measure any possible dependence on leakage with loop-seal bed height. The measurements analysed by the pressure transducers and gas analyser during the course of the investigation were recorded by a TC-08 data-logger from Pico Industries and accompanying software suite for process monitoring.

$$LR_{CO_2} = P_{CO_2} \cdot Q_{riser} \frac{100}{Q_{LS}} \qquad \textbf{Equation 6-1}$$

## 6.3 **Results and Discussion**

### 6.3.1 **Minimum fluidisation and transport velocities**

The resistance co-efficient of the riser's gas distributer was measured by determining pressure drop above and below the distributer with varying gas velocities. Once this had been determined, the riser was filled with solid particles to a bed height of 550 mm. A step-wise increase in gas velocity (upstream) was applied to the bed material until fluidisation was observed and then decreased step-wise (downstream). The pressure curves for the molochite and the FE100 particles are shown in Figure 6-2 and Figure 6-3 respectively. The downstream curves were utilised to determine $U_{mf}$, which were estimated as 0.11 m/s and 0.023 m/s for the molochite and FE100 particles respectively. It can be seen that there is a clear and noticeable difference when comparing the upstream curves of the two particles. Whilst molochite displays smooth transition into fluidisation, the FE100 particles shows an overshoot of pressure drop when changing into the incipient fluidising regime. This was also visually observed by a sudden increase in bed height in the upstream and whilst a smooth transition was observed when decreasing the fluidising gas velocity.

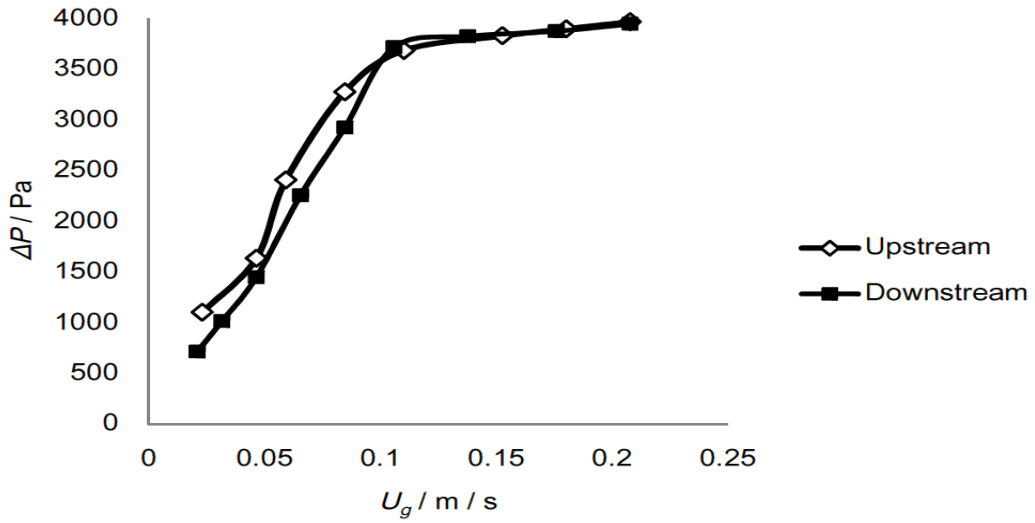


**Figure 6-2 Minimum fluidisation velocity of molochite**

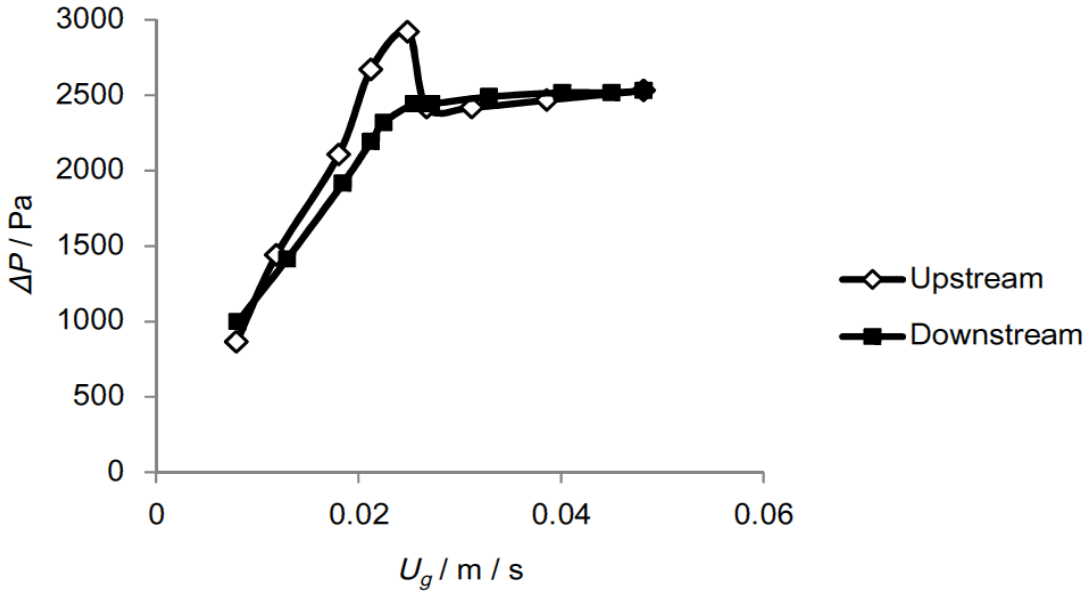


**Figure 6-3 Minimum fluidisation velocity of FE100**

The pronounced hysteresis seen in Figure 6-3 is indicative of Geldart group A particles which typically exhibit greater particle-particle cohesion (Geldart, 1973). The specific position of the molochite and FE100 particles employed in

this study in context to Geldart classifications are shown in Figure 6-4. It can be seen that while both classifications define the particles as group B, FE100 particles are located in close proximity to the particle A/B border and exhibit group A properties with respect to particle cohesion. The transport velocity $U_{tr}$ was determined by visual observation of particles dropping from the cyclone to the return leg, coupled with the pressure drop of the bed, the transport velocity was determined to be 1.70 m/s and 1.38 m/s for molochite and FE100 respectively which is quite close to the theoretical value obtained by calculation Bi and Fan 1991, which is 1.75m/s (Yang, W.-C., 2003).

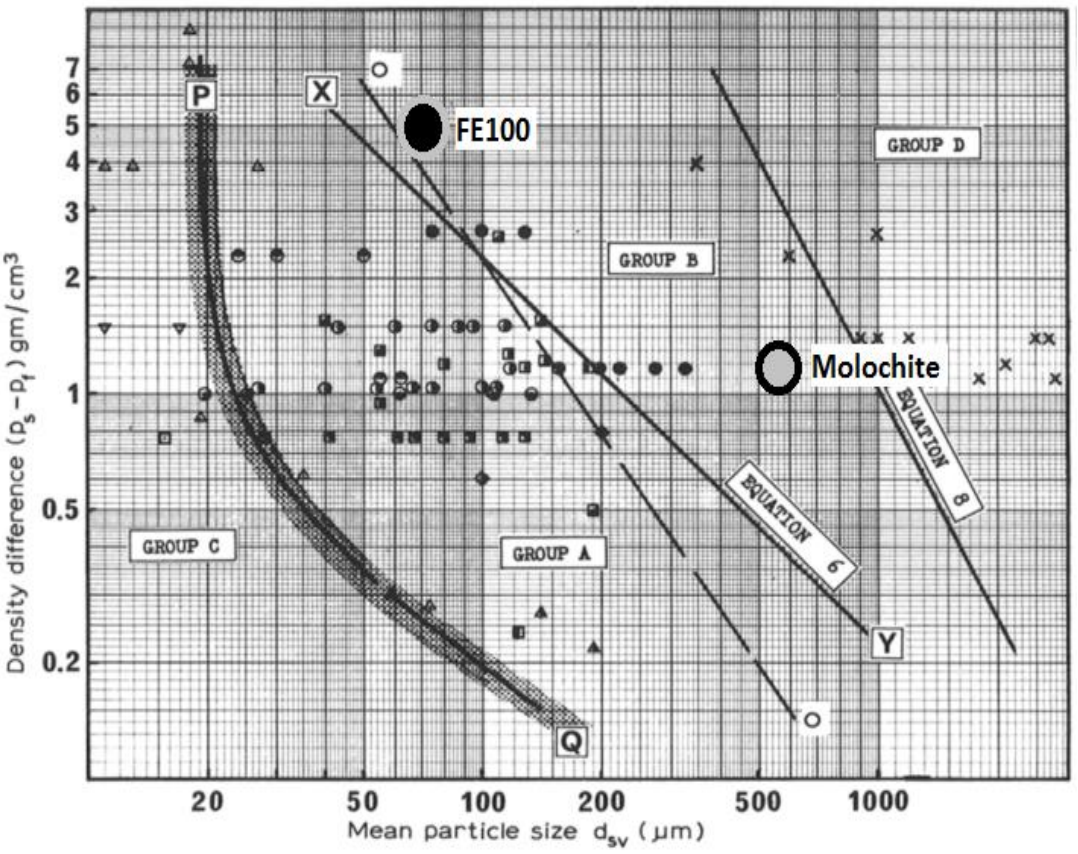


**Figure 6-4 Geldart particle classification of molochite and FE100 (Adapted from(Geldart, 1973))**

### 6.3.2 **Density profiles at varying velocities**

The density profiles with varying fluidisation velocities for molochite and FE100 are shown in Figure 6-5 and Figure 6-6. The general trends with both particles employed, are that the solid concentration ($\xi_s$) decreases as the height of the riser increases. In the case of molochite, at velocities below $U_{tr}$, the solid concentration is near 0.55, similar to that in a bubbling bed. As gas velocity increases, molochite particles are increasingly carried out of the dense bed and enter the freeboard. At velocities just above $U_{tr}$, (1.7 and 1.9 m/s) at a height of 0.45m, the bed has a greater solid concentration (0.1) when compared to the solid concentration of 0.07 corresponding to increased fluid gas velocities (≥2.1 m/s). At the height of 0.75m, this solid concentration decreases for velocities close to $U_{tr}$ indicating that this region is the source of where most particles are elutriated.

In the case of the FE100 particles, the elutriation zone is higher than compared to that of molochite. At a height of 0.75m the bed has a greater solid concentration for velocities greater than $U_{tr}$, particles are carried out of the dense phase at greater height between 0.75 and 2m. This could be attributed to the shorter static bed height where gas hold up is limited in shorter beds. The density profile of FE100 shows an increase in density at the very top of the riser. Due to the particles high density and small diameter, the wall effects became important at this height as particles hit the top of the riser before being finally carried through to the cyclone.

The pressure profiles of both the AR and FR risers at steady state conditions are shown in Figure 6-7. It can be seen that for varying fluidising velocities, the pressures in both reactors are very similar. This indicates that the solid exchange between the two reactors can be maintained in stable operation despite the fact that the solid handling is controlled through pneumatic transport.

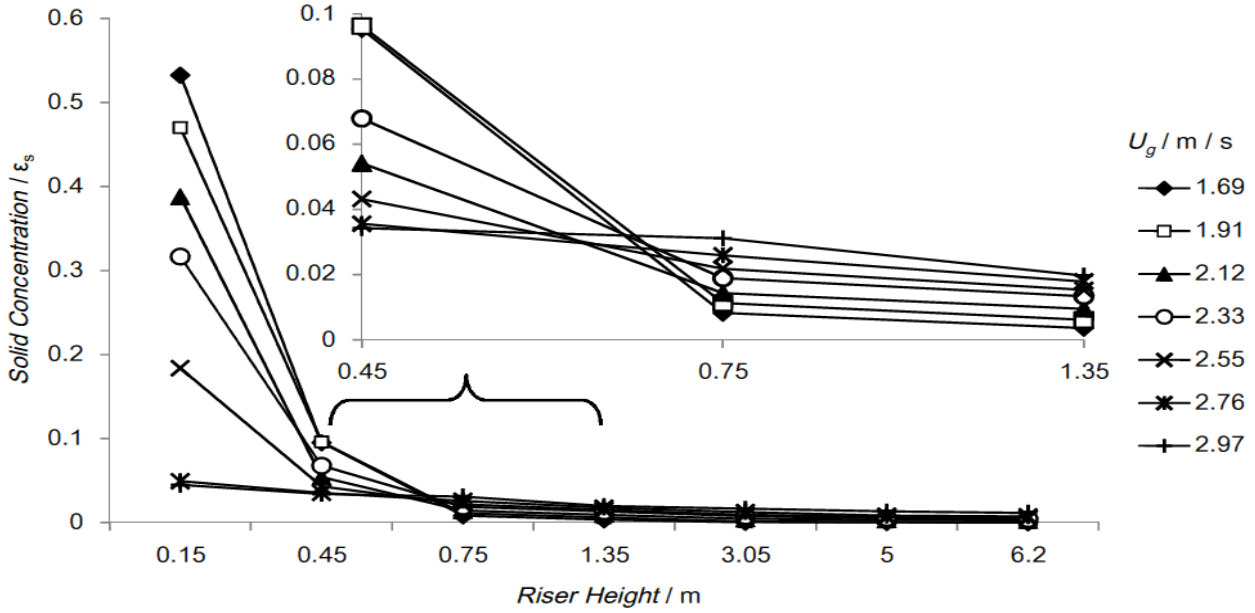


**Figure 6-5 Density profiles at varying fluidisation velocities (molochite static bed height 550mm)**

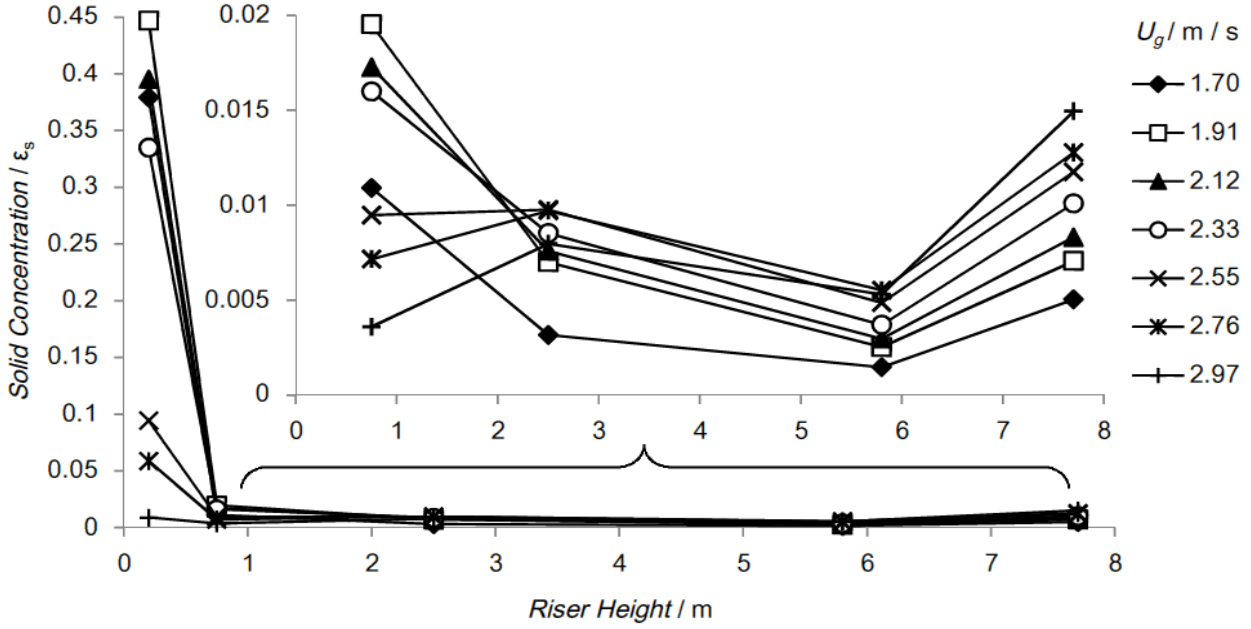


**Figure 6-6 Density profiles at varying fluidisation velocities (Fe100 static bed height 230mm)**

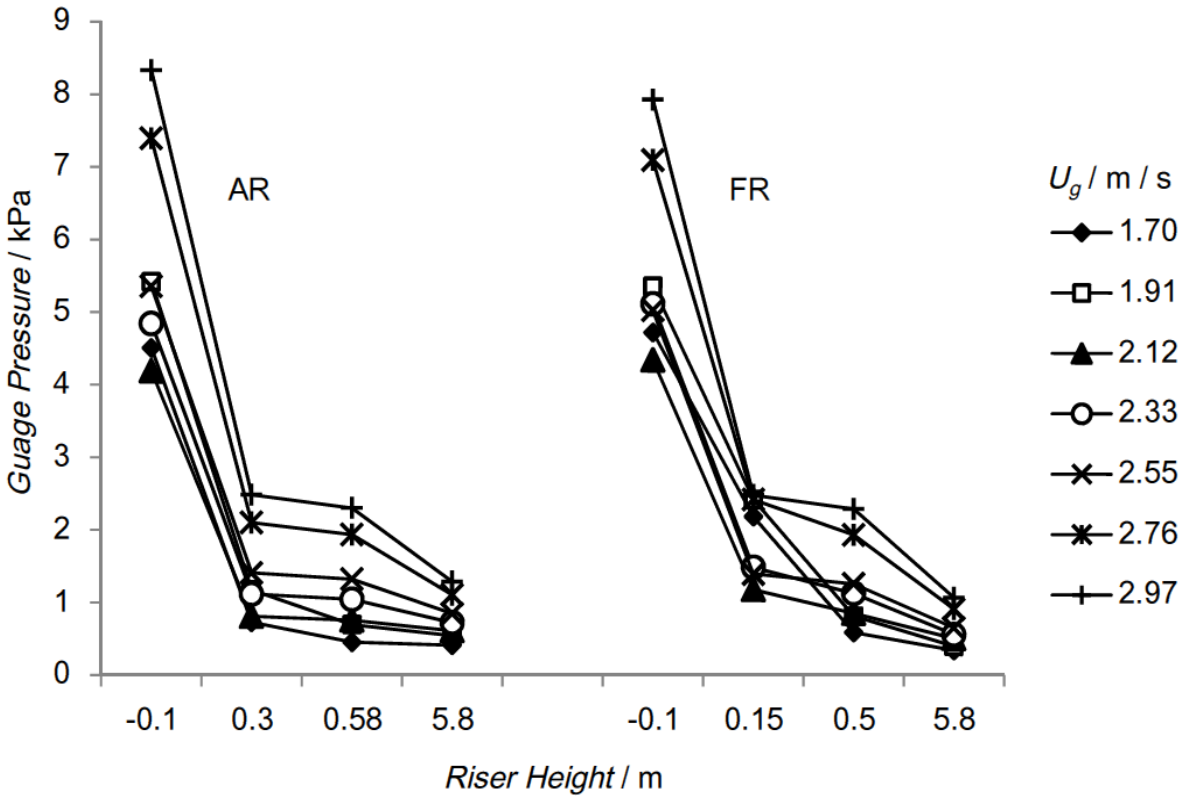


**Figure 6-7 Pressure profile of both risers at steady state (static bed height 550mm)**

### 6.3.3 **Solid circulation rate**

The effect of varying static-bed height and fluidising velocity on the solid circulation rate was investigated for molochite and FE100 particles and are shown in Figure 6-8 and Figure 6-9 respectively. Typical behaviour is observed, with the particle transfer rate increasing with greater gas velocity. In the case of molochite, for a static bed height of 550mm and a gas velocity increased from 2.33 to 2.76 m/s, the transfer of solids increases from 1.66 to 4.32 kg /$m^2$/s. With higher fluidising velocities (2.55-2.76 m/s) the increase in solid transfer rate is fairly linear. Whist at a lower velocity and a bed height varying from 600 to 770mm, the increase in rate of solids transferred is minimal with a rise of 0.3 kg /$m^2$/s. At a velocity between 2.55-2.76 m/s the bed circulation appears to be sensitive, when the bed height is in the region of 430mm to 600mm with the difference in solids transferred is 1.4 kg /$m^2$/s.

The FE100 particles followed the expected trend of increasing solids transfer with increasing fluidising velocity. At lower velocity (2.33 m/s) the difference between the solids transferred with increasing static bed height from 200 – 450mm was minimal and exhibited a rise of 1.8 kg /$m^2$/s. The rise in solid transfer with greater static bed height is greater for fluidising velocities between 2.33 and 2.97 m/s. The dependence of increasing fluidising gas velocity and a larger static bed yields an average rise of 6.4 kg /$m^2$/s. These results indicate that the circulation rate can be controlled in the dual CFB system by adjusting the fluidising velocity, though re-circulation rate can also be increased with the further addition of bed material. This scenario is not ideal due to the thermal losses and energy penalty of adding cold particles for 'hot' operation and requirement of an increased pressure head in the wind-box.

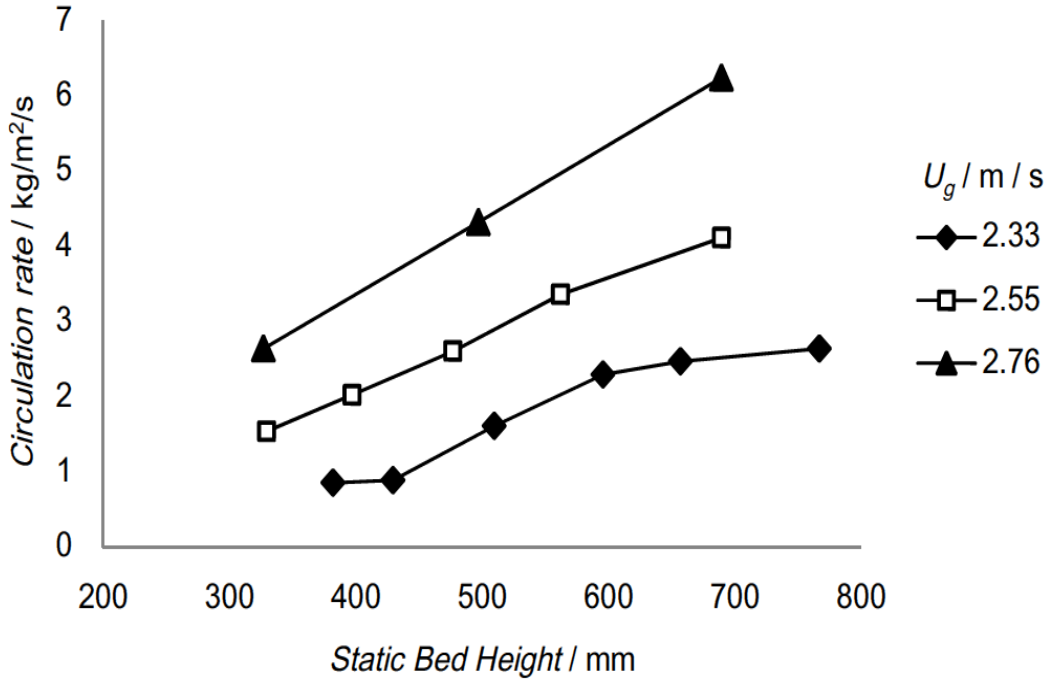


**Figure 6-8 Solid transfer rate at varying velocity and static bed height (molochite)**

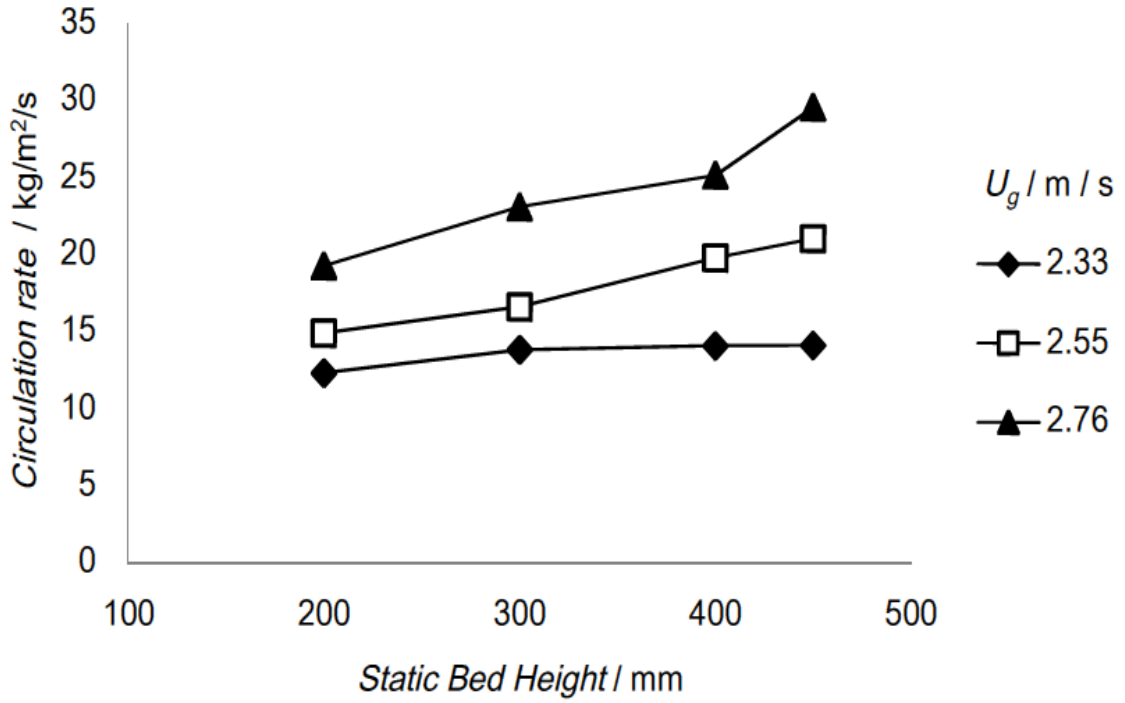


**Figure 6-9 Solid transfer rate at varying velocity and static bed height (FE100)**

### 6.3.4 **Gas bypass leakage**

In the chemical looping fast bed reactor design it is essential to ensure that we have almost pure $CO_2$ at the exit of the FR cyclone. Gas bypass or leakage from the AR will dilute this $CO_2$ and can potentially increase the cost of $CO_2$ purification and separation. Therefore the potential for gas leakage and methods for its reduction is important. Three modes of leakage have been identified;

1) The gas back pass from the outlet of the FR loop seal through the FR return leg upward towards the FR cyclone.

2) Gas bypass from the AR riser through the interconnected loop seal into the FR return leg leading to the FR cyclone.

3) Gas transferred from the AR riser via the solids return leg through the loop seal into the FR riser then being led to the FR cyclone.

Though these modes of potential leakage have been identified, previous experimental studies (Johansson et al., 2003) have indicated that Mode 1 poses the greatest potential for dilution of the $CO_2$ stream at the outlet of the FR cyclone, and Modes 2 and 3 have a negligible effect.

As air is used as the primary fluidising gas in the CFM, the leakage ratio was determined by introducing $CO_2$ as the trace gas to be monitored. $CO_2$ replaced air as the fluidising gas in the outlet of the FR loop seal.

Figure 6-10 shows the gas leakage ratio with FE100 particles where the main considerations for investigation were loop seal fluidising gas velocity and the bed heights above the loop seal in the return leg. The riser flow rates were kept constant at 1000 L/min (2.12 m/s). Whilst maintaining stable and balanced operation, the system shows that $CO_2$ concentration at the exit of the FR cyclone can be maintained at very low level. When the loop seal fluidising velocity is maintained below 0.05 m/s the system exhibits a leakage ratio of up to 2.5 corresponding to a $CO_2$ concentration of 0.7% with a minimal loop seal bed height of 350mm. The leakage ratio increases dramatically to 3.75-3.9 equivalent to a $CO_2$ concentration of 1.5-1.6% when increasing the loop seal fluidising velocity from 0.04 – 0.055 m/s. This indicates that at this bed height, the system is sensitive to fluidising gas flow and velocity. These results indicate that the loop seal bed height must be maintained above 600mm in order to minimize gas leakage from the riser. As seen from Figure 6-10, maintaining the loop seal bed height above 600mm results in $CO_2$ concentrations of 0.5%, which cannot be accommodated given the limits of analysis methods employed here, and indicates that it is critical to avoid dilution of the stream exiting the FR reactor by maintaining an acceptable bed height. The investigation provides acceptable indicators for gas leakage control for transfer to the dual fast bed system.

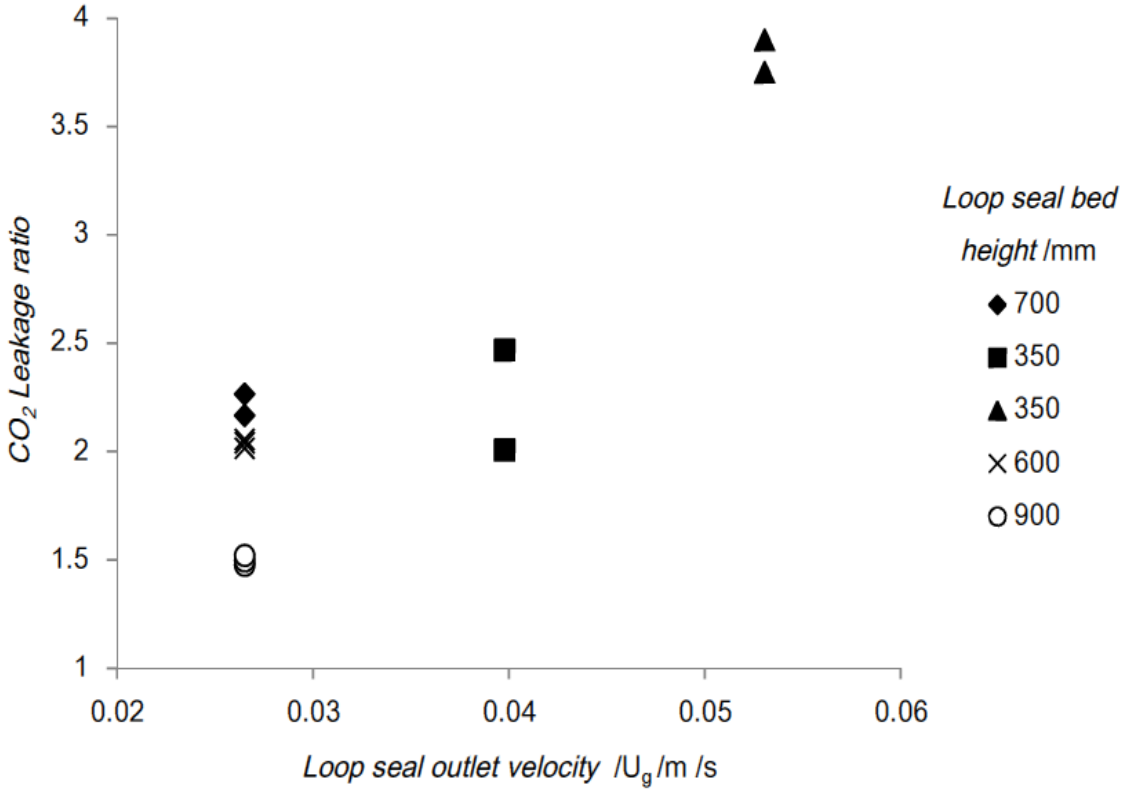


**Figure 6-10 Leakage ratio at varying fluidising gas velocities and loop seal bed heights**

## 6.4 **Conclusions**

The cold-flow hydrodynamic investigation has provided useful and transferable information for the operational philosophy for the CLC reactor. The CFM was operated with two different particles (molochite and FE100) as bed material for a comprehensive understanding of the systems hydrodynamic characteristics whilst observing close similarity to Glicksman's applicable simplified scaling laws.

The solids transfer between the dual CFB reactors can be controlled and maintained to a high level of stable operation in spite of the control philosophy governed by pneumatic transport.

The circulation rate can be flexibly controlled with fluidising gas velocity in the riser. The experimental investigation determines that recirculation rate can also be adjusted through solid make-up of bed inventory.

Gas leakage investigations have shown that dilution of the output stream, from the FR cyclone can be minimal, if the loop seal bed height is maintained above 600mm.

The consequence of this investigation allows a deeper understanding for the operational strategy of the Cranfield CLC reactor to operate in its intended dual CFB configuration. Special attention should be implemented towards maintaining a constant loop-seal bed height in order to minimise cross reactor leakage and would ensure operation is conducted whilst ensuring the fuel reactor flue gas stream to remain undiluted with air and $N_2$ from the air reactor.

In order to allow one to operate the CLC reactor with an optimised strategy, modifications to the CLC reactor can include the addition of view ports in the return leg above the loop-seal to ensure solids are maintained above the required height.

The significance of this investigation and its concluding results contributes to the optimisation of operation and therefore serves to meet the requirements of objective 1a detailed in the PhD aims and objectives.

# 7 Conclusions and Future Work

This chapter discusses the findings resulting from the experimental investigations conducted during this research project. It evaluates the effectiveness of how well the defined aims and objectives in chapter 1 have been met, as well as their contributions to the scope of knowledge within the field. It also discusses recommendations for future studies related to the investigations conducted.

## 7.1 **Conclusions**

The main results and conclusions are drawn from the investigations conducted as a part of this research project, and are detailed below.

### 7.1.1 **Oxygen carrier development**

Oxygen carriers produced from low-cost materials were investigated for CLC processes. Their performance for stability and gaseous fuel conversion were examined using a laboratory-scale fluidised-bed reactor. Their cyclic performance was investigated by subjecting the carriers to alternating oxidation and reduction conditions. Oxidation conditions corresponded to a 5% $O_2$ concentration. Reduction conditions consisted of either, $CH_4$, $CH_4$ 5% in $N_2$, CO 50% in $H_2$ or 10%CO in $N_2$.

The investigation of the development or iron and manganese ores showed that:

- The method of impregnation successfully modified the ores and promoted the formation of combined Fe/Mn oxygen carrier;
- Impregnation of the ores positively influenced their mechanical properties. The measured force required to fracture the oxygen carriers shows the modified iron and manganese ores were 11 and 26% higher than the iron and manganese ore respectively;
- The modified ores also showed positive behaviour in terms of their attrition resistance with an increase between 31 - 37% in attrition resistance for modified iron and manganese ore respectively compared to the unmodified iron and manganese ores;

- The low porosity of the iron ore saw the impregnated $Mn_2O_3$ form a shell on the outside of the oxygen carrier particle from EDX analysis. XRD analysis showed the formation of the mixed $(Fe,Mn)_2O_3$ bixbyite phase;
- The impregnation of $Fe_2O_3$ on to the manganese ore showed improved distribution of iron within the oxygen carrier from EDX analysis;
- Both the oxygen carriers consisting of iron ore exhibited increased reaction rates with syngas (CO 50%, H2 50%) with accumulative redox cycles at 850ºC. Syngas conversion yield was enhanced as was the reducibility of the modified and un-modified ore. The impregnated iron ore exhibited full syngas conversion above 950ºC and outperformed the other oxygen carriers examined in this experimental investigation. The formation of the bixbyite phase allows the phase change to the spinel formation resulting in oxygen release;
- This was further validated, as the impregnated iron ore was the only oxygen carrier investigated to decompose to the spinel phase in an inert atmosphere thereby yielding gaseous oxygen. This corresponded to 0.2% $O_2$ molar concentration by the end of the inert period;
- The oxygen carriers consisting of manganese ore had reduced mass based and syngas conversion (approximately 35%) in comparison to the iron ore containing oxygen carriers at 950ºC. Neither an activation stage nor accumulative redox cycles improved the syngas conversion. Conversely, the reducibility of the oxygen carrier and conversion yield reduced with increasing cycle numbers;
- The unmodified manganese ore exhibited approximately 7% and 10% enhanced methane conversion at 900ºC and 950ºC respectively over the other oxygen carriers tested. The effect of increasing cycle number improving conversion or reducibility was not observed, except for the impregnated iron ore, with negligible improvement;
- Impregnation of iron ores can enhance mechanical stability as well as heighten its reactivity with syngas. Manganese ore also see mechanical improvements, but reduced in efficacy for gas conversion when impregnated.

The investigation of the development of copper-based oxygen carriers showed that:

- Two scalable methods for the production of oxygen carriers were explored; the ball mill method and pelletisation. The pelletisation method was the most feasible method for producing CuO based oxygen carriers supported on alumina cement and CaO based supports;
- The support materials were chosen for their low relative cost and used in order to attempt to stabilise the active CuO, for use in a fluidised-bed investigation with alternating redox cycles;
- The series of produced oxygen carriers were first assessed with CO 10%, after this assessment, select oxygen carriers were chosen for investigation with $CH_4$ as the reducing gas;
- A parallel characterisation study found that the supporting material improved the fracture resistance through crushing strength tests by a minimum of 280% over a pelletised CuO particle;
- EDX analysis of the fresh produced particles shows general uniformity with respect to distribution of different materials within the oxygen carrier particle. Even greater uniformity would be achieved with using as smaller material particle size as possible;
- All of the oxygen carriers tested in this investigation exhibited high CO conversion and were fully reducible from CuO to Cu. Alumina cement supported oxygen carriers saw the greatest extent of this conversion, with conversion increasing with CuO ratio as expected;
- It was apparent that the alumina cement supported suffered reduced performance as the number of redox cycles accumulated. This corresponded to a 20% and 10% reduction in CO conversion between the $1^{st}$ and $25^{th}$ cycles in Cu50Al50 and Cu75Al25 respectively;
- CaO-supported oxygen carriers also exhibited high conversion of CO but in comparison did not deactivate over the cyclic experiment, except in the case of 75% CuO containing oxygen carrier. This behaviour could be largely attributed to the deactivation of the active CuO through pore expansion as seen through the changes in morphology in the

SEM/SFEG imaging and is more evident in oxygen carriers with higher CuO ratios. The reduced performance seen in the alumina cement supports could also be due to interactions between the support and active phase;

- Only one of the oxygen carriers didn't suffer from signs of agglomeration, and its effect was more evident in carriers with higher ratios of CuO. Cu25Al75, which did not suffer from agglomeration, did however show the greatest attrition, with a loss of approximately 8% of its initial mass throughout the 25 redox-cycle investigation;
- The reduction with methane saw a limited reducibility and gas conversion. Methane conversion was limited to 15-25% and 50% for Cu25Ca75 and Cu25Al75 respectively. Cu25Ca75 saw conversion improve, where Cu25Al75 saw a decrease in conversion with increasing redox cycles, although its fuel and oxygen carrier conversion was consistently greater than Cu25Ca25;
- Pelletisation of oxygen carriers with low cost support material as support material is quite scalable. The characterisation of the produced oxygen carriers suggest, a greater suitability towards production with limestone based supports due to its increased crushing strength and sphericity. While the fluid bed investigations yielded that, the chemical interactions between the two materials used here could not reduce the agglomeration that typically occurs with CuO oxygen carriers. But due to the generally good performance of CuO in the conversion of gaseous fuels, the use of lower ratios of the active material could be more beneficial for longer-term use.

### 7.1.2 **Pilot plant operational strategy**

A component of this research project was the installation, commissioning and operation of the dual-fast bed CLC reactor. The commissioning and single column operation yielded the following conclusions:

- Installation and commissioning of the system were successful. The commissioning phase saw the validity and applicability of the ignition and oxygen carrier loading strategies. An initial reaction temperature of 725ºC was required for ignition of injected methane into the wind-box to further elevate the temperature. This strategy was deemed successful with temperatures elevated to over 900ºC;
- The single column-commissioning test utilised 50g of 60%wt CuO 40%wt $Al_2O_3$ oxygen carrier produced by the ball mill method in sand as inert bed. Results saw good methane conversion with a gas yield of 90% and full reduction of the oxygen carrier, during the reduction phase;
- The single column CLOU test utilised a full bed (7kg) of oxygen carrier material. Sustained oxygen release corresponding to approximately 1.5 vol% was observed in the flue-gas outlet concentrations for the inert period of 30mins;
- During this time, the oxygen carrier experienced significant attrition and became elutriated out of the bed, furthermore the oxygen carrier also agglomerated. It was therefore not possible to conduct re-oxidation and reduction phases;
- Operating this system in a dual-column mode has some engineering challenges that are required to be addressed. For operation at the design condition of 50kW heat input with a CuO 60%wt oxygen carrier, balance of the solid transfer between the two reactors requires approximately 23 $nm^3/h$ of $CO_2$ recirculation in the fuel reactor. This strategy can be simulated through additional supply and benefits fuel conversion through CLOU processes;
- Due to the exothermic oxidation reaction of the CuO-based oxygen carrier, the AR would require the removal of 22kW of heat. The only

manageable means of operation of this facility would be to decrease the heat input to 20kW.

To this effect a parallel hydrodynamic study was operated in order to investigate the operation and solid handling characteristics of this reactor system for balanced operation.

- Two bed materials were used; iron particles and clay particles in order to have dynamic similarity with the reactor and for investigation of global control. The $U_{mf}$ and $U_{tr}$ of both particles were determined, with 0.023 and 1.38 m/s for iron and 0.11 and 1.70 m/s for clay respectively;
- The elutriation zones at velocities just above $U_{tr}$ were at a taller height (0.75m) up the riser for iron than for clay particles (0.45m). The density profiles of the two risers were similar to each other, as expected;
- Stable and balanced flow for the system could be achieved. For this specific system, the circulation rate, varies with velocity and can be controlled with the use of the loop-seals for solids hold up to determine static bed height;
- The leakage between the reactors can be minimised by varying the fluid velocity in the loop-seals and ensuring the solids hold-up in bed height is above 600mm in the return leg;

## 7.2 **Research findings comparison with research objectives**

This research project set out to satisfy the two identified PhD aims which concerned; 1) To evaluate the operation of the pilot CLC reactor. 2) The development of oxygen carriers with an emphasis on low cost materials. These aims are described in chapter 1. In order to meet these aims, associated objectives were outlined, and as a consequence of the research conducted in this project are reviewed below in order to evaluate their fulfilment.

**Objective 1a** *Assess the fast-bed design chemical looping reactor's operability through a study of hydrodynamics through the operation of a hydrodynamically scaled cold flow model.*

**Outcome 1a** A method of operation and control philosophy was established through an investigation into the hydrodynamic behaviour of newly designed CLC reactor. The study utilised a cold flow model and suggests that balanced operational flow can be maintained successfully. In the designs current configuration, loop seal can be used to control global circulation as can the fluid velocity. Methods for the control of reactor-reactor leakage have been established in order to minimise its effect. The results from this study have been accepted for publication in Energy Technology journal.

**Objective 1b** *Evaluate the operability of a dual-fast bed chemical looping pilot plant reactor. Detail engineering challenges addressed for an operation campaign.*

**Outcome 1b** The dual-fast bed design presents engineering challenges associated with its operation. These have been explored and discussed. In its current design configuration, heat must be removed for operation. The alternative strategy includes, operation with reduced heat input. The reactor was installed, commissioned, and successfully operated in a single column configuration, with an oxygen carrier demonstrating the CLOU effect and successful methane conversion.

**Objective 2a** *Conduct an experimental campaign exploring the use of ores as oxygen carriers for chemical looping combustion cycles with gaseous fuel.*

*Assess these ores for potential oxygen release under inert conditions, for indications for suitability towards chemical looping with oxygen uncoupling processes. Assess employable methods for the possible improvement of the ores, in order to enhance their properties for increase efficacy and performance in chemical looping cycles.*

**Outcome 2a** Ores can offer a low-cost alternative for use as oxygen carriers at the expense of reduced performance and conversion. An investigation was conducted in order to modify ores for enhancing their CLC performance. The results were very promising for modified iron ore in terms of gas conversion and potential CLOU properties. The modification of manganese ore showed reduced performance in comparison but had enhanced mechanical stability. The results of this study have been published in Applied Energy (163) 2016.

**Objective 2b** *Assess methods for producing oxygen carriers at a feasible scale for pilot plant operation. Evaluate oxygen carriers produced by feasible methods, in bench scale reactors to determine their performance in oxidation and reducing environments with gaseous fuels.*

**Outcome 2b** Two potentially scalable methods were developed and utilised in order to produce oxygen carriers with CuO as the active material. The oxygen carriers produced by both methods were used during the research project for gaseous fuel conversion.

**Objective 2c** *Conduct an experimental campaign exploring the use of feasible supports for Copper (II) oxide as oxygen carriers, whilst assessing their morphology, characterising their physical properties and fuel conversion performance.*

**Outcome 2c** A detailed investigation of gaseous fuel conversion and characterisation was conducted to assess pelletised oxygen carriers of CuO with low-cost support materials. The results of this investigation are intended to be submitted for publication.

From the evaluation of the PhD objectives against their associated outcomes it is believed that the PhD aims and objectives have been met satisfactorily.

## 7.3 **Future work and recommendations**

The research accomplished throughout the course of the project contributes to the field of CLC and carbon capture research. The analysis of the findings contained within this thesis and the limitations encountered during the research project can lead to addressing areas of research, which could be suitable for future investigative studies.

### 7.3.1 **Future oxygen carrier development**

The use of low-cost oxygen carriers or materials in their production continues to be an interesting area of CLC research. The use of ores in the CLC process is one avenue for material cost reduction. In the author's opinion, the use of both iron ores and manganese ores should be maximised. The modification of ores presents great opportunity for improving their mechanical stability and chemical performance. The way that this is achieved, should be scrutinised for its cost/performance effectiveness. The production method assessment is important, where impregnation with nitrates produces $NO_2$ and may not be as scalable as mechanical mixing methods.

Ores that can undergo CLOU processes shows great promise for solid fuel conversion, where CLC is most competitive as a $CO_2$ capture technology. In this study the modification of iron ore exhibited improved mechanical and chemical stability. The long-term effectiveness of this strategy should be investigated in order to develop an estimate of oxygen carrier 'life expectancy'. Modifying the manganese ore saw a decrease in gas conversion. It is therefore recommended to explore the use of other materials, for its modification. Materials such as CuO could be a potential candidate. The requirement for a stable support in which CuO can react and not agglomerate is evident from the results presented and ores could provide a potential material for stable support.

### 7.3.2 **Future pilot plant modifications**

Several limiting factors had been met during the course of this research. The main issues are concerned with the operation of the pilot-scale CLC reactor. As a consequence of the operational experience with the reactor system, the following recommendations are suggested for greater success in operational campaigns.

The main requirement is an oxygen carrier that is robust enough to withstand circulation within a dual fast bed system.

The trace heating system and gaseous preheaters can achieve fluidising gas/ reactor temperatures of around 725ºC, which is sufficient for the heating by methane injection, but reaching this temperature is at the thermal working limits of the heating equipment. Several testing campaigns during the commissioning phase have not reached this required temperature. Moreover, the point that methane is injected (wind-box) is not designed for explosive environments, and will have contributed to the agglomeration of the oxygen carrier in situ and the deterioration of the gas distributor as pictured in chapter 5. It is therefore suggested that the heating strategy is re-designed. The trace-heating elements should be used for supplementary heating and maintaining temperature, instead of its current configuration, where they are used in reactor start-up heating. The amount of power required to heat up electrically in this manner is not efficient either. The recommendation is to install gas burners which should be located in the dense bed, as is commonly found in industrial CFB units (Price, Gittinger and Lindsey, 1997). The suggested method of heating would be beneficial to the reactor in its current configuration and could potentially operate and circulate material. However, the current configuration is not optimised for fuel conversion and maintaining a high $CO_2$ capture efficiency. In order to achieve this, the fuel reactor requires re-designing, as in order to increase its dimensions so as to operate as a bubbling bed, instead of a transport bed.

# REFERENCES

Abad, A. et al. (2012) ‘Demonstration of chemical-looping with oxygen uncoupling (CLOU) process in a 1.5kWth continuously operating unit using a Cu-based oxygen-carrier’, *International Journal of Greenhouse Gas Control*, 6, pp. 189–200. Available at: 10.1016/j.ijggc.2011.10.016 (Accessed: 16 July 2012).

Abad, A. et al. (2007a) ‘Mapping of the range of operational conditions for Cu-, Fe-, and Ni-based oxygen carriers in chemical-looping combustion’, *Chemical Engineering Science*, 62(1-2), pp. 533–549. Available at: 10.1016/j.ces.2006.09.019 (Accessed: 24 August 2012).

Abad, A. et al. (2007b) ‘The use of iron oxide as oxygen carrier in a chemical-looping reactor’, *Fuel*, 86(7-8), pp. 1021–1035. Available at: 10.1016/j.fuel.2006.09.021 (Accessed: 3 September 2012).

Abad, A. et al. (2006) ‘Chemical-looping combustion in a 300 W continuously operating reactor system using a manganese-based oxygen carrier’, *Fuel*, 85(9), pp. 1174–1185.

Abanades, J.C. (2002) ‘The maximum capture efficiency of $CO_2$ using a carbonation / calcination cycle of CaO / $CaCO_3$’, *Chemical Engineering Journal*, 90(3), pp. 303–306.

Adánez, J. et al. (2012) ‘Progress in Chemical-Looping Combustion and Reforming technologies’, *Progress in Energy and Combustion Science*, 38(2) Elsevier Ltd, pp. 215–282. Available at: 10.1016/j.pecs.2011.09.001 (Accessed: 24 July 2012).

Adánez, J. et al. (2014) ‘Design and Operation of a Coal-fired 50 kWth Chemical Looping Combustor’, *Energy Procedia*, 63, pp. 63–72.

Adánez, J. et al. (2010) ‘Ilmenite activation during consecutive redox cycles in chemical-looping combustion’, *Energy and Fuels*, 24(2), pp. 1402–1413.

Adánez, J. et al. (2004) ‘Selection of oxygen carriers for chemical-looping

combustion', *Energy and Fuels*, 18(2), pp. 371–377.

Adánez, J. et al. (2006) 'Chemical Looping Combustion in a 10 kW th Prototype Using a CuO / $Al_2O_3$ Oxygen Carrier : Effect of Operating Conditions on Methane Combustion', *Industrial & Engineering Chemistry Research*, 45, pp. 6075–6080.

Anthony, E.J. (2008) 'Solid Looping Cycles: A New Technology for Coal Conversion', *Industrial & Engineering Chemistry Research*, 47(6), pp. 1747–1754.

APGTF (2011) *Cleaner Fossil Power Generation in the 21 st Century – Maintaining a Leading Role*.

Arjmand, M. et al. (2011) 'Prospects of $Al_2O_3$ and $MgAl_2O_4$ -Supported CuO Oxygen Carriers in Chemical-Looping Combustion ( CLC ) and Chemical-Looping with Oxygen Uncoupling ( CLOU )', *Energy & Fuels*, 25, pp. 5493–5502.

Arjmand, M. et al. (2012) 'Use of manganese ore in chemical-looping combustion (CLC)—Effect on steam gasification', *International Journal of Greenhouse Gas Control*, 8 Elsevier Ltd, pp. 56–60. Available at: 10.1016/j.ijggc.2012.02.001 (Accessed: 16 July 2012).

Arjmand, M. et al. (2014) 'Investigation of different manganese ores as oxygen carriers in chemical-looping combustion (CLC) for solid fuels', *Applied Energy*, 113 Elsevier Ltd, pp. 1883–1894.

Azimi, G. et al. (2013) 'Investigation of different Mn-Fe oxides as oxygen carrier for chemical-looping with oxygen uncoupling (CLOU)', *Energy and Fuels*, 27, pp. 367–377.

Azimi, G. et al. (2015) 'Comprehensive study of Mn–Fe–Al oxygen-carriers for chemical-looping with oxygen uncoupling (CLOU)', *International Journal of Greenhouse Gas Control*, 34 Elsevier Ltd, pp. 12–24. Available at: 10.1016/j.ijggc.2014.12.022 (Accessed: 19 March 2015).

Bayham, S.C. et al. (2013) ‘Iron-Based Coal Direct Chemical Looping Combustion Process: 200-h Continuous Operation of a 25-kW th Subpilot Unit’, *Energy & Fuels*, 27(3), pp. 1347–1356.

Bischi, A. et al. (2011) ‘Performance analysis of the cold flow model of a second generation chemical looping combustion reactor system’, *Energy Procedia*, 4, pp. 449–456.

Bischi, A. et al. (2012) ‘Hydrodynamic viability of chemical looping processes by means of cold flow model investigation’, *Applied Energy*, 97, pp. 201–216.

Blamey, J. et al. (2010) ‘The calcium looping cycle for large-scale $CO_2$ capture’, *Progress in Energy and Combustion Science*, 36(2) Elsevier Ltd, pp. 260–279.

Bolhàr-Nordenkampf, J. et al. (2009a) ‘Comprehensive modeling tool for chemical looping based processes’, *Chemical Engineering and Technology*, 32(3), pp. 410–417.

Bolhàr-Nordenkampf, J. et al. (2009b) ‘Performance of a NiO-based oxygen carrier for chemical looping combustion and reforming in a 120 kW unit’, *Energy Procedia*, 1(1) Elsevier, pp. 19–25. Available at: 10.1016/j.egypro.2009.01.005 (Accessed: 21 May 2013).

Boot-Handford, M.E. et al. (2014) ‘Carbon capture and storage update’, *Energy & Environmental Science*, 7(1), pp. 130–189.

BP (2013) *Energy Outlook 2016*. (Available at https://www.bp.com/content/dam/bp/pdf/energy-economics/energy-outlook-2016/bp-energy-outlook-2016.pdf (Accessed 02 February 2016)

Cao, Y. et al. (2006) ‘Investigation of chemical looping combustion by solid fuels. 2. Redox reaction kinetics and product characterization with coal, biomass, and solid waste as solid fuels’, *Energy & Fuels*, 20(4), pp. 1845–1854.

Chiu, J. and Andrus, H. (2014) *Alstom’ s Chemical Looping Technology Program Update CO2 Capture Technology Meeting Overview CLC Concepts*.

Cho, P. et al. (2006) ‘Defluidization Conditions for a Fluidized Bed of Iron Oxide-

, Nickel Oxide-, and Manganese Oxide-Containing Oxygen Carriers for Chemical-Looping Combustion', *Industrial & Engineering Chemistry Research*, 45(3), pp. 968–977.

Cho, P. et al. (2004) 'Comparison of iron-, nickel-, copper- and manganese-based oxygen carriers for chemical-looping combustion', *Fuel*, 83(9), pp. 1215–1225. Available at: 10.1016/j.fuel.2003.11.013 (Accessed: 28 May 2013).

D'Alessandro, D.M. et al. (2010) 'Carbon dioxide capture: Prospects for new materials', *Angewandte Chemie - International Edition*, 49(35), pp. 6058–6082.

de Diego, L.F. et al. (2014) 'Reduction and Oxidation Kinetics of a $CaMn_{0.9}Mg_{0.1}O_3^{-\delta}$ Oxygen Carrier for Chemical-Looping Combustion', *Industrial and Engineering Chemistry Research*, 53, pp. 87–103.

De Diego, L.F. et al. (2004) 'Development of Cu-based oxygen carriers for chemical-looping combustion', *Fuel*, 83(13), pp. 1749–1757.

de Diego, L.F. et al. (2005) 'Impregnated $CuO/Al_2O_3$ Oxygen Carriers for Chemical-Looping Combustion: Avoiding Fluidized Bed Agglomeration', *Energy & Fuels*, 19(5), pp. 1850–1856.

Donat, F. et al. (2015) 'Characteristics of Copper-based Oxygen Carriers Supported on Calcium Aluminates for Chemical-Looping Combustion with Oxygen Uncoupling (CLOU)', *Industrial & Engineering Chemistry Research*, 54(26), p. 150615135406002.

Eyring, E.M. et al. (2011) 'Boucle chimique pour la combustion du charbon avec un transporteur d'oxyg??ne ?? base d'oxyde de cuivre', *Oil and Gas Science and Technology*, 66(2), pp. 209–221.

Fan, L.-S. (2010) *Chemical Looping Systems for Fossil Energy Conversions*. Wiley.

Fennell, P.S. and Anthony, E.J. (2015) *Calcium and chemical looping Technology for power generation and Carbon dioxide capture*. Woodhead publishing.

Figueroa, J.D. et al. (2008) ‘Advances in $CO_2$ capture technology-The U.S. Department of Energy’s Carbon Sequestration Program’, *International Journal of Greenhouse Gas Control*, 2(1), pp. 9–20.

Fossdal, a. et al. (2011) ‘Study of inexpensive oxygen carriers for chemical looping combustion’, *International Journal of Greenhouse Gas Control*, 5(3), pp. 483–488. Available at: 10.1016/j.ijggc.2010.08.001 (Accessed: 4 April 2013).

Gallagher, P.K. and Schrey, F. (1971) ‘The thermal decomposition of aqueous manganese (II) nitrate solution’, *Thermochica Acta*, 2, pp. 405–412.

Gayán, P. et al. (2012a) ‘Development of Cu-based oxygen carriers for Chemical-Looping with Oxygen Uncoupling (CLOU) process’, *Fuel*, 96, pp. 226–238.

Gayán, P. et al. (2012b) ‘Testing of a highly reactive impregnated Fe2O3/Al2O3 oxygen carrier for a SR–CLC system in a continuous CLC unit’, *Fuel Processing Technology*, 96, pp. 37–47.

Geldart, D. (1973) ‘Types of Gas Fluidization’, *Powder Technology*, 7, pp. 285–292.

Glicksman, L.R. et al. (1994) ‘Dynamic similarity in fluidization’, *International Journal of Multiphase Flow*, 20(94), pp. 331–386.

Glicksman, R. (1982) ‘Scaling relationships for fluidized beds’, *Chemical Engineering Science*, 39(9), pp. 1373–1379.

Global CCS Institute (2011) *The global status of CCS: 2011*., *Canberra, Australia*

Gu, H. et al. (2011) ‘Chemical looping combustion of biomass/coal with natural iron ore as oxygen carrier in a continuous reactor’, *Energy and Fuels*, 25(1), pp. 446–455.

Gu, H. et al. (2015) ‘Cement/CaO-modified iron ore as oxygen carrier for chemical looping combustion of coal’, *Applied Energy*

Hallberg, P. et al. (2013) ‘Chemical Looping Combustion and Chemical Looping

with Oxygen Uncoupling Experiments in a Batch Reactor Using Spray-Dried $CaMn_{1-x}M_xO_3^{-\delta}$ (M = Ti, Fe, Mg) Particles as Oxygen Carriers', *Energy & Fuels*, 27, pp. 1473–1481.

Hansen, J. (2004) 'Defusing the global warming time bomb', *Scientific American*, (290), pp. 68–77.

Hester, R.E. and Harrison, R.M. (2010) *Issues in Environmental Science and Technology, 29 Carbon Capture: Sequestration and Storage*. Royal Society of Chemistry.

Hossain, M.M. and de Lasa, H.I. (2008) 'Chemical-looping combustion (CLC) for inherent separations—a review', *Chemical Engineering Science*, 63(18), pp. 4433–4451. Available at: 10.1016/j.ces.2008.05.028 (Accessed: 24 August 2012).

Hughes, L. (2000) 'Biological consequences of global warming: is the signal already apparent?', *Trends in Ecology & Evolution*, 15(2), pp. 56–61.

IEA (2015) *Energy and Climate Change*. (Available at https://www.bp.com/content/dam/bp/pdf/energy-economics/energy-outlook-2016/bp-energy-outlook-2016.pdf) (Accessed 02 February 2016)

IEA (2010) *Energy Technology Perspectives: Scenarios & Strategies To 2050*.

Imtiaz, Q. et al. (2013) 'Review of Oxygen Carriers for Chemical Looping with Oxygen Uncoupling (CLOU): Thermodynamics, Material Development, and Synthesis', *Energy Technology*, 1, pp. 633–647.

IPCC (2014) *Climate Change 2014: Synthesis Report. Contribution of Working Groups I, II and III to the Fifth Assessment Report of the Intergovernmental Panel on Climate Change*.

IPCC (2007) *Climate Change 2007 : AR4 Synthesis Report*., *Intergovernmental panel on climate change*

Ishida, M. and Hongguang Jin (1994) A novel combustor based on chemical-looping reactions and its reaction kinetics *Journal of Chemical Engineering of*

*Japan*.

Ishida, M. and Jin, H. (1996) 'A Novel Chemical-Looping Combustor without NOx Formation', *Industrial & Engineering Chemistry research*, 5885(95), pp. 2469–2472.

Ishida, M. and Jin, H. (1994) 'A new advanced power-generation system using chemical-looping combustion', *Energy*, 19(4), pp. 415–422.

Jerndal, E. et al. (2006) 'Thermal analysis of chemical-looping combustion.', *Chemical Engineering Research and Design*, 84(A9), pp. 795–806.

Jia, L. et al. (2007) 'Attrition of Calcining Limestones in Circulating Fluidized-Bed Systems', *Industrial & Engineering Chemistry Research*, 46, pp. 5199–5209.

Johansson, E. et al. (2003) 'Gas leakage measurements in a cold model of an interconnected fluidized bed for chemical-looping combustion', *Powder Technology*, 134(3), pp. 210–217. Available at: 10.1016/S0032-5910(03)00125-6 (Accessed: 5 May 2013).

Källén, M. et al. (2013) '$CaMn_{0.9}Mg_{0.1}O_3^{-\delta}$ as Oxygen Carrier in a Gas-Fired 10 kW th Chemical-Looping Combustion Unit', *Industrial & Engineering Chemistry Research*, 52(21), pp. 6923–6932.

Kidambi, P.R. et al. (2012) 'Interaction of Iron Oxide with Alumina in a Composite Oxygen Carrier during the Production of Hydrogen by Chemical Looping', *Energy & Fuels*, 26(1), pp. 603–617.

Kim, H.R. et al. (2013) 'Coal direct chemical looping combustion process: Design and operation of a 25-kWth sub-pilot unit', *Fuel*, 108 Elsevier Ltd, pp. 370–384.

Koornneef, J. et al. (2007) 'Development of fluidized bed combustion—An overview of trends, performance and cost', *Progress in Energy and Combustion Science*, 33(1), pp. 19–55. Available at: 10.1016/j.pecs.2006.07.001 (Accessed: 27 March 2013).

Kramer, G.J. and Haigh, M. (2009) 'No quick switch to low-carbon energy', *Nature*, 462(December), pp. 3–4.

Kronberger, B. et al. (2005) 'Design and Fluid Dynamic Analysis of a Bench-Scale Combustion System with $CO_2$ Separation - Chemical-Looping Combustion', *Industrial Engineering Chemistry Research*, 44(3), pp. 546–556.

Lambert, A. et al. (2011) 'Spinel mixed oxides as oxygen carriers for chemical looping combustion', *Energy Procedia*, 4 Elsevier, pp. 318–323.

Lambert, A. et al. (2009) 'Synthesis and characterization of bimetallic Fe/Mn oxides for chemical looping combustion', *Energy Procedia*, 1, pp. 375–381. Available at: http://www.sciencedirect.com/science/article/pii/S1876610209000526 (Accessed: 10 September 2012).

Larring, Y. et al. (2015a) 'Evaluation of a Mixed Fe–Mn Oxide System for Chemical Looping Combustion', *Energy & Fuels*, 29(5), pp. 3438–3445.

Larring, Y. et al. (2015b) 'Fe-Mn based minerals with remarkable redox characteristics for chemical looping combustion', *Fuel*, 159 Elsevier Ltd, pp. 169–178.

Lee, J.-B. et al. (2005) Redox characteristics of various kinds of oxygen carriers for hydrogen fueled chemical-looping combustion *Journal of Industrial and Engineering Chemistry*.

Leion, H. et al. (2009a) 'Solid fuels in chemical-looping combustion using oxide scale and unprocessed iron ore as oxygen carriers', *Fuel*, 88(10) Elsevier Ltd, pp. 1945–1954. Available at: 10.1016/j.fuel.2009.03.033 (Accessed: 4 September 2012).

Leion, H. et al. (2009b) 'Use of $CaMn_{0.875}Ti_{0.125}O_3$ as oxygen carrier in chemical-looping with oxygen uncoupling', *Energy and Fuels*, 23(10), pp. 5276–5283.

Leion, H. et al. (2008) 'Solid fuels in chemical-looping combustion', *International Journal of Greenhouse Gas Control*, 2(2), pp. 180–193. Available at:

10.1016/S1750-5836(07)00117-X (Accessed: 16 July 2012).

Leion, H. et al. (2009a) ‘Use of Ores and Industrial Products As Oxygen Carriers in Chemical-Looping Combustion Use of Ores and Industrial Products As Oxygen Carriers in Chemical-Looping Combustion’, *Energy and Fuels*, 23, pp. 2307–2315.

Leion, H. et al. (2009b) ‘Using chemical-looping with oxygen uncoupling (CLOU) for combustion of six different solid fuels’, *Energy Procedia*, 1(1) Elsevier, pp. 447–453.

Lewis, W.K. and Gilliland, E.R. (1954) *Production of Pure Carbon Dioxide*.

Linderholm, C. et al. (2008) ‘160h of chemical-looping combustion in a 10kW reactor system with a NiO-based oxygen carrier’, *International Journal of Greenhouse Gas Control*, 2(4), pp. 520–530. Available at: 10.1016/j.ijggc.2008.02.006 (Accessed: 12 March 2013).

Linderholm, C. et al. (2012) ‘Chemical-looping combustion of solid fuels - Operation in a 10 kW unit with two fuels, above-bed and in-bed fuel feed and two oxygen carriers, manganese ore and ilmenite’, *Fuel*, 102 Elsevier Ltd, pp. 808–822.

Linderholm, C. and Schmitz, M. (2016) ‘Chemical-looping combustion of solid fuels in a 100kW dual circulating fluidized bed system using iron ore as oxygen carrier’, *Journal of Environmental Chemical Engineering*, 4(1) Elsevier B.V., pp. 1029–1039.

Linderholm, C. et al. (2016) ‘Chemical-looping combustion in a 100-kW unit using a mixture of ilmenite and manganese ore as oxygen carrier’, *Fuel*, 166 Elsevier Ltd, pp. 533–542.

Luo, S. et al. (2014) ‘Conversion of metallurgical coke and coal using a Coal Direct Chemical Looping (CDCL) moving bed reactor’, *Applied Energy*, 118 Elsevier Ltd, pp. 300–308.

Lyngfelt, a. (2011) ‘Oxygen Carriers for Chemical Looping Combustion - 4000 h

of Operational Experience', *Oil & Gas Science and Technology – Revue d'IFP Energies nouvelles*, 66(2), pp. 161–172. Available at: 10.2516/ogst/2010038 (Accessed: 20 April 2013).

Lyngfelt, A. (2013) Successful Operation of a 100-kW Chemical-Looping Combustor for Solid Fuels, *Greenhouse News IEAGHG*, (109), pp. 1–13.

Lyngfelt, A. et al. (2008) 'Chemical looping combustion - Status of Development', *9th International Conference on Fluidized Beds*.

Lyngfelt, A. et al. (2004) 'The GRACE Project: Development of Oxygen Carrier Particles for Chemical-Looping Combustion. Design and Operation of a 10 kW Chemical-Looping Combustor', *7th International Conference on Greenhouse Gas Control Technologies*.

Lyngfelt, A. and Leckner, B. (2015) 'A 1000MWth boiler for chemical-looping combustion of solid fuels – Discussion of design and costs', *Applied Energy*, 157, pp. 475–487.

Lyngfelt, A. et al. (2001) 'A fluidized-bed combustion process with inherent CO 2 separation; application of chemical-looping combustion', *Chemical Engineering Science*, 56, pp. 3101–3113.

Lyngfelt, A. and Thunman, H. (2003) 'Construction and 100 h of operational experience of a10 kW chemical looping combustor', *The $CO_2$ Capture and Storage Project (CCP) for Carbon Dioxide Storage in Deep Geologic Formations For Climate Change Mitigation, Thomas, D. (Ed.), Elsevier Science: London*, 1(36), pp. 625–645.

Markström, P. et al. (2012) 'Chemical-looping combustion of solid fuels-Design and operation of a 100 kW unit with bituminous coal', *International Journal of Greenhouse Gas Control*, 15, pp. 150–162. Available at: http://publications.lib.chalmers.se/publication/160152-chemical-looping-combustion-of-solid-fuels-design-and-operation-of-a-100-kw-unit-with-bituminous-coa (Accessed: 20 May 2013).

Markström, P. and Lyngfelt, A. (2012) 'Designing and operating a cold-flow

model of a 100kW chemical-looping combustor', *Powder Technology*, 222, pp. 182–192. Available at: 10.1016/j.powtec.2012.02.041 (Accessed: 28 March 2013).

Mattisson, T. et al. (2014) 'Innovative Oxygen Carriers Uplifting Chemical-looping Combustion', *Energy Procedia*, 63 Elsevier B.V., pp. 113–130.

Mattisson, T. et al. (2007) 'Chemical-looping combustion using syngas as fuel', *International Journal of Greenhouse Gas Control*, 1(2), pp. 158–169. Available at: 10.1016/S1750-5836(07)00023-0 (Accessed: 4 April 2013).

Mattisson, T. et al. (2004) 'Multicycle Reduction and Oxidation of Different Types Chemical-Looping Combustion', *Energy & Fuels*, 18, pp. 628–637.

Mattisson, T. et al. (2001) 'The use of iron oxide as an oxygen carrier in chemical-looping combustion of methane with inherent separation of $CO_2$', *Fuel*, 80(13), pp. 1953–1962.

Mattisson, T. et al. (2009) 'Chemical-looping with oxygen uncoupling for combustion of solid fuels', *International Journal of Greenhouse Gas Control*, 3, pp. 11–19.

Miller, D.D. et al. (2015) 'Fluidized-bed and fixed-bed reactor testing of methane chemical looping combustion with MgO-promoted hematite', *Applied Energy*, 146 Elsevier Ltd, pp. 111–121.

Moldenhauer, P. et al. (2014) 'Chemical-looping combustion with fuel oil in a 10 kW pilot plant', *Energy and Fuels*, 28(9), pp. 5978–5987.

Ohlemüller, P. et al. (2015) 'Development of a process model for coal chemical looping combustion and validation against 100kWth tests', *Applied Energy*, 157, pp. 433–448.

Ohlemüller, P. et al. (2016) 'Chemical-Looping Combustion of Hard Coal: Autothermal Operation of a 1 $MW_{th}$ Pilot Plant', *Journal of Energy Resources Technology*, 138(4), p. 042203.

Orth, M. et al. (2012) 'Design and Operation of a 1 MW th Chemical Looping

Plant', *2nd International Conference on Chemical Looping*., pp. 26–28.

Penthor, S. et al. (2015) 'Investigation of the performance of a copper based oxygen carrier for chemical looping combustion in a 120kW pilot plant for gaseous fuels', *Applied Energy*, 145, pp. 52–59.

Pires, J.C.M. et al. (2011) 'Recent developments on carbon capture and storage: An overview', *Chemical Engineering Research and Design*, 89(9), pp. 1446–1460. Available at: 10.1016/j.cherd.2011.01.028 (Accessed: 13 July 2012).

Price, C.E. et al. (1997) 'Internal Recirculation CFB Boiler for Southern Illinois University - Update on Start-Up and Initial Operation', *ASME International Joint Power Generation Conference*., pp. 1–6.

Pröll, T. et al. (2009a) 'Natural minerals as oxygen carriers for chemical looping combustion in a dual circulating fluidized bed system', *Energy Procedia*, 1(1), pp. 27–34. Available at: 10.1016/j.egypro.2009.01.006 (Accessed: 21 May 2013).

Pröll, T. et al. (2009b) 'Cold Flow Model Study on a Dual Circulating Fluidized Bed (DCFB) System for Chemical Looping Processes', *Chemical Engineering & Technology*, 32(3), pp. 418–424.

Rackley, S.A. (2010) *Carbon capture and storage*. Elsevier. Available at: http://www.knovel.com/web/portal/browse/display?_EXT_KNOVEL_DISPLAY_bookid=2739&VerticalID=0 (Accessed: 10 September 2012).

Rydén, M. et al. (2014a) 'Combined oxides as oxygen-carrier material for chemical-looping with oxygen uncoupling', *Applied Energy*, 113, pp. 1924–1932.

Rydén, M. et al. (2011a) 'CaMn0.875Ti0.125O3 as oxygen carrier for chemical-looping combustion with oxygen uncoupling (CLOU)-Experiments in a continuously operating fluidized-bed reactor system', *International Journal of Greenhouse Gas Control*, 5(2), pp. 356–366.

Rydén, M. et al. (2011b) ‘Combined manganese/iron oxides as oxygen carrier for chemical looping combustion with oxygen uncoupling (CLOU) in a circulating fluidized bed reactor system’, *Energy Procedia*, 4 Elsevier, pp. 341–348.

Rydén, M. et al. (2014b) ‘Measuring attrition resistance of oxygen carrier particles for chemical looping combustion with a customized jet cup’, *Powder Technology*, 256 Elsevier B.V., pp. 75–86.

Sedor, K.E. et al. (2008) ‘Reactivity and stability of Ni/Al2O3 oxygen carrier for chemical-looping combustion (CLC)’, *Chemical Engineering Science*, 63, pp. 2994–3007.

Shakun, J.D. et al. (2012) ‘Global warming preceded by increasing carbon dioxide concentrations during the last deglaciation’, *Nature*, 484(7392) Nature Publishing Group, pp. 49–54.

Shrestha, S. et al. (2016) ‘Cold flow model of dual fluidized bed : A review’, *Renewable and sustainable energy reviews*, 53, pp. 1529–1548.

Shuai, W. et al. (2011) ‘Fluid dynamic simulation in a chemical looping combustion with two interconnected fluidized beds’, *Fuel Processing Technology*, 92(3), pp. 385–393.

Shulman, A. et al. (2009a) ‘Manganese/iron, manganese/nickel, and manganese/silicon oxides used in chemical-looping with oxygen uncoupling (CLOU) for combustion of methane’, *Energy and Fuels*, 23(10), pp. 5269–5275.

Shulman, A. et al. (2009b) ‘High reactivity and mechanical durability of $NiO/NiAl_2O_4$ and $NiO/NiAl_2O_4/MgAl_2O_4$ oxygen carrier particles used for more than 1000 h in a 10 kW CLC reactor’, *Industrial and Engineering Chemistry Research*, 48(15), pp. 7400–7405.

Sim, C.Y. et al. (2012) ‘Particle characterisation in chemical looping combustion’, *Chemical Engineering Science*, 69(1), pp. 211–224. Available at: 10.1016/j.ces.2011.10.026 (Accessed: 17 October 2012).

Simmonds, M. et al. (2004) ‘Oxyfuel technologies for $CO_2$ capture: a techno-

economic overview', *Proceedings of GHGT*, 44(0), pp. 1–5. Available at: http://uregina.ca/ghgt7/PDF/papers/nonpeer/470.pdf (Accessed: 10 September 2012).

Sozinho, T. et al. (2012) 'Main results of the 10 kW th pilot plant operation', *2nd International Conference on Chemical Looping, 26-28 September 2012, Darmstadt, Germany*, (September), pp. 26–28.

Stobbe, E.R. et al. (1999) 'The reduction and oxidation behaviour of manganese oxides', *Catalysis Today*, 47(1-4), pp. 161–167.

Stocker, T.F. et al. (2013) *Technical Summary: Supplementary Material World* Energy Outlook Special Report (Available at: https://www.iea.org/publications/freepublications/publication/WEO2015SpecialReportonEnergyandClimateChange.pdf) (Accessed 02 February 2016)

Ströhle, J. et al. (2014) 'Design and operation of a 1MWth chemical looping plant', *Applied Energy*, 113, pp. 1490–1495.

Thon, A. et al. (2013) 'Operational Experience With a Coupled Fluidized Bed System for Chemical Looping Combustion of Solid Fuels', *The 14th International Conference on Fluidization*, (September), pp. 26–28.

Thon, A. et al. (2014) 'Operational experience with a system of coupled fluidized beds for chemical looping combustion of solid fuels using ilmenite as oxygen carrier', *Applied Energy*, 118 Elsevier Ltd, pp. 309–317.

UKCCSRC (2016) *CCS Process*., *What is CCS?* Available at: https://ukccsrc.ac.uk/about/what-ccs (Accessed: 16 February 2016).

UNFCCC (2015) *Adoption of the Paris Agreement*. Available at: https://unfccc.int/resource/docs/2015/cop21/eng/l09r01.pdf (Accessed 02 February (2016)

Wang, J. and Anthony, E.J. (2008a) 'Clean combustion of solid fuels', *Applied Energy*, 85, pp. 73–79.

Wang, J. and Anthony, E.J. (2008b) 'Clean combustion of solid fuels', *Applied*

*Energy*, 85(2-3), pp. 73–79.

Wieczerok-Ciurowa, K., Kozak, A.J. (1999) ‘THE THERMAL DECOMPOSITION OF $Fe(NO_3)_3 \times 9H_2O$’, *Journal of Thermal Analysis and Calorimetry*, 58(3), pp. 647–651.

Wilcox, J. (2012) *Carbon Capture*. Springer.

Xiao, R. et al. (2012) ‘Pressurized chemical-looping combustion of coal using an iron ore as oxygen carrier in a pilot-scale unit’, *International Journal of Greenhouse Gas Control*, 10 Elsevier Ltd, pp. 363–373.

Xu, L. et al. (2014) ‘Cu-Modified Manganese Ore as an Oxygen Carrier for Chemical Looping Combustion’, *Energy & Fuels*, 28, pp. 7085–7092.

Yang, W.-C. (ed.) (2003) *Handbook of Fluidization and Fluid-Particle Systems*. CRC Press, Chemical Industries.

Zafar, Q. et al. (2007) ‘Reduction and oxidation kinetics of $Mn_3O_4$/Mg-$ZrO_2$ oxygen carrier particles for chemical-looping combustion’, *Chemical Engineering Science*, 62(23), pp. 6556–6567.

# APPENDICES

## Appendix A

### A.1 CLC reactor installation and ancillaries pictures

**Figure A-1 Installation of the risers, cyclones and trace heating elements**

**Figure A-2 Installation of return legs, and reactor insulation**

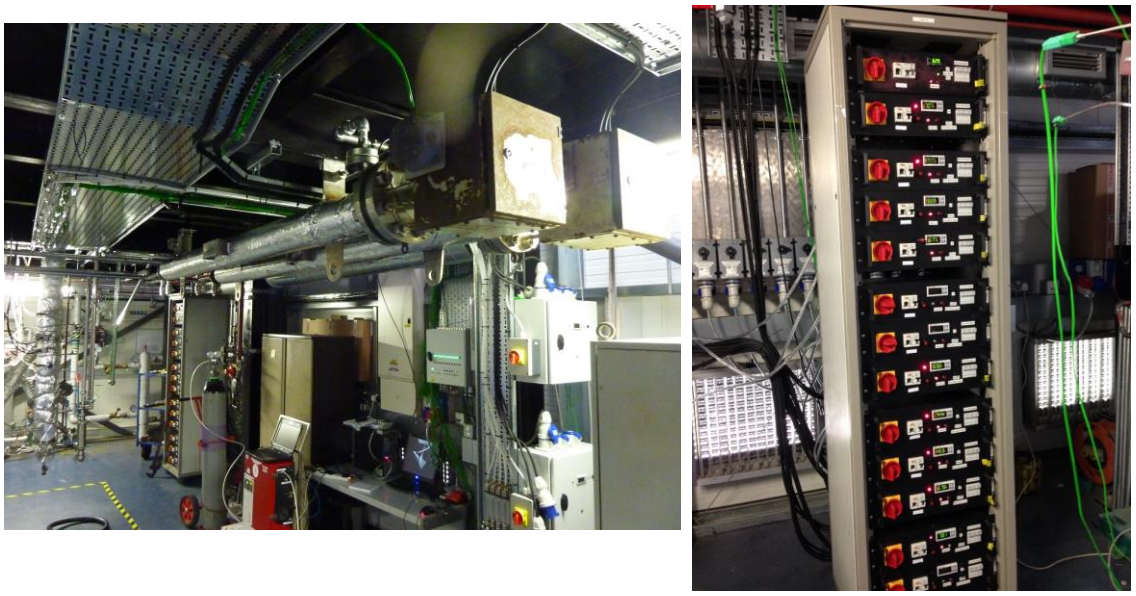

**Figure A-3 (left) Gas preheaters (right) Trace heating control units**

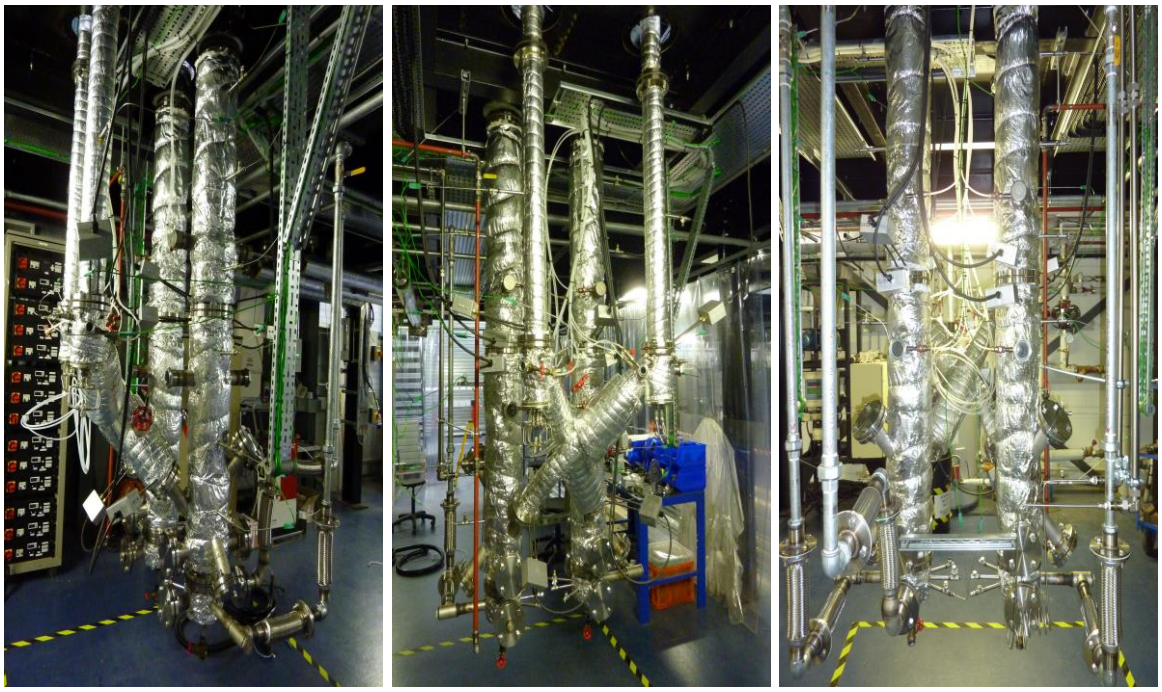

**Figure A-4 Installed loop seals and flexible joints for reactor expansion relief**

## A.2 Engineering diagrams

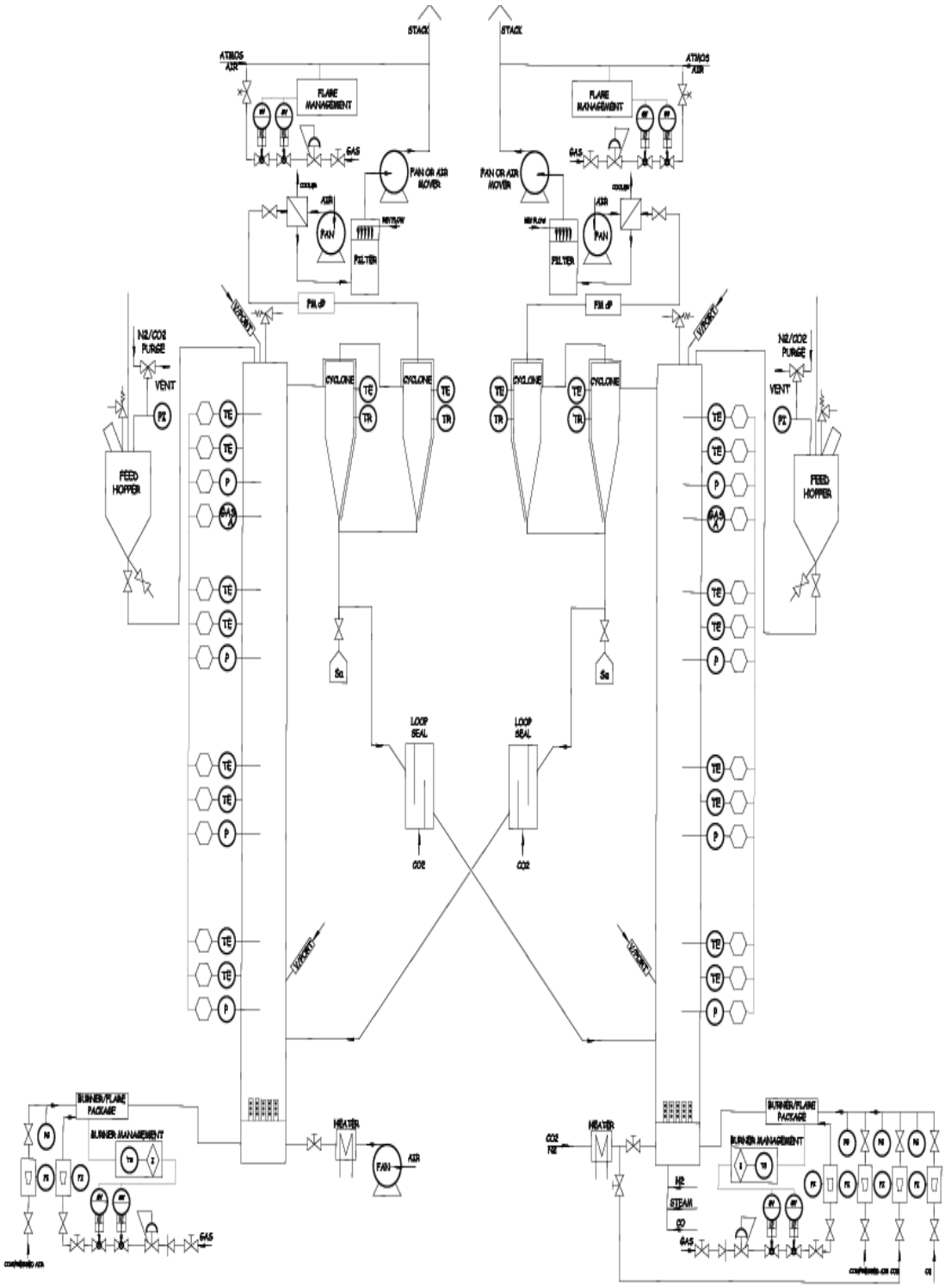


**Figure A-5 Engineering scheme of CLC reactor**

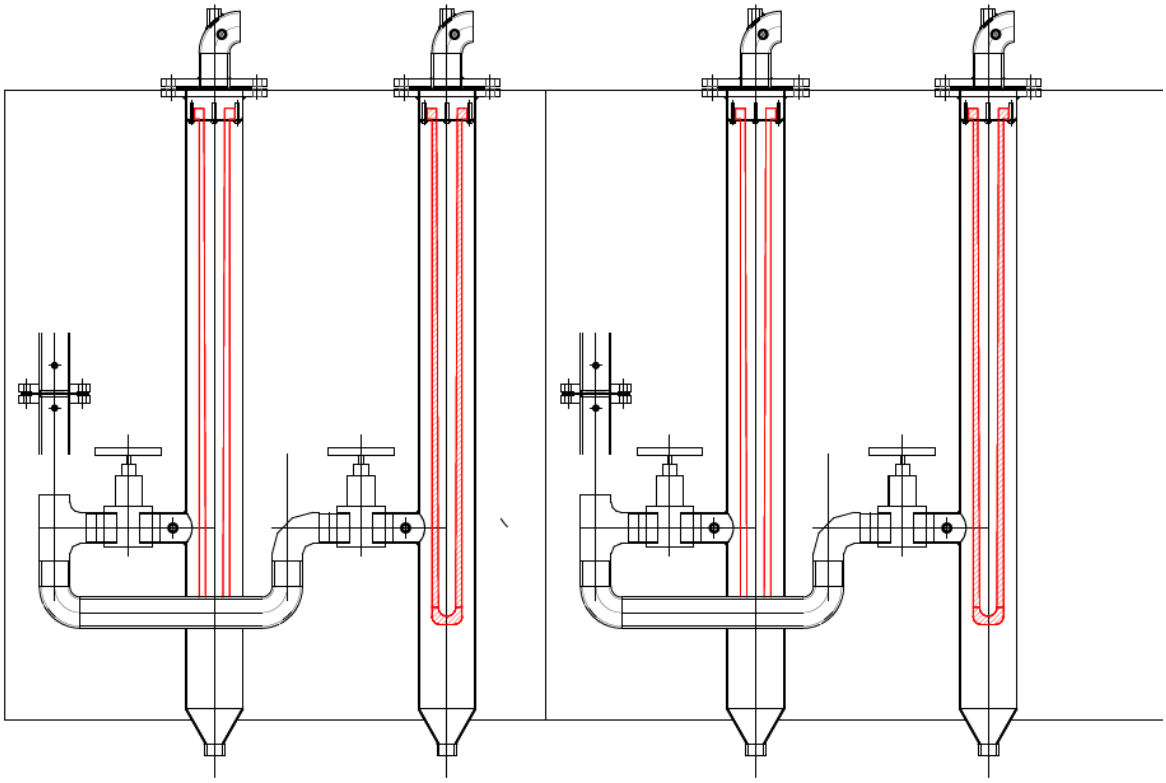

**Figure A-6 Design of candle particulate filter. Two per riser, designed to allow continuous operation if one becomes full or blocked.**

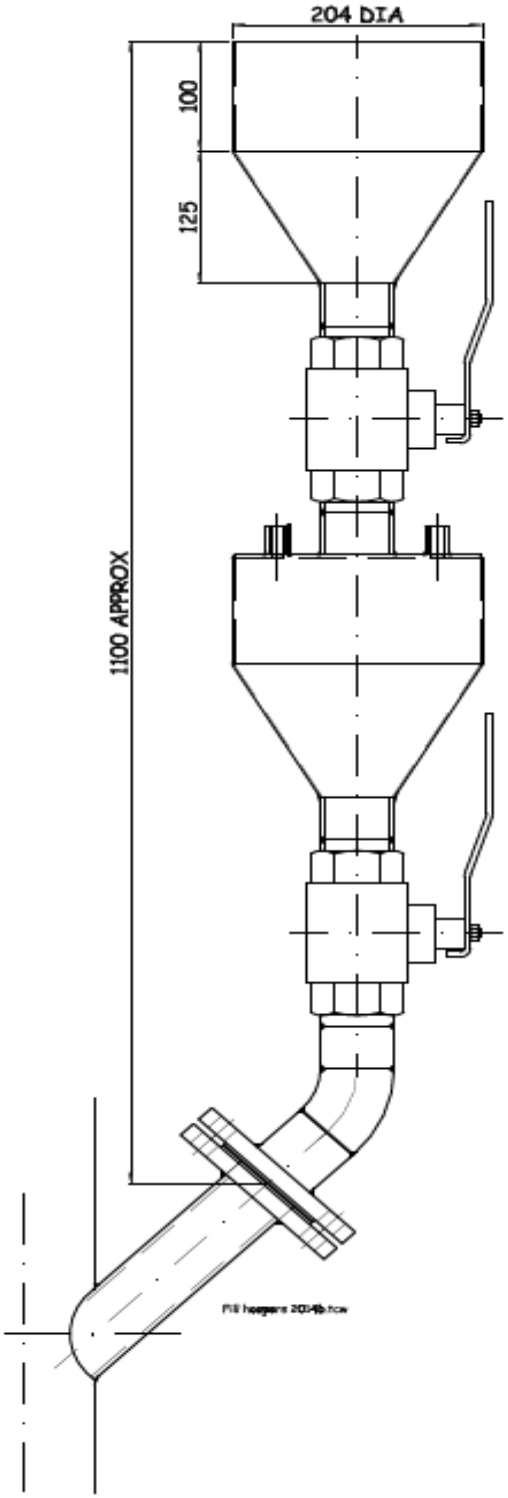


**Figure A-7 Design of feed lock hopper for the oxygen carrier feeding**

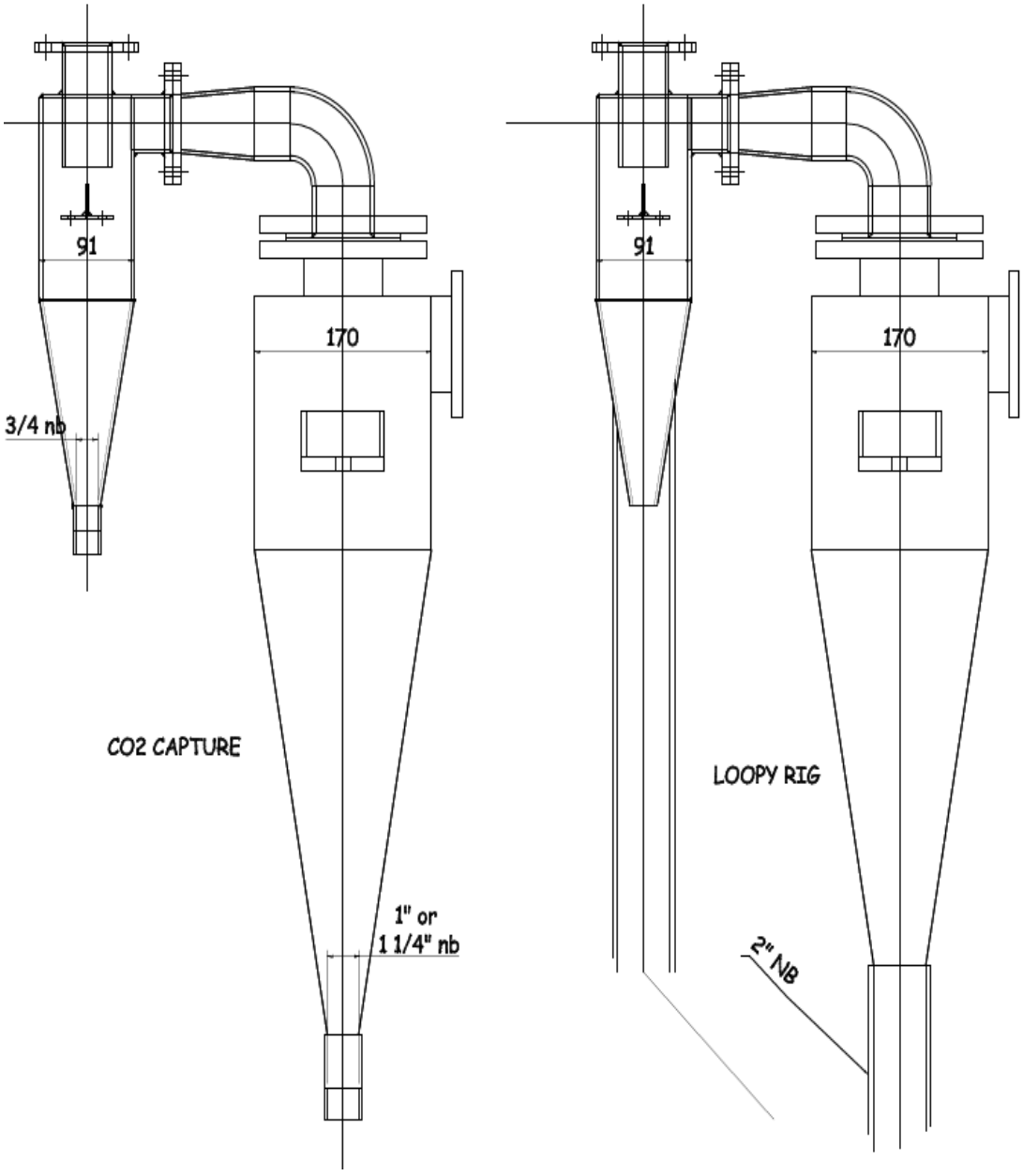


**Figure A-8 Design of primary and secondary cyclones**

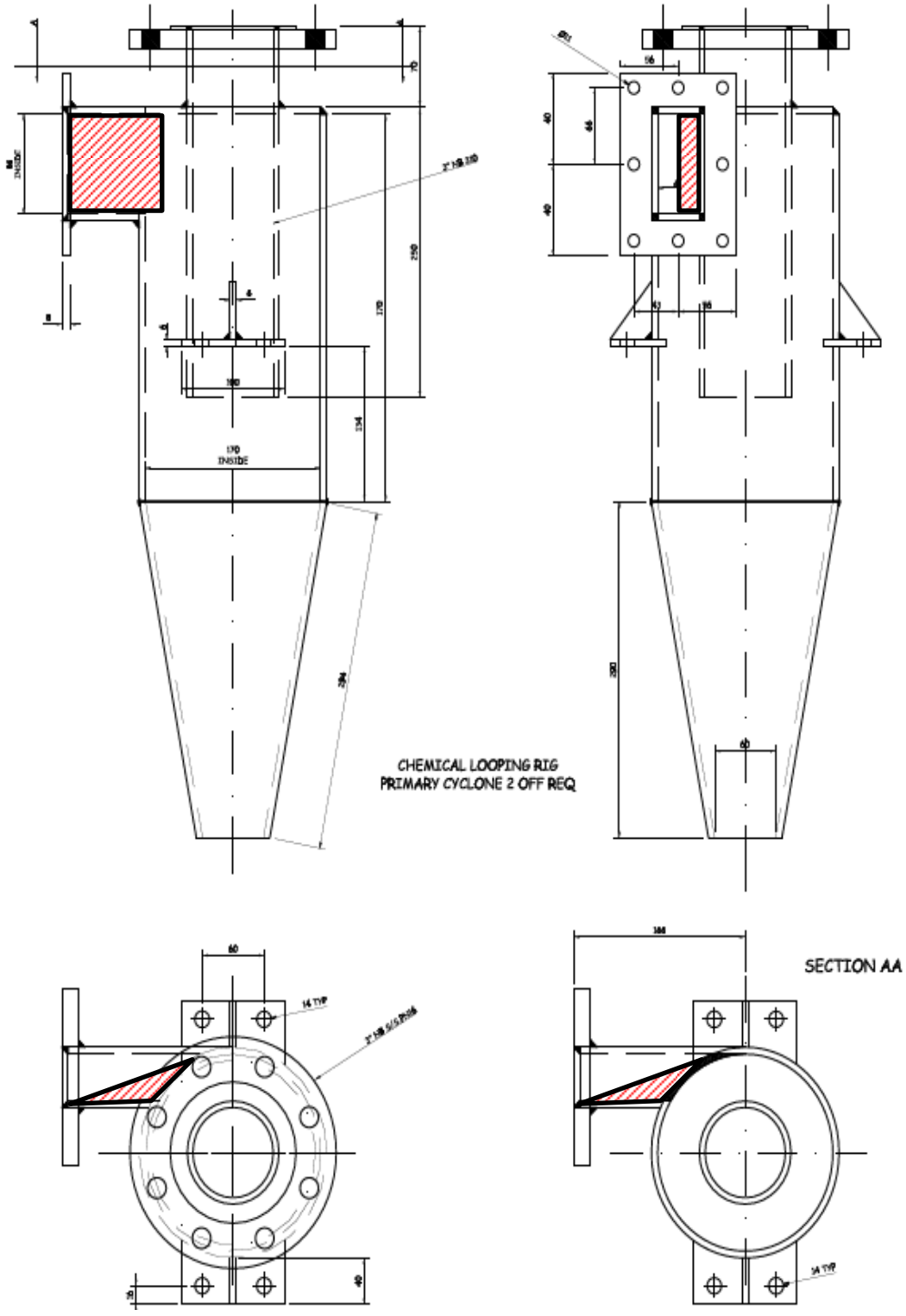


**Figure A-9 Primary cyclone modification to enhance entry velocity and cyclonic effect. Plate installed (indicated in red) to reduce cyclone inlet aperture**

# Appendix B

## B.1 Start-up procedure

- Switch on extraction system (1st floor mezzanine)
- Ensure personal gas monitor on the person, switched on and functioning
- Check mains gas detection system is functioning
- Ensure downstream valves on filters and cyclones are open to atmosphere
- Switch on logging computer
- Calibrate the gas analysers, zero pressure transducers ensure methane detection system is functioning.
- Open LabVIEW software, initialisation will check communication with data logging equipment
- Open CLC.vi and run the software vi and Open the brooks mass flow controller software and initialise communication with the mass flow controllers
- Check mains compressor is switch on and warmed up
- Open valves on mass flow controller manifold for $CO_2$ and $N_2$
- Open pneumatic safety valves, upstream of the gas manifold and on the control box, flick switches $CO_2$ and $N_2$ to up position
- Supply 300L/min of air to both of the reactors
- Turn on the single phase power switches for the trace heating controllers and preheaters.
- Turn on the controllers and ensure they are set to correct target temperatures [Password 77] select mode ST1 790 for both the trace heating and preheaters
- Wait for reactor to reach required temperature (725°C)
- When reactor wind-box has reached methane ignition temperature ask technician to switch on flare
- Reduce air flow to 150 L/min and introduce 5 L/m of methane to elevate reactor temperature.
- Load required oxygen carrier in the feed hopper approx. 200g per load, and introduce into reactor slowly.

## B.2 Shut-down procedure

- Switch off preheating and trace heating controllers (red switch to off)
- Switch off controllers from single phase supply points
- Switch off any combustible gases
- Allow reactor to fluidise and cool in inert gases minimum 200 L/min ($N_2$)
- Save data on LabVIEW by exporting graphs to excel and save as .xls
- Once the reactor temperature of the reactor has reached 350$^{o}$C use brooks software to switch off mass flow controllers
- Continue to log the temperatures until the reactor cools to 100$^{o}$C
- Switch off extraction system
- Close opened mass flow controller manifold valves
- Close pneumatic safety valves

### Post operation procedures

- In clean receptacles, empty filters by opening valves and tap with rubber mallet. Ensure particulate mask is worn additional to lab PPE
- Empty reactors by opening drainage valve and tapping with rubber mallet
- Check integrity of pressure measurement tubing and thermocouple wires
- Ensure data is saved and shut-down computer

# Appendix C

## C.1 XRD spectra of oxygen carrier after commissioning test

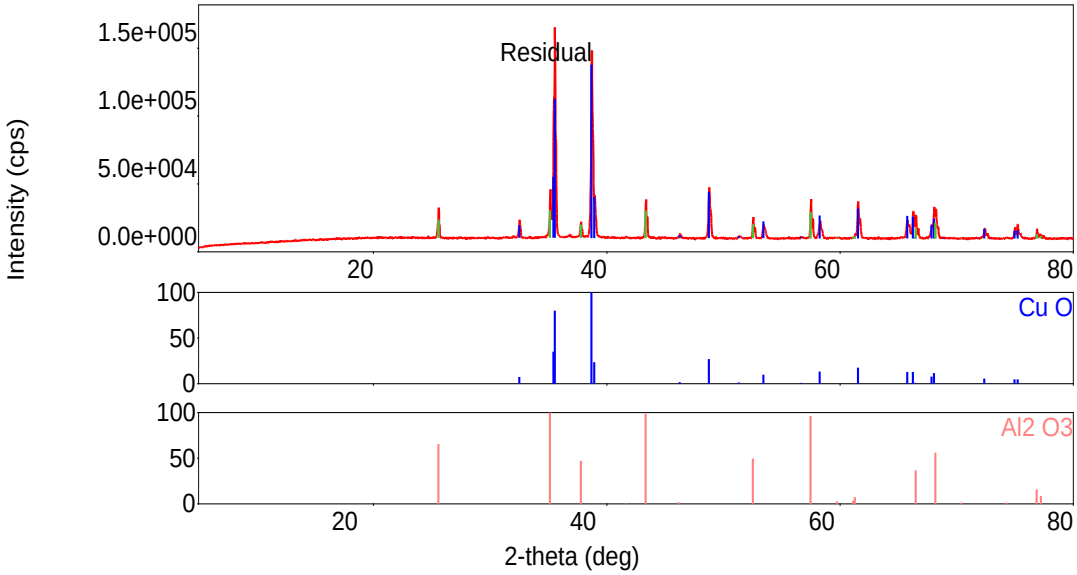


**Figure C-1 XRD spectra of CuO 60% $Al_2O_3$ 40% after commissioning test, showing no interaction between active oxide and support material.**